1999

Chip-controlled 3-D complex cutting tool insert design and virtual manufacturing simulation

Shizhuang Luo
Iowa State University

INFORMATION TO USERS

This manuscript has been reproduced from the microfilm master. UMI films the text directly from the original or copy submitted. Thus, some thesis and dissertation copies are in typewriter face, while others may be from any type of computer printer.

The quality of this reproduction is dependent upon the quality of the copy submitted. Broken or indistinct print, colored or poor quality illustrations and photographs, print bleedthrough, substandard margins, and improper alignment can adversely affect reproduction.

In the unlikely event that the author did not send UMI a complete manuscript and there are missing pages, these will be noted. Also, if unauthorized copyright material had to be removed, a note will indicate the deletion.

Oversize materials (e.g., maps, drawings, charts) are reproduced by sectioning the original, beginning at the upper left-hand corner and continuing from left to right in equal sections with small overlaps. Each original is also photographed in one exposure and is included in reduced form at the back of the book.

Photographs included in the original manuscript have been reproduced xerographically in this copy. Higher quality 6" x 9" black and white photographic prints are available for any photographs or illustrations appearing in this copy for an additional charge. Contact UMI directly to order.

UMI®

Bell & Howell Information and Learning
300 North Zeeb Road, Ann Arbor, MI 48106-1346 USA
800-521-0600

Chip-controlled 3-D complex cutting tool insert design and virtual manufacturing simulation

by

Shizhuang Luo

A dissertation submitted to the graduate faculty

in partial fulfillment of the requirements for the degree of

DOCTOR OF PHILOSOPHY

Major: Mechanical Engineering

Major Professor: X. Daniel Fang

Iowa State University

Ames, Iowa

1999

Graduate College

Iowa State University

This is to certify that the Doctoral dissertation of

Shizhuang Luo

has met the dissertation requirements of Iowa State University

Signature was redacted for privacy.

Major Professor

Signature was redacted for privacy.

For the Major Program

Signature was redacted for privacy.

For the Graduate College

TABLE OF CONTENTS

ACKNOWLEDGEMENTS

I would like to thank my major professor, Dr. X Daniel Fang, for his supervision and generous assistance and encouragement during the period of this study. I am grateful to all members in my graduate program of study committee for their invaluable advice on my graduate study.

I would also like to acknowledge the generous assistance given by other staff of the department, especially Mr. Larry Couture.

ABSTRACT

Designing suitable tools for the turning operation is of vital interest to manufacturers. The tool inserts used nowadays adopt complex geometric shapes. A question facing many manufacturers is how to effectively design complex shaped tool inserts and how to prove the validity of such design. One of the important criteria for selecting inserts is the ability to control chip formation and chip breaking.

The research work described in this dissertation attempted to bring innovation into the cutting tool insert design process by using feature-based modeling and by proposing a predictive chip model and integrating it into the design process. Such model integration makes the tool insert design a much more effective process and also enhances the decision-making required in insert design

A new 3-D kinematic chip model was developed to depict chip behavior in a complex groove insert. The model derived showed the analytical relationships between chip shape parameters and chip motion parameters. This dissertation explained how the kinematic model could be modified to take into account all possible 3-D complex groove shapes. A mathematical model was also developed from experimental data to serve the current need for cutting tool design.

Other research work presented in this dissertation is the simulation of the machining process in a virtual environment. The virtual machining simulation can be of great benefit for researchers in manufacturing to use the platform as a testbed for product development and testing.

CHAPTER 1 INTRODUCTION

1.1 Scope of the dissertation

Machining is a key activity in a manufacturing environment. Within machining processes, the lathe turning operation is a major component of the manufacturing process. Designing suitable tools for the turning operation is of vital interest to the manufacturers. With the advance of machining technology, and especially with the introduction of high speed cutting, the requirements of cutting tools have become more demanding than ever before. The tool inserts used nowadays adopt complex geometric shapes. A question facing many manufacturers is how to effectively design complex shaped tool inserts and how to prove the validity of such design.

Modern CAD tools are quite powerful in assisting with design visualization. These software packages, however, have no knowledge of the functionality of a specific design. They are actually "blind" in such areas. It is up to the designer to classify the functional requirements for the parts and calculate (if possible) the design parameters. When the CAD tools are used to perform complex geometric design of cutting tool inserts, it is very troublesome for the CAD tools to create insert shapes and it is very difficult for the designers to modify once a design is created. The motivation here is to find a way to systematically approach the problem of complex geometric design of cutting tool inserts and find a convenient and customized solution to it.

An advanced unmanned manufacturing process demands tool inserts that can ensure high quality products and low cost. One of the important criteria for selecting inserts is the ability

to control chip formation and chip breaking. Metal chips from the cutting process have been a major problem in unmanned machining. If the cutting tool insert design process can somehow predict the chip formation performance of the insert being designed, only valid designs would be allowed to come through. Thus, the design process would avoid many days of trials and errors and become an intelligent process. What is needed, then, is a prediction algorithm for chip formation based on complex insert geometry. Once this algorithm is developed, it also needs to be successfully integrated into the design process.

The research work described in this dissertation attempted to bring innovation into the cutting tool insert design process by using feature-based modeling and by proposing a predictive chip model and integrating it into the design process. Such model integration makes the tool insert design a much more effective process and also enhances the decision-making required in insert design

Other research work presented in this dissertation is the simulation of the machining processes in a virtual environment. Prior to actual machining, an effective platform is needed to demonstrate current understanding of the process and to simulate the execution of different manufacturing tasks. If this platform can perform correctly or at least as accurately as possible compared to the real machines, it can be a great benefit for researchers in manufacturing to use the platform as a testbed for product development and testing. The design and implementation of such platform is discussed in this dissertation.

This dissertation is divided into seven chapters. Chapter 1 introduces the scope of the dissertation and provides some background on cutting tool design and design theories. Chapter 2 focuses on the introduction and literature review of chip control. Chapter 3 analyzes 3-D chip formation for complex groove tools and establishes a prediction model for

chip formation. Chapter 4 integrates the model in complex geometry design of tool insert. Chapter 5 reviews virtual reality (VR) in manufacturing. Chapter 6 proposes VR as an testbed for chip control simulation and Chapter 7 will discuss all the conclusions from the research work.

1.2 Background of the cutting tool design

The sole purpose of a cutting tool is to remove material using its cutting edge. This process is referred to as the machining process. The machining process involves not only the cutting tools, but also the tool holder, the workpiece and the cutting conditions. All of these together contribute to the quality of the final product. A successful design of cutting tools for the turning operation requires a complete understanding of cutting tool function and its geometry. The cutting tool design diagram is shown in Fig. 1.1.

As shown in Fig. 1.1, cutting tool design has always involved material design and geometric design. Material design includes material properties, such as material life, strength, hardness and so on. These directly determine the maximal allowed cutting conditions (i.e., maximal cutting speed, maximal cutting forces, etc). Geometric design of tool insert deals with basic geometry of an insert (i.e., nose radius, rake angle, etc). Tool geometry plays an important role in product quality. The aim of geometric design is to provide a tool insert that has optimal finish quality on a workpiece.

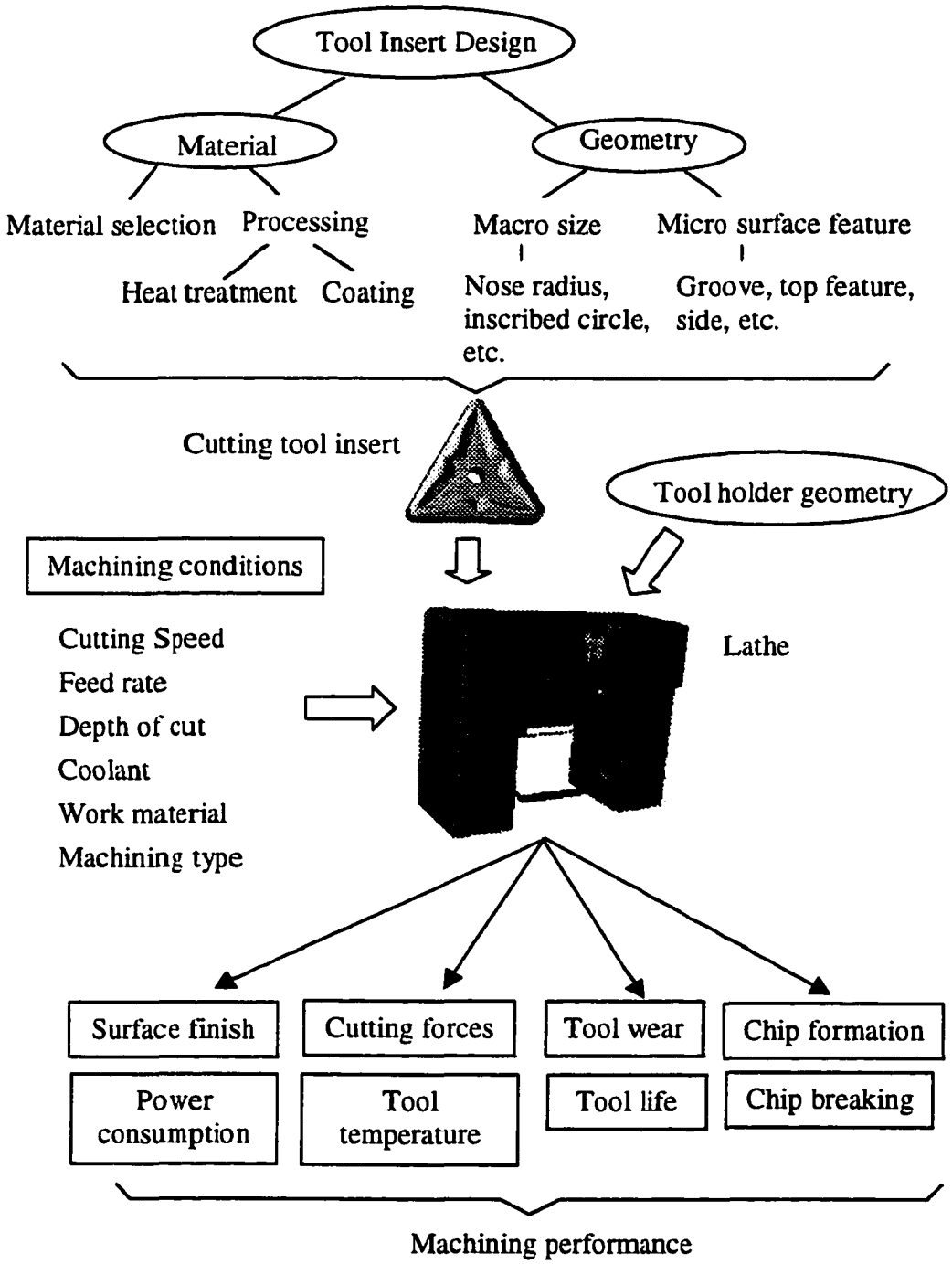

Fig. 1.1 Cutting tool design diagram

1.2.1 Cutting tool geometry

Since the introduction of cutting tools, they have experienced several stages of development, from basic flat rake face tools to 2-D modified tools and then to complex 3-D tools.

1.2.1.1 Basic single-point tools: flat rake face

The basic shape of a single point cutting tool is shown in Fig. 1.2. As Fig. 1.2 shows, main sections of a tool are face, nose, heel, shank and the cutting edge. The shank is the part of the tool on which the tip is supported. The cutting edge is the portion of the face along which the chip is separated from the workpiece. For common tools, the cutting edge is composed of the side cutting edge, the nose radius, and the end cutting edge. The flank is the end surface adjacent to the cutting edge. In the early days of cutting practice (before 1950s), the tool rake face was a simple flat shape.

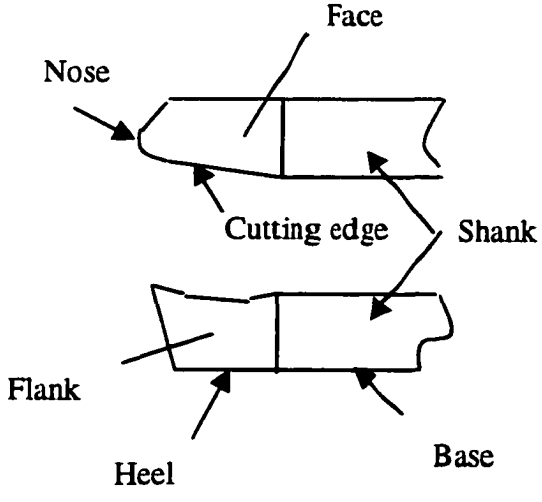

Fig. 1.2 Basic single-point cutting tool geometry

Cutting tools are usually divided into two categories: left-cut and right-cut. On a left-cut tool, the cutting edge is on the left side when viewed face up from the point end of the tool. Respectively, a right-hand tool's cutting edge is on the right side.

A single-point tool has several basic tool angles that are important in the metal-removal process: back rake angle, side rake angle, end relief angle, side cutting edge angle and end cutting edge angle. The angles are illustrated in Fig. 1.3. Each tool angle plays a different role in the cutting process.

As Fig. 1.3 shows, the back rake angle is the angle between the face of the tool and a line parallel to the base of the shank. Variation of the back rake angle affects the direction of chip flow, chip contact length and cutting forces.

The side rake angle is defined as the angle between the tool face and a plane parallel to the tool base. This angle is related to cutting forces, tool life and surface finish.

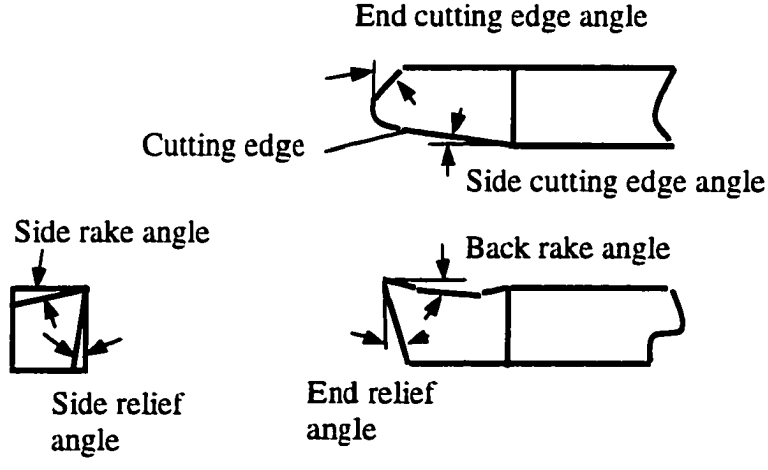

Fig. 1.3 Basic tool angle of a single-point tool

The end relief angle affects the tool tip strength, which determines the tool wear and tool life.

Side cutting edge, end cutting edge and nose radius make up the cutting edges of a cutting tool. The two cutting edge angles determine how the edges are blended together.

1.2.1.2 Modified tools: 2-D modification

As a flat rake face tool had a short life and poor chip control performance, it could not satisfy the need for high volume and automatic production. Manufacturing operators realized the troubles with cutting tools at high volume production (Kauffman, 1954). Because of the need for increased cutting speed and feed rate, modifications were made to reduce cutting forces, extend tool life and improve chip control.

As the machining practice improved, some cutting tools began to use chip breakers. A chip breaker is a step or groove in the face of a tool or a separate piece attached to the tool in order to cause the chip to break up or curl properly. The 2-D modification of cutting tool referred to simple chip breakers because the chip breakers' cross-section were approximately uniform throughout the cutting edge. The typical chip breaker shapes for 2-D modifications are shown in Fig. 1.4.

During the 1950s, researchers started doing the chip flow and chip breaking analysis (ten Horn, 1954 and Henriksen, 1954). Some results of this early research are still used in today's chip control practice.

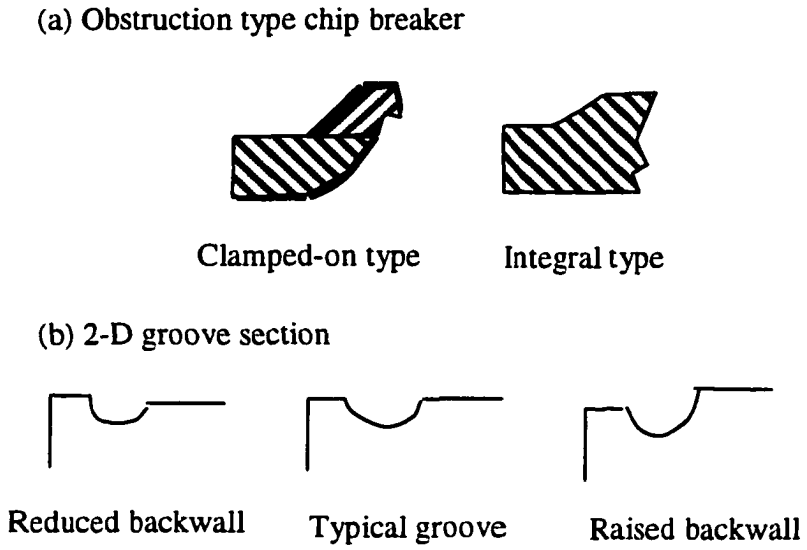

Fig. 1.4 Typical shape of 2-D modified cutting tool

1.2.1.3 Complex tool inserts: 3-D modification

Since the 1950s, indexable metal cutting inserts have become widely used. In this kind of tooling configuration, a tool holder and a tool insert are used together.

The tool holder provides some basic geometry similar to that shown in Fig. 1.2 and Fig. 1.3, while the tool insert determines the shape of the cutting edge and the chip breaker. The tool insert usually has multiple cutting edges to increase the life of a single insert. This configuration increases productivity by enabling the operator to easily change inserts without needing to calibration of the machine tool. This configuration also helps reduce operating costs because tool inserts cost less than single-body tools.

Much research has been conducted to study the dynamic model of the cutting process, especially the chip formation and chip breaking process. Some researchers have also studied

the effects of different geometrical shapes towards cutting forces and chip control. More detailed discussion of this previous research will be provided in Chapter 2.

Modern cutting tool inserts usually have molded-in chip breakers. There is no need for separate clamped-on type chip breakers. The groove geometry gets more complex as it includes variable groove profiles and variable rake face profiles. On some tool inserts, small extrusions work as obstruction type chip breakers. These geometric variations may work in combination to optimize the chip control result. Fig. 1.5 shows some complex tool insert configuration.

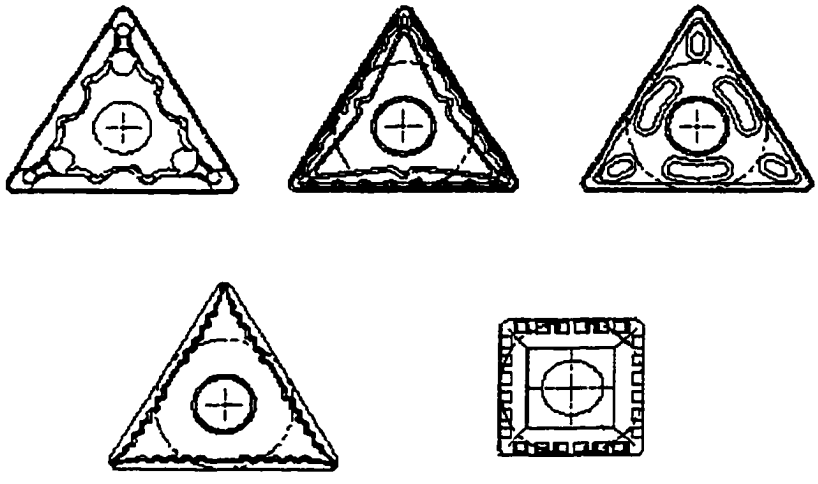

Fig. 1.5 Complex 3-D insert designs

The design of complex shape inserts becomes a challenging task for designers as the selection of geometry relies heavily on the experience of the tool designer. Because there is no CAD program to hasten the creation and modification of insert design, it is an art to design an effective insert.

1.2.2 Cutting tool material design

Tool material must be carefully chosen in relation to the workpiece material to be machined, the machining condition (feed, speed and depth of cut), the kinematics and stability of the machine tool and required surface finish quality. The tool material will also influence the tool life and production costs.

There are three criteria for material selection: high-temperature physical and chemical stability, abrasive wear resistance, and resistance to brittle fracture. These criteria can be expressed as thermal behavior, hardness, and tensile strength. A given type of material tends not to perform highly in all three areas. For example, if a material performs well on one criterion, it is unlikely that it performs highly in both of the others. This variability among material types is why it is important for designers to carefully select tool material for particular machining need.

The following are the major cutting tool materials, listed in order of increasing hardness and decreasing tensile strength: carbon steel, high-speed steel, cast alloy, Tungsten carbides, cermets, Titanium carbides, ceramic, polycrystalline diamond and cubic Boron Nitride, and single crystal diamond. For example, the first generation tool material is High-speed steel. It is still used in some areas. Tungsten carbides have been used for at least 50 years. Their ability to combine high strength and hardness with excellent thermal shock resistance made them highly successful as cutting tool material. By varying the cobalt level, the relative balance of tool toughness and hardness can be modified.

Cermets are metal bonded materials containing a very high proportion of cubic carbides (especially TiC), and often employ significant quantities of NI. Cermets are primarily used

for light cuts at relatively high cutting speeds on cast iron and steel. Ceramic (Al_2O_3) tools have proven to be of greatest usefulness in machining cast iron and hard steel.

Modern carbide tools are often coated. Coating can improve the hardness and surface properties of the cutting tool inserts. A thin coating of hard, chemically inert and lubricious compounds can be applied to the surface of cutting tools. The coating compounds are usually a combination of TiC, TiN and Al_2O_3. There are two basic coating methods: chemical vapor deposition (CVD) and physical vapor deposition (PVD). CVD done in gases of 1000 degrees Celsius; PVD tools are treated at around 400 degrees Celsius.

With all the materials and techniques, the material design of cutting tools requires designers to consider cutting conditions and tool geometry in order to choose appropriate material. Material properties can also influence the cutting forces and the chip formation process during machining. As material technology advances, material design can be satisfied with the selection of commercial material products.

1.3 Development of the design theories

Engineering design is an art. It is an art because it requires someone special to put things in order, especially when there are not many rules that can help with the designing process. Designing is an information transformation process that converts the requirement information into design parameters.

Designers have tried hard to make the designing process a science rather an art. Researchers have always tried to find ways to develop a system of rules and theories that may facilitate the designing process. The development of computer-aided design over the last 40 years has driven even more engineers to examine this information transformation process.

Suh (1977, 1982) first discussed the different design spaces and introduced the axiomatic design theory. The axiomatic design theory used the concepts of functional requirements and design parameters. Suh argued that a design process should map the functional requirements to various design parameters. He initially proposed seven axioms, which he later reduced to two axioms: first, maintain the independence of functional requirements; second, minimize the information content. Suh's axioms also set forth rules for information transformation.

To use Suh's theory in design automation, the functional requirement (FR) need to be mapped into some design parameters (DR). This mapping was not widely discussed in the axiomatic design theory as the axiomatic design focused only on the meta-processing. Mapping between FRs and DRs is actually the most difficult part of a designing process. Determining how to define FRs and DRs is another problem with the axiomatic design.

Takeda (1990) moved towards building a computable design process model; such a model is a prerequisite for realizing intelligent computer-aided design systems. The concept of meta-model was used by Takeda in describing the evolutionary nature of design. Stepwise refinement and model evolution were discussed. The evolutionary design cycle is shown in Fig. 1.6. Shimomura et al, improved the model to a functional evolutionary process model (1998).

Kirschman (1998) described the decomposition process of design. He proposed that based on mechanical functions, FRs should be decomposed into taxonomy. With such taxonomy in place, rather than an exhaustive search process of possible parameters, a simple set of generic forms may be used to represent the necessary design concepts. Design can then be effectively accomplished.

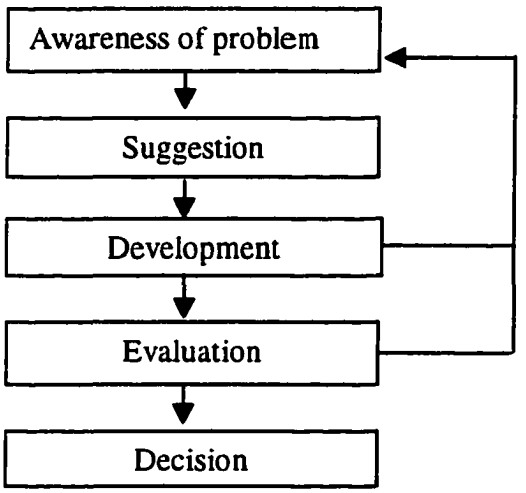

Fig. 1.6 Evolutionary design cycle

Other designers regard the design process as a decision-making process. Every choice that a designer makes is a decision. A successful design process requires correct decisions. As the design process becomes automated, one key question that arise is how to make the decision-making intelligent. Intelligent decision-making processes often involve AI technologies, such as neural networks and fuzzy logic.

Up to now, design is still by and large an art rather than science. Despite attempts by researchers, computers are still not intelligent enough to fully automate the design process. With some theories in place, previous research has, however, made it easier to identify the needs of a particular design.

In the particular design problem of cutting tool insert, complex geometry and design validation could be achieved using a systematic approach. The systematic approach views the design process as a combination of many small decision-making steps. Each step contributes to a bit of information to the final design model. Through modeling the design process,

suggestions are made to improve the performance of the design process. The goal is make the design process closer to a science.

CHAPTER 2 LITERATURE REVIEW ON CHIP CONTROL

Chip forming and chip breaking are important processes of metal-cutting. Many researchers have studied various aspects of the processes in attempts to model them and to direct the results into cutting tool design. Chip control has become a crucial criterion in the performance judgement for a cutting tool design. This chapter looks at research achievements in the chip control field and indicates the need for further study.

2.1 Chip control importance

Before the 1950s, machining practice had aimed at improving productivity by focusing on high cutting speed, high feed and high machine tool accuracy. Chip control was rather neglected until problems came up with machining automation (Kauffman, 1954 and ten Horn, 1954). In an unmanned automatic machining, any chip tangled on the machine would delay production and might cause serious damage to both the workpiece and the cutting tool. These undesirable results made researchers realize the importance of chip control.

Chip control is vital to manufacturers' interests because unwanted chips may cause several problems: (Jawahir, 1993; Shaw, 1984)

- Personal injuries (in a manual operation);
- Poor surface finish quality and workpiece damage;
- Damage to cutting tools and machine tools;
- High cutting forces, high tool temperature, excessive tool wear and shorter tool life;
- High volume of chips produced;

- Delay in production and increase in production costs.

Owing to all the above factors, more and more attention has been focused on the subject of chip control. There are many approaches to this problem. Some researchers have tried to understand the complicated mechanics model of the metal-removal process, such as Johnson, Usui and Oxley, while others have studied the role of tool geometry in chip formation, such as Nakayma and Jawahir. All these efforts, theoretical and experimental, work towards a goal of total chip control in machining. The following sections will introduce development in chip formation and chip breaking, and then discuss the research work in chip control.

2.2 Basic chip forms

When the cutting tool removes a layer of work material from the workpiece, the removed material forms cutting chips. Due to the characteristics of work material, cutting chips come in different forms: continuous chips, segmented chips and elemental chips. Continuous chips are the result of stable metal deformation. The segmented and elemental chips are often referred to as discontinuous chips. Discontinuous chips exist when material like cast iron is cut. Some chips may be something in between these forms, such as a wavy chip with no constant thickness. Continuous chips are produced in steel cutting.

The shape of a continuous chip is influenced by many factors. When a flat-faced tool is used, the chip would have motions as shown in Fig 2.1. The chip has one linear velocity and two angular velocities (Nakayama et al., 1978). Any freely-shaped chip can be constructed with these motions. When a helical chip is uncoiled by removing the up-curling, it becomes a circular chip. When the circular angular velocity equals zero, the chip becomes a straight chip.

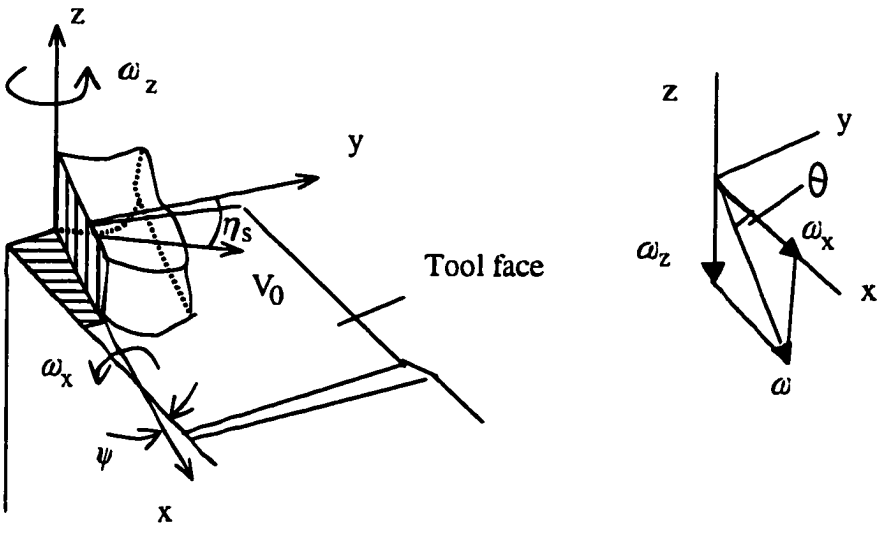

Fig. 2.1 Motion of chip on a flat face cutting tool

The values of angular velocities are given as Eq. 2-1 and Eq. 2-2. Their motions are illustrated in Fig. 2.2.

$$\omega_x = \frac{V_0 \cos\eta_s}{R_u} \tag{2-1}$$

$$\omega_z = \frac{V_0}{R_s} \tag{2-2}$$

where R_u is the up-curl radius, R_s is the side curling radius, V_0 is the speed of chip flow and η_s is the chip (side)flow angle. The angular velocities forms ω, while the angle between ω and x is obtained by Eq. 2-3.

$$\tan\theta = \frac{\omega_z}{\omega_x} = \frac{R_u}{R_s \cos\eta_x} \tag{2-3}$$

The helical chip resulting from the motions is determined by radius R (Eq. 2-4) and pitch p (Eq. 2-5).

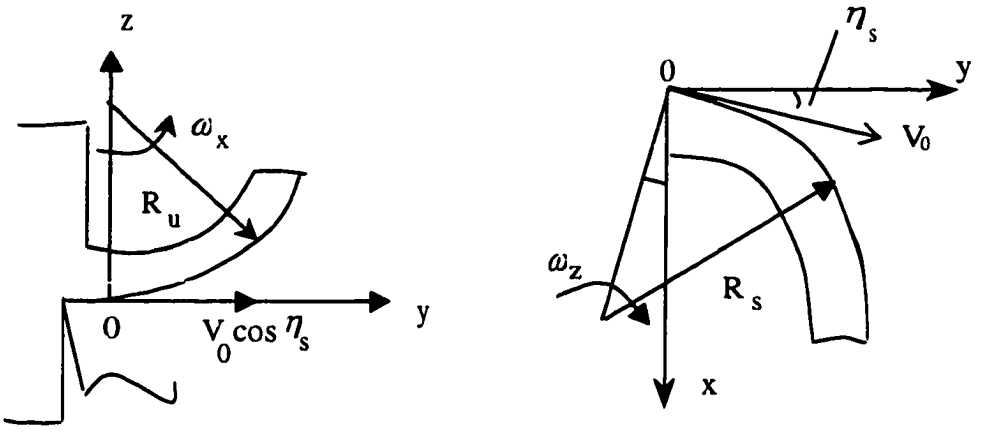

Up-curl Side-curl

Fig. 2.2 Up-curling and side-curling effect of free chip from flat face cutting

$$R = \sqrt{\frac{1-\sin^2 \eta_s \cos^2 \theta}{(\cos \eta_s / R_u)^2 + (1/R_s)^2}} \tag{2-4}$$

$$p = \frac{2\pi R \sin \eta_s \cos 6}{\sqrt{1-\sin^2 \eta_s \cos^2 \theta}} \tag{2-5}$$

These basic chip forms are considered free if they do not hit any obstacles. Usually, the chip will meet obstacles such as a chip breaker and become a forced chip. The model described above is for a flat face cutting tool. With complex tool geometry, other motions like twisting are included. The effect of twisting will be described in section 2.5.

2.3 Chip formation: chip flow and chip curling

In a cutting process, the chip moves across the tool face. Most research to date deals with orthogonal cutting conditions. When a tool face is perpendicular to the cutting speed and the depth of cut is at least five times the feed rate, the cutting is considered as orthogonal cutting.

Otherwise, it is considered as oblique cutting. Under orthogonal cutting conditions, the width of the chip is equal to the undeformed chip width. The undeformed chip thickness corresponds to the feed rate while the depth of cut corresponds to the chip width.

There are two basic chip flow modes in a cutting process: chip side-flow and chip back-flow. Chip side-flow is viewed in the tool face plane, and chip back-flow is viewed in the plane perpendicular to the cutting edge. Chip back-flow is also known as chip streaming. The result of chip flow is chip curling. Similar to chip flow, there are two chip curling modes: chip side-curl and chip up-curl. Chip side-curl happens in the same plane as chip side-flow and chip up-curl is in the plane as chip back-flow. Both chip flow and chip curling modes have been studied in detail by various researchers. The next section summarize key elements of this research.

2.3.1 Chip side-flow and chip side-curl

In a cutting process, the chip always leaves the cutting edge at some angle to the cutting edge. This occurrence is known as the chip side-flow and had been studied by several researchers. Colwell (1954) used a cutting edge method to analyze the chip flow. His analysis showed that the chip flows approximately perpendicular to the chord representing the major axis of the cut. Fig. 2.3 shows Colwell's method of determining the chip flow angle for nose radius tools.

If the side cutting edge angle C is zero and the depth of cut d is greater than the nose radius r (as shown in Fig. 2.3 (a)), then chip side-flow angle η_s is given by Eq. 2-6.

$$\eta_s = \tan^{-1}\left(\frac{r + f/2}{d}\right) \tag{2-6}$$

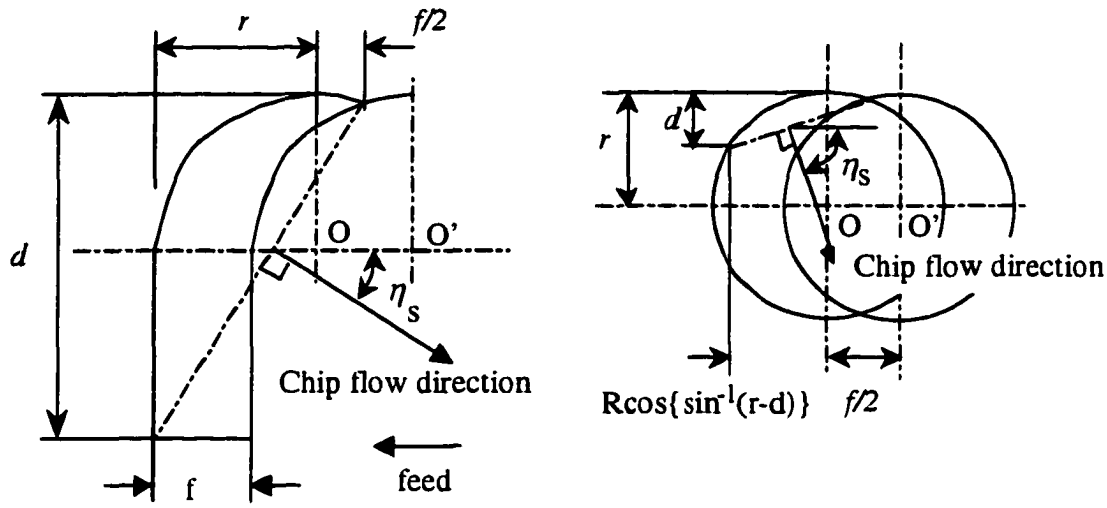

(a) when $d>r$

(b) when $d<r$

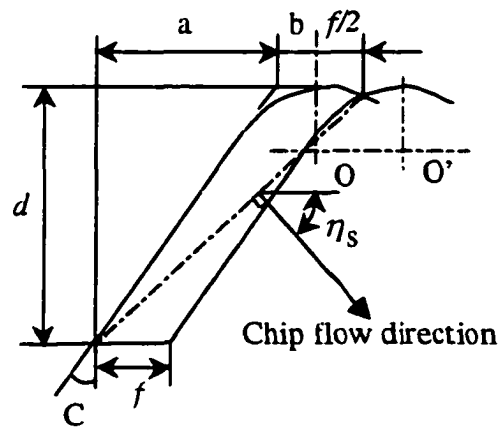

(c) general case

Fig. 2.3 Colwell's method of determining the chip flow angle for nose radius tools

where η_s is measured from the axis perpendicular to the cutting edge, f is the feed rate, r is the nose radius of the cutting tool.

When the depth of cut is small enough compared to the nose radius r (as shown in Fig. 2.3(b)), then the flow angle can expressed as shown in Eq. 2-7:

$$\eta_s = \tan^{-1}\{\frac{(2rd - d^2)^{1/2} + f/2}{d}\} \tag{2-7}$$

For a general case, where the side cutting edge angle is other than zero and the depth of cut is greater than the nose radius (as shown in Fig. 2.3 (c)), the chip side-flow direction can be expressed as in Eq. 2-8.

$$\begin{aligned}\eta_s &= \tan^{-1}\{\frac{a+b+f/2}{d}\} \\ &= \tan^{-1}\{\frac{d\tan C + r\tan(\pi/4 - C/2) + f/2}{d}\}\end{aligned} \tag{2-8}$$

Stabler (1951 and 1964) also analyzed important angles in the cutting model, including the side-flow angle. He examined the velocity and force diagrams for oblique cutting in Merchant's shear theory, which led to some fundamental machining equations.

Okushima and Minato (1959) suggested that the chip flow is the actual result of each particle that passes into the chip from the workpiece to flow perpendicular to the edge that cut it. They assumed that the chip would take up a flow direction that was the average of the directions of its constituents, as shown in Eq. 2-9.

$$\overline{\eta} = \frac{\int \eta_s(s)ds}{\int ds} \tag{2-9}$$

where ds is a small length of the cutting edge and $\eta_s(s)$ is the local chip flow angle of the corresponding chip element leaving that portion of the edge.

Spaans (1971) reviewed all these methods and derived an empirical equation to predict the chip flow angle. Young et al. (1987) studied the nose radius effects for oblique cutting and derived an equation for predicting the resultant friction force on the tool face. Through

analytical work and experiments, he showed that the frictional force on the tool face was directly associated with the chip flow.

The chip side-curl does not happen in every cutting condition. Nakayama (1972) and Van Luttervelt (1976) pointed out some factors that produced side-curl:

- the cutting edge is not straight;
- the primary motion of chip is not rectilinear;
- the cutting edge is not perpendicular to the primary motion;
- the chip compression rate varies along the chip width.

It has also been proven that the chip side-curl is influenced by the chip contact length. Van Luttervelt (1989) further studied the chip side-curl effect. His experimental work showed a direct relationship between the chip side-curl radius and the chip side-flow angle. Nakayama (1992) developed the chip form diagram that presented combined effects of chip up-curl and side-curl. Yet, he could not theoretically derive the side-curl curvature because of a lack of comprehensive understanding of its physical model.

2.3.2 Chip back-flow and chip up-curl

Chip back-flow and chip up-curl are closely related subjects. The following subsections will introduce current understanding of them in detail.

2.3.2.1 Chip back-flow

Chip back-flow or chip streaming is probably the subject that attracted most studies in the chip formation process. As show in Fig. 2.4 (a), the chip will keep moving on the tool rake face for a while before it starts curling. The natural contact length between chip and tool face

is h. When a tool is designed to have a shorter contact length than the natural contact length as in Fig. 2.4(b), the chip will flow towards the tool groove at an angle. This effect is called the back-flow or chip streaming. The angle is, therefore, called the back-flow angle or the streaming angle. The chip back-flow angle η_b is defined as the angle between a plane perpendicular to the cutting speed and the chip flow direction after restricted contact.

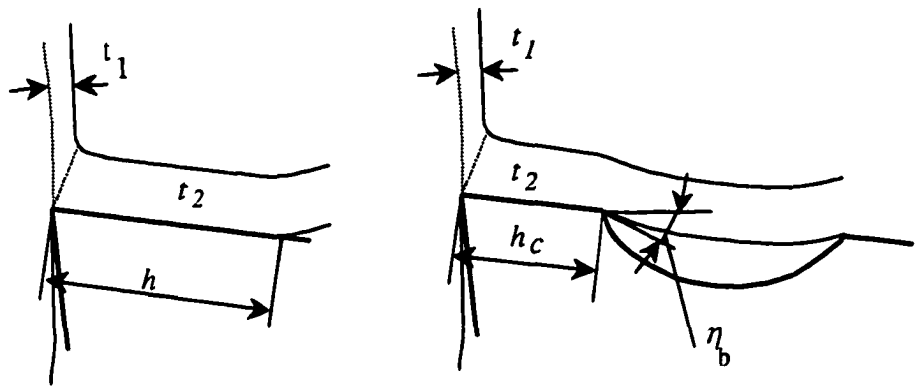

(a) Chip flow with natural contact (b) Chip flow with restricted contact

Fig. 2.4 Chip streaming effect on a cutting tool face

Johnson (1962) presented the first slip-line field model and the corresponding hodograph for orthogonal machining with a restricted contact tool. Usui et al (1963, 1964) also worked on this subject. Usui and Hirota (1978) used cutting model and the energy methods together in predicting chip formation and cutting force. Jawahir and Oxley (1988) found the equations of chip-back flow angle towards the cutting conditions and tool geometry. However, the results of the theoretic studies were not satisfactorily matched with the experimental results.

2.3.2.2 Chip up-curl

The chip up-curl is due to the fact that the chip velocity is not constant across the chip thickness. In a machining process, chips will curl up and away from the tool surface. This creates the chip up-curl effect. Henriksen (1954) first studied the geometry of chip up-curl curvature in relationship to the chip breaker geometry. He concluded that the radius could be calculated as shown in Eq. 2-10,

$$B=w^2/2h+h/2 \tag{2-10}$$

where B is the chip up-curl radius, w is the width of chip breaker and h is the height of the chip breaker. Henriksen's model is shown in Fig. 2.5. In the model, Henriksen omitted feed even though his experimental results showed the radius is related to the feed rate.

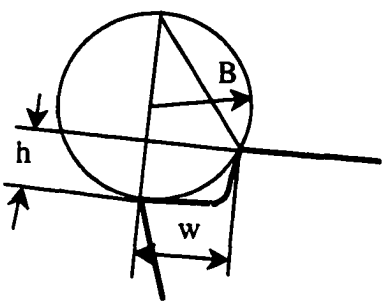

Fig. 2.5 Henriksen's chip up-curl model

Despite its inaccuracy, Henriksen's model is the mostly widely used model when calculating the chip up-curl radius. Using a similar approach, Nakayama (1962) defined the chip up-curl radius for obstruction type tool as shown in Fig. 2.6 (a) and Eq. 2-11.

$$R=(W-L)\cot(\theta/2) \tag{2-11}$$

where R is the up-curl radius, W is the length between tool tip to the chip breaker, and L is the chip-tool contact length. Nakamura (1982) defined the chip up-curl radius for a groove-type breaker. The tool is shown in Fig. 2.6 (b) and Eq. 2-12.

$$R=H/2 + W^2/(8H) \tag{2-12}$$

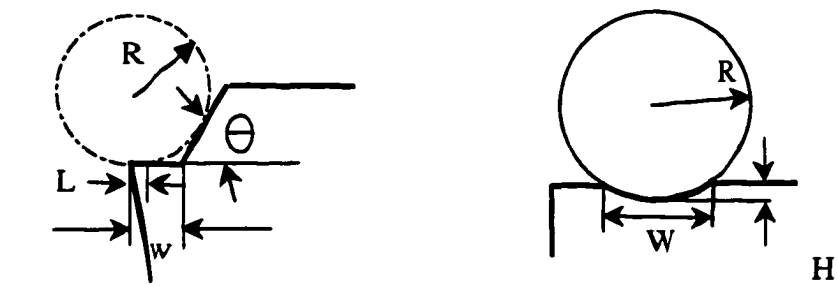

(a) Obstruction type tool (b) Groove tool

Fig. 2.6 Chip curl models developed by different researchers

Experimental results showed that chip thickness is an important factor in chip curl radius. Trim and Boothroyd (1968) took the chip thickness into consideration and found that

$$R=H/2 + W^2/(8H) \tag{2-12}$$

$$R= (W-t)^2/(2h) +h/2 \tag{2-13}$$

where W is the width of chip breaker, h is the height of it, and t is the chip thickness.

Worthington (1975 and 1976) and Worthington and Rahman (1979) proposed a new model that included chip thickness:

$$K=(h-h_s)(R-R_{min}) \tag{2-14}$$

where h is the undeformed chip thickness, h_s is the undeformed chip thickness at which its value equals the length of the sticky friction zone, R is the chip up-curl radius, R_{min} is the minimum value of chip curl radius for a particular groove configuration, and K is a constant determined by the equation. R can be derived as follows,

$$R = b/C(h-ab)+W*2^{1/2}/2 \qquad (2\text{-}15)$$

where a is a constant determined by work material, b is the restricted contact length and W is the groove width.

There are many researchers who worked on chip back-flow using a slip-line field model and tried to get the radius through calculating chip streaming angle. Van Luttervelt (1976) introduced the concept of "dead zone" in the chip formation and predicted the chip flow radius for machining operations at a small diameter. Zhang et al (1989) examined the theoretical calculation of the naturally curling radius of a cutting chip using the slip-line model. Such a model could be modified to include rake face boundary conditions to simulate chip curl in other tool faces. Shi and Ramalingam (1991 and 1993) reviewed previous slip-line models and used a new slip-line solution to calculate chip geometry from a groove tool. Liu et al. (1995) worked on their slip-line field model for prediction of chip curl radius.

2.3.3 Other research work on chip formation

Considerable efforts have been expended on developing the theory of chip formation. The number of approaches used indicates that the task was not an easy one and in each subsequent attempt, the approach was changed somewhat by each researcher in the hope of obtaining better agreement of theory with experiment. The next subsections are research work on theoretical and experimental work related to chip formation.

2.3.3.1 Cutting forces models

Cutting forces have always been essential to machinability and tool life. They even affect the chip formation process and chip breaking. Many models have been developed for cutting

forces; These models attempt to establish the relationships between the cutting forces and the resultant chip formation parameters, like chip flow angle.

Albrecht (1961) introduced the concept of ploughing into the metal-cutting process. Under this approach, the chip formation mechanism showed that increased bending action at shear zone reduces the shear angle.

Oxley (1961) and Yellowley (1983) worked on orthogonal cutting with restricted tool-chip contact. Venu Vinod et al. (1978) and Rubenstein et al. (1986) analyzed the oblique cutting with controlled contact tools using mechanics analysis. Mesquita and Barata Marques (1992) described a method for predicting cutting forces on a parallel-groove type chip breaker. The model considers the ploughing effect, chip-breaker geometry and the effective side-rake angle. Their results showed a good match between theoretical prediction and experiments. Sikdar et al. (1991) used statistical analysis to determine the variation of the geometrical and process parameters on the chip reduction coefficient, chip contact length and the cutting forces.

2.3.3.2 Chip formation for special tool shape

Due to different tool use, many forms of cutting tools are available. The cut-off tools perform considerably different than indexable tool inserts. Usui and Shaw (1962) experimented with the cutting of free machining steel and analyzed the effects of cut-off tools with reduced contact length. Rotberg et al. (1991) studied this special case of machining in chip forming and chip flow.

Armarego (1966) developed models for symmetrical triangular cut. Armarego and Wiriyacosol (1978) investigated oblique machining V grooves with triangle form tools. They

developed two oblique cutting analyses and also identified and designed the fundamental tool angles for oblique machining with form tools.

2.3.3.3 Cutting tool temperature

Cutting tool temperature is a factor that influences cutting tool life and the chip curl effect. It has been difficult to study due to lack of heat-sensitive equipment and computational complexity. In an early attempt, Wright et al. (1980) experimented with the cutting tool temperature distribution and compared that with theoretical results. Later, Sadik and Lindstrom (1993) analyzed the role of tool-chip contact length in the cutting process, especially the cutting forces, flank wear and tool temperature. Venkatesh et al. (1993) studied the chip surface characteristics and found that color can be used to identify the temperature of chip and strains. In these studies, there is still far from a clear understanding of the effect of temperature on the chip formation.

2.3.3.4 Chip formation with different material

Until present, the majority of chip formation research used medium carbon steel as the testing material, and tried to improve models to make results in agreement with testing on the medium carbon steel. However, with the extensive use of other metals in the industry, it has become urgent to study the behavior of metal cutting with materials other than steels.

Trigger and von Turkovich (1963) presented metal-cutting data for the high-speed machining of copper and aluminum. They found that cutting behavior is influenced by the purity of work material, its initial temperature and the tool-chip contact length. Mittal et al. (1980) modeled deformation of aluminum with high speed steel tools.

In aluminum alloy cutting with a flat rake face cutting tool, Strenkowski and Moon (1990) simulated orthogonal metal cutting with an Eulerian finite element model. The model can predict chip geometry and temperature distribution in the workpiece, chip, and tool without the need for empirical data. The tool-chip contact length can also be found, as can the characteristics of the flow field in the vicinity of the tool. Similarly, Ueda and Manabe (1992) used the Rigid-Plastic Finite Element Method (RPFEM) to simulate the chip formation mechanism of amorphous metals.

The study of chip formation makes it possible to understand the exact process that a chip is formed. The research work in this dissertation used previous research as a basis for building 3-D chip models for complex groove tools. The 3-D chip model can be used in the design process to predict possible chip forms for a complex groove insert design.

2.4 Chip breaking

Chip breaking is a relatively neglected subject within chip control. The chip breaking mechanism is not clear as yet. It may be a result of chip/workpiece surface contact and chip/tool face contact. Yet, some researchers have considered that chip vibration may contribute to the breaking. Others even considered chip weight as a factor of chip breaking.

Nakayama (1960) introduced the very first criterion of chip breaking. He asserted that a chip, which was born with a radius of R_0, would be broken up if the strain of its skin reaches the maximum elongation of the chip material. The condition will be

$$\varepsilon < \frac{t}{2}\left(\frac{1}{R_0} - \frac{1}{R_L}\right) \tag{2-16}$$

where ε is the strain at which the chip material is ruptured, t is the chip thickness, and R_L is the maximum radius of curvature when the point of chip reaches the bottom of the tool shank. Eq.2-16 applies to chip breaking in two dimensional curling and was later modified to Eq. 2-17.

$$\varepsilon < \alpha * t * (\frac{1}{R_0} - \frac{1}{R_L}) \tag{2-17}$$

Nakayama et al. (1981) studied a special means for breaking thin chips, using a cutting tool with curved rake face. This type of tool is especially important to produce thin chips in finish turning, face, and fine boring operations. They discussed the mechanism of chip breaking under curved rake face and suggested a deep groove design to break the thin chip.

Jawahir (1988) provided additional results from experimental work on chip breaking. In his study, all the chips were cut with restricted contact tool. He studied the effect of contact length on chip breaking results and suggested the factors that influence chip breaking. In a brief technical review, Stier (1990) suggested four ways to break the chip: using the chip breaker, applying tool oscillating movements, occasionally interrupting the feed to reduce the chip length and reversing the spindle turning direction to allow the chips to fall down unobstructed.

Fang and Jawahir (1991) and Fang et al. (1996) found that it is difficult to estimate the chip breakability of hundreds of different chip groove geometries. A cutting tool produces broken chips under specific cutting conditions on selected work material. When the conditions changes, the breakability changes. They introduced a fuzzy set-based knowledge-based system which quantified the chip breakability through a membership value u(x), ranging from 0 to 1. The database system stored fuzzy information about different cutting

tools chip breakers, different work materials and different tool geometries. These studies concluded that with fuzzy logic operation, the chip breakability of a new cutting tool can be calculated given the database.

Although these previous researchers have made important contributions, chip breaking is still a difficult but important area that requires extensive research and analysis. This dissertation will focus on using 3-D mathematical model to predict the chip breaking size. The model is derived as a result of theoretical study on chip kinematics and 3-D cutting tests.

2.5 Chip control method

Chip control has long been a subject of interest to machining operators. The goal of chip control is to get only desired chip forms and break them at certain length. This, in turn, will reduce chip volume, minimize production down time and save costs. In order to achieve this goal, chips are classified in different categories as acceptable and unacceptable chips. In the effort to predict chip breakability, some research has been carried out on classifying chips and on modeling the chip formation and chip breaking.

2.5.1 Chip classification

Not all chip forms are desired in a machining process. Some types of chip are easily entangled with workpieces and tools. It is necessary to identify and classify different chip forms into categories so as to avoid unwanted types.

Henriksen (1954) classified chips into six categories: straight chips, snarling chips, infinite helices, regular intermittent , full turn, and fragments and splinters. Only three of these categories (infinite helices, regular intermittent and full turn) are considered acceptable

in cutting practice. Nakamura and Wuebbling (1982) added the categories of short helix and compressed crescent to Henriksen's classification scheme.

A further study by Shin and Betts (1993) indicated that the chip up-curl radius also characterizes the possible type of chips and suggested the usability of a chip. A graph showing Shin and Betts' effective chip breaking range is shown in Fig. 2.7. The experimental results shown in Fig. 2.7 were obtained by cutting 4150 steel using speed of 2m/s with a depth of cut of 3.175 mm.

Nakayama and Arai (1992) used a general helix mathematical model to represent all the chip forms. They considered chips with and without side-curling. The resultant forms from their analysis are shown in Fig. 2.8.

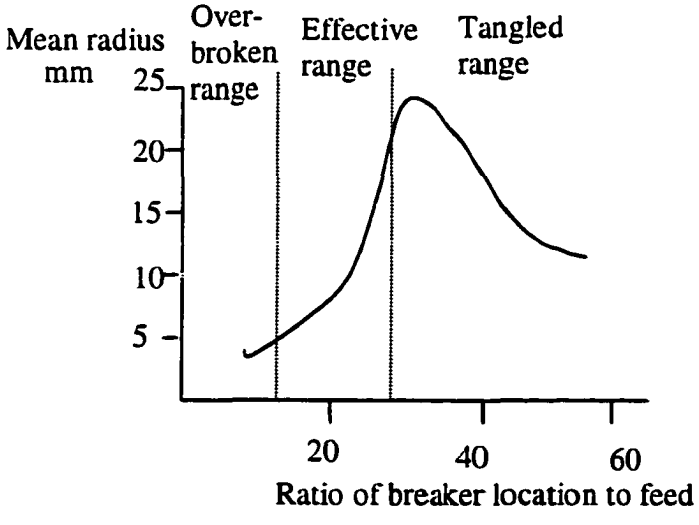

Fig. 2.7 Effective chip breaking range (Shin and Betts, 1993)

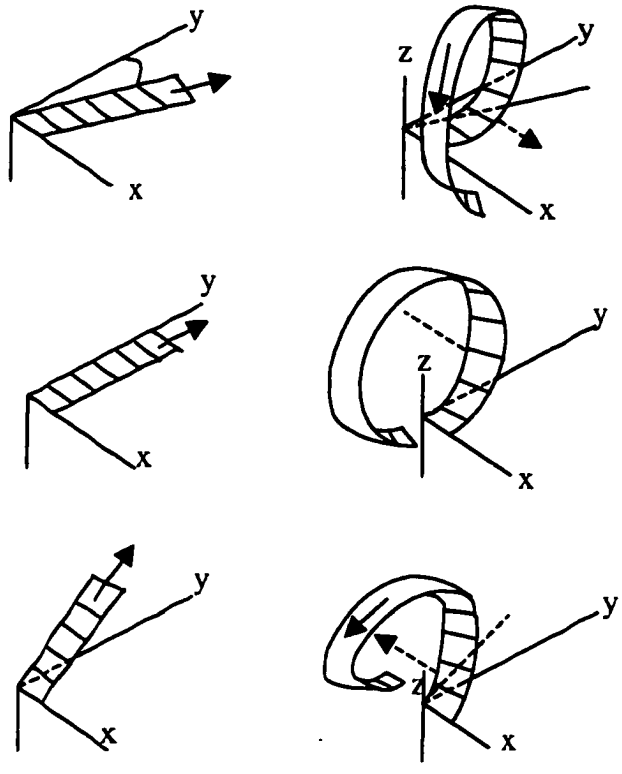

Fig. 2.8 General mathematical model of helix chips (Nakayama and Arai, 1992)

2.5.2 Chip modeling: 2-D cyclic chip

Cyclic chip is a special chip form generated in machining. Its geometry can be characterized in two dimensions. Yao et al. (1990) used an expert process planning system to simulate and animate chip flow and chip curl. Fang and Jawahir (1996) fully explained how a typical 2-D up-curl machining can generate a chip, as shown in Fig. 2.9

The chip model of Fang and Jawahir use spiral shape curve.

$$\rho = \rho_0 + K \cdot \omega \tag{2-18}$$

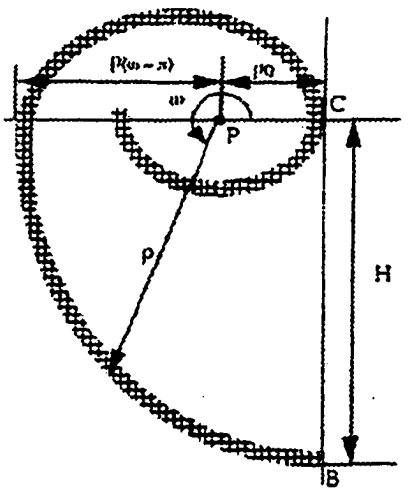

Fig. 2.9 Spiral shape chip model (Fang and Jawahir, 1996)

$$\rho = \sqrt{\rho_0^{\,2} + H^2} = \rho_0 + K \cdot (\frac{3}{2}\pi + \arctan\frac{\rho_0}{H}) \tag{2-19}$$

From this geometric model cyclic chip, the tool/chip contact length can be approximated from the following recursive equations.

$$\frac{h_{t+1}}{h_t} = \frac{(R_c)_{t+1}}{(R_c)_t} \tag{2-20}$$

$$R_c = \frac{1}{chip \quad curvature} = \frac{(\rho^2 + (\frac{d\rho}{d\omega})^2)^{3/2}}{\rho^2 + 2(\frac{d\rho}{d\omega})^2 - \rho(\frac{d^2\rho}{d^2\omega})^2} \tag{2-21}$$

The tool/chip contact length is needed for calculating the cutting forces and determining chip breaking. The animation of Fang and Jawahir's model is shown in Fig. 2.10. The animation gives the different stages of chip curling, which is in agreement with results from high speed filming. Thus, their model can be used in predicting cyclic chip geometry and breaking.

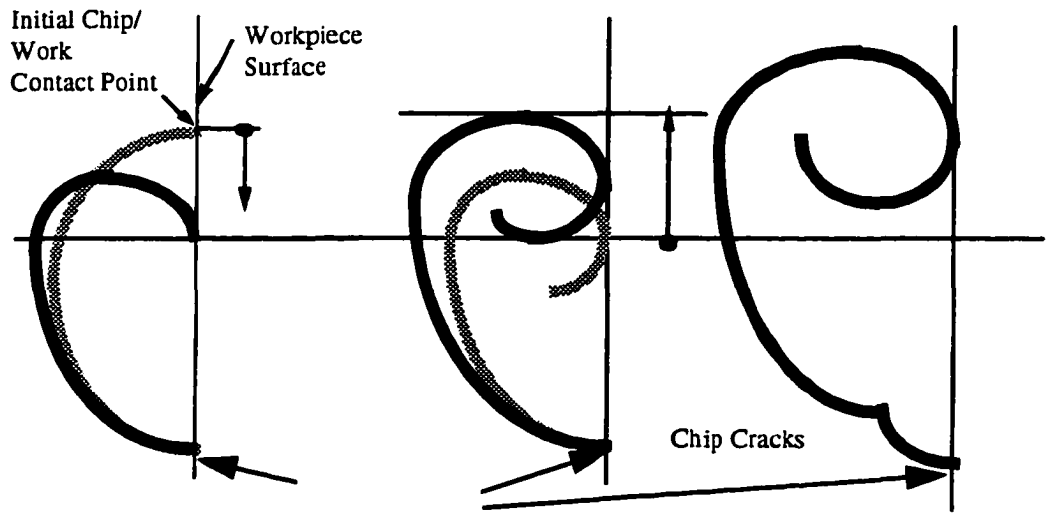

Fig. 2.10 2-D cyclic chip forming and breaking

2.5.3 Chip modeling: 3-D chip

3-D chip modeling is a challenging task. The analysis of chip forming and chip breaking in 3-D had just begun quite recently, and there is not much previous work available for reference. In 3-D chip modeling, one has to enhance models obtained in 2-D cutting conditions and make 3-D models compatible with all the conclusions drawn in 2-D analysis.

Fang et al. (1997a) presented computer model for 3-D chip animation in oblique cutting conditions. The model had successfully produced animated chips similar to all forms of actual cutting chips. In a further attempt, Fang et al (1997b and 1997c) analyzed the 3-D chip behavior and introduced a 3-D kinematic model of complex chip curling with chip breaker. This model not only considered the side-curling and up-curling effects, but also introduced twisting as one of the curling effects in chip formation. The 3-D curling models are shown in Fig. 2.11. The 3-D chip model considers a cutting chip that has 3-axis angular velocities, given by equations as follows:

$$\omega_z = \frac{-\partial V}{\partial(x\cos\eta)} = \frac{V_0 - V_0\cos(\eta_0' - \eta_0)}{B\cos\eta_0} \tag{2-23}$$

$$\omega_x = \frac{-\partial(V\cos\eta)}{\partial z} = \frac{(V_0 - V_0'')\cos\eta_0}{t_0} \tag{2-25}$$

$$\omega_y = \frac{\nabla\varphi V_0 \cos\eta_0}{W} \tag{2-26}$$

The resultant angular velocity is calculated as follows:

$$\omega = \sqrt{\omega_x^2 + \omega_y^2 + \omega_z^2}$$

$$= V_0\cos\eta_0\sqrt{(\frac{1}{\rho_{x0}})^2 + (\frac{\nabla\varphi}{W})^2 + (\frac{1}{\rho_{z0}\cos\eta_0})^2} \tag{2-27}$$

Using Fig. 2.12 to analyze the velocities, a kinematic model of complex chip may be derived.

$$\cos\beta_0 = \sqrt{1 - (\sin\eta_0\frac{\omega_x}{\sqrt{\omega_x^2+\omega_y^2}}\frac{\sqrt{\omega_x^2+\omega_y^2}}{\sqrt{\omega_x^2+\omega_y^2+\omega_z^2}} + \cos\eta_0\frac{\omega_y}{\sqrt{\omega_x^2+\omega_y^2}}\frac{\sqrt{\omega_x^2+\omega_y^2}}{\sqrt{\omega_x^2+\omega_y^2+\omega_z^2}})^2}$$

$$= \sqrt{\frac{(\omega_x\cos\eta_0 - \omega_y\sin\eta_0)^2 + \omega_z^2}{\omega_x^2+\omega_y^2+\omega_z^2}} \tag{2-28}$$

Eq.2-28 gives the helical angle of a curling chip, and Eq.2-29 defines the radius of helical chip. Eq. 2-30 is the helical chip pitch.

$$\rho_0 = \frac{V_0\cos\beta_0}{\omega} = V_0\frac{\sqrt{(\omega_x\cos\eta_0 - \omega_y\sin\eta_0)^2 + \omega_z^2}}{\omega_x^2+\omega_y^2+\omega_z^2} \tag{2-29}$$

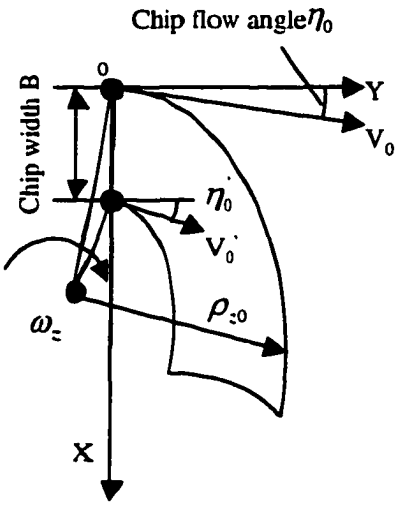

(a) Side-curling effect

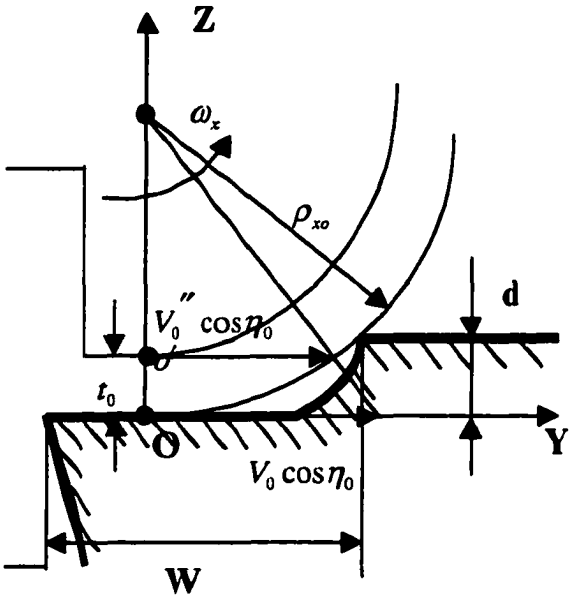

(b) Up-curling effect

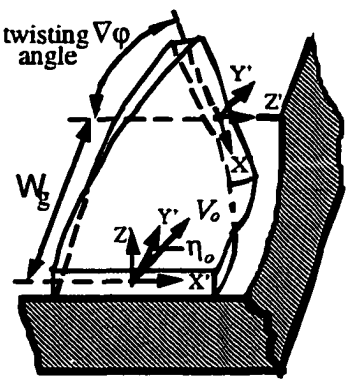

(c) Twisting effect

Fig. 2.11 3-D models of chip curling effects

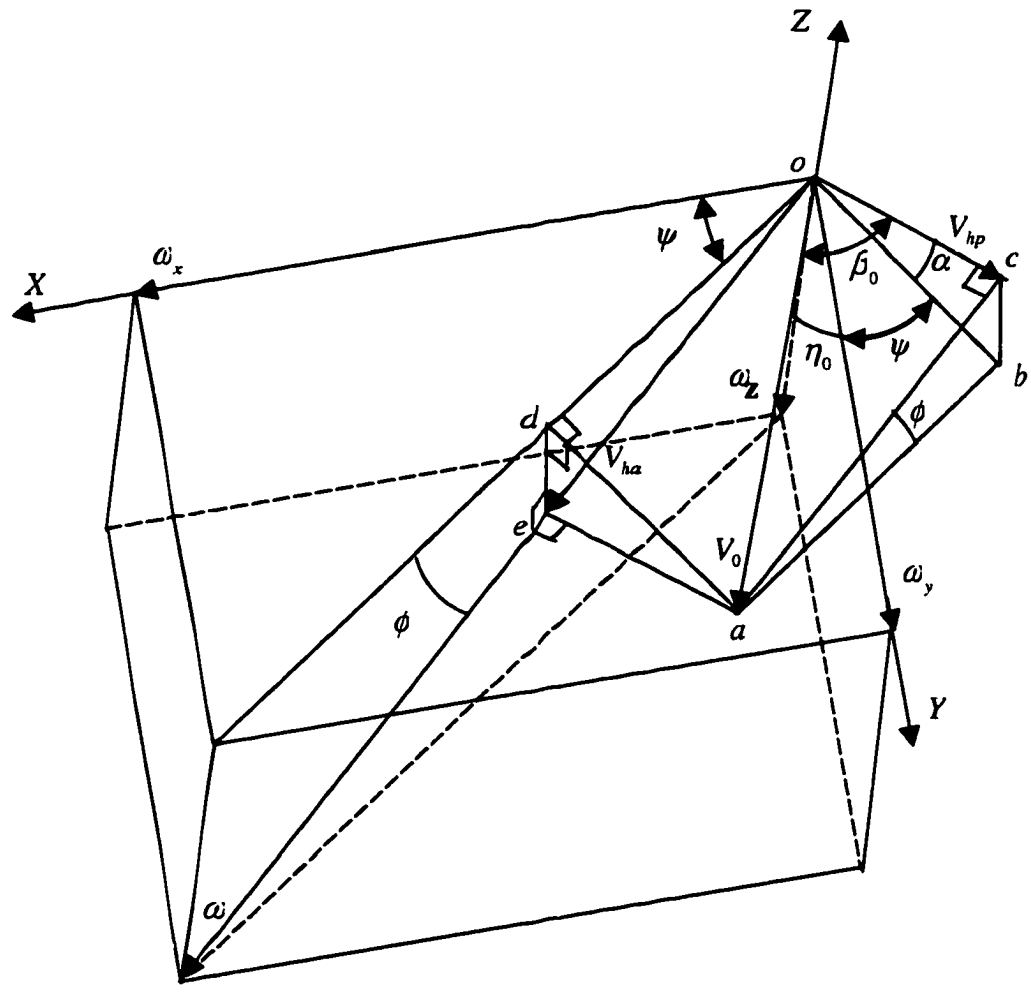

Fig. 2.12 Chip velocity analysis (Fang et al., 1997)

$$h = 2\pi V_0 \frac{(\omega_x \sin\eta_0 + \omega_y \cos\eta_0)}{\omega_x^2 + \omega_y^2 + \omega_z^2} \tag{2-30}$$

Further analysis of this model by Fang et al. demonstrated that it was in agreement with existing facts about chip geometry. The significance of the 3-D kinematic model is that it could be used to predict the 3-D chip curling effect and could also be used with simulation and analysis programs. The limitation of this model is that the chip breaker is an obstruction type and most commercial inserts are groove types. Also, in a cutting process, the angular

velocities are subjected to the cutting conditions. The chip formation modeling still requires a mechanism to model the relationship between cutting conditions and angular velocities.

2.5.4 Chip control

Chip control has long been a major concern in turning operations, and technologies to deal with it have been varied. Creative turning-insert geometry design, with lots of bumps and grooves, is one of the most popular approaches. Zhang (1980) summarized the important factors affecting chip curl and breaking: the thickness of the chip, the radius of curvature of the chip and the mechanical properties of the chip material removed from the workpiece. He suggested a groove type chip-breaker design based on the mechanics model.

As manufacturers and machining operators began to realize the significance of the groove in the insert, it became known that the existence of a groove eliminates the need for a separate and additional part for chip breaker. Besides, the groove serves to provide chip control over a wider range of feeds and depths. A novice design from Kennametal (Feinberg, 1975) introduced the idea of land type (no-groove) insert that may reduce the cutting force and lead to better chip performance. Katbi (1990) from GTE Valenite summarized chip control factors and presented the relationship between selecting chip groove design and chip control. Kluft et al (1979), Jawahir (1988) and later Jawahir and van Luttervelt (1993) reviewed chip control research and suggest potential future research directions. Using a totally different approach, Zdeblich and Mason (1992) proposed a unique chip breaking method, using high-pressure coolant flow to break cutting chip.

All these different methods serve a common goal of chip control, which is still to effectively break chip into desired form.

This dissertation will extend previous study on 3-D chip formation model on complex groove tools. A mathematical model from cutting tests will serve as the basis for chip control performance prediction. The chip control prediction can lead to a jump in the design of complex 3-D cutting tool inserts.

CHAPTER 3 CHIP MODELS FOR COMPLEX GROOVE

From the literature review of Chapter 2, it is clear that current studies do not have a complete picture of chip control information for complex tool insert designs. This chapter attempts to identify the nature of this gap, and then to propose a new kinematic model for complex groove tools, and to subsequently derive a key simulation model from cutting experiments.

3.1 Current gap in chip simulation model for complex groove tools

As seen in Chapter 1, current tool insert designs make use of complex 3-D geometric shapes. These advanced designs typically have dips (known as grooves) and tiny extrusions (known as lumps). These geometrical entities are designed specifically for chip control purposes. Current practice attempts to design tool chip breaker geometry through trials and errors. The only way to test the effectiveness of the insert is to go through lengthy tests. It is very difficult to achieve optimal design effects in this manner.

The type of cutting tool insert that is the focus of this dissertation is one with complex groove shapes. A typical groove section is shown in Fig. 3.1. It consists of a rake face that is usually shorter than the natural length of chip tool contact. Next to the restricted contact area, there is a groove curve in the cross-section. The groove curve shape may vary depending on the position of the cross-section along the cutting edge. The earliest groove curve was a circular shape. When the tool design improved since the 1950s, the selection of groove curve became rather random because there were no criteria upon which to base the design.

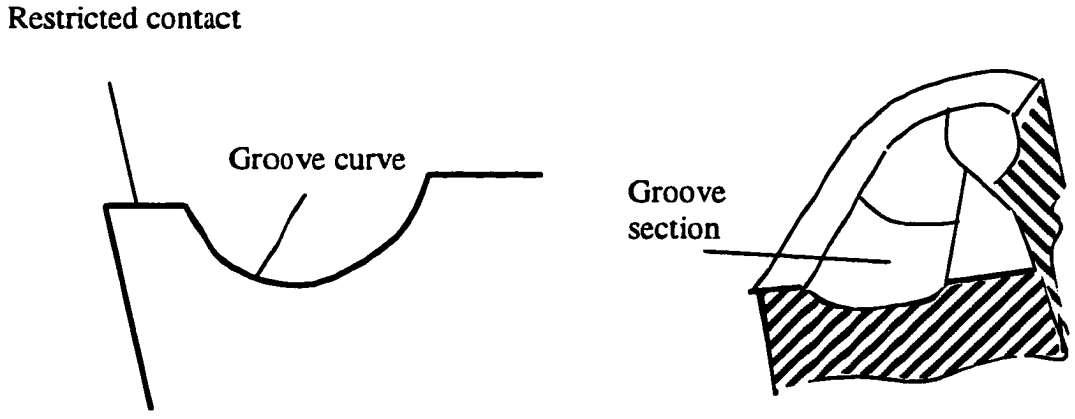

Fig. 3.1 Groove type tool insert cross-section

As discussed in chapter 2, the cutting chip enters a groove at an angle of η_b. This is the chip streaming effect. Two questions then arise:

A. How will the cutting chip behave after it enters into the cross-section?

B. What is the effect of the groove curve shape on the chip forms?

Nakayama and Arai (1992) used a general helix mathematical model to represent all the chip forms. They considered chips with and without side-curling. This mathematical model was further studied by Fang et al. (1997a), who enabled the computer animation of oblique cutting chips. The animation results revealed that all chip forms generated from a practical cutting environment can be reproduced by the mathematical model. If all the parameters required by the mathematical model can be obtained accurately, then the shape of the cutting chip can be predicted. These parameters are the side-curl radius, up-curl radius, chip tilting angle and the pitch.

The accuracy of parameters for the mathematical model then becomes a key concern. The animation model developed by Fang et al. used several equations developed by previous

researches. Some of the equations were not devised for the use of complex groove tools, and hence may require further study. One obvious example is the up-curl radius calculation used in the animation model. It used Nakamura and Wuebbling's (1982) estimation (shown in Eq. 2-16), which assumes that the chip would follow the exact shape of the groove. The same assumption existed for Henriksen's (1954) model. Henriksen indicated that the up-curl radius is proportional to the feed rate, though not linearly (1954). This nonlinear relationship is can be shown in Fig. 3.2. Other researchers indicated that the radius is also related to the depth of cut.

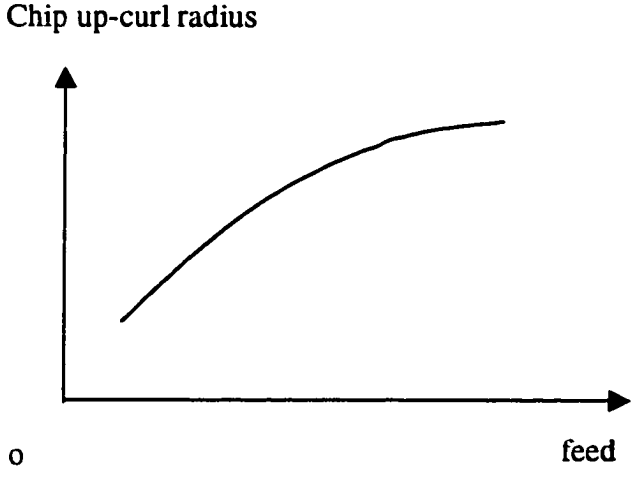

Fig. 3.2 Relationship between feed rate and up-curl radius

It is clear that there is some sort of relationship between cutting conditions and chip parameters. But the cause and nature of such relationship is not known. Therefore, in addition to the problems presented by chip behavior and groove curve shape, there is still a third question that need to be addressed to fill the gap:

C. How do cutting conditions affect chip model parameters?

All of the questions discussed above relate to the modeling of chip parameters, which is known to be a difficult task, especially when complex groove geometry is considered as well. However, if the gap relating to the effects of cutting conditions on chip model parameters can be filled completely or tentatively, as this dissertation attempts to do, the answers can lead to greater improvement in tool design strategy.

3.2 New kinematic model for groove tools

According to the characteristics of a 3-D metal cutting model with a complex groove chip breaker, the chip undergoes deformation in three dimensions: longitudinal bending, transversal bending, and torsional deformations. As shown in Fig. 3.3, These spatial forces result in the side-curling, up-curling and twisting motions in the chip "growing."

Fang et al. (1997a) demonstrated that the combination of these three motions can form any 3-D chips. In a further analysis, Fang et al. (1997b) worked on a kinematics model of a typical obstruction type chip-breaker. Although this analysis showed the influence of 3-D deformations forces on the final chip shape, it study cannot be used directly in the complex groove geometry shown in Fig. 3.1. The streaming effect has to be considered in a complex groove insert. Therefore, the next section describes the derivation of a new kinematic model that takes into account this streaming effect.

3.2.1 A kinematic model considering complex groove geometry

A kinematic model is very important to understand the chip behavior. The next subsections will present a new kinematic model for complex groove geometry.

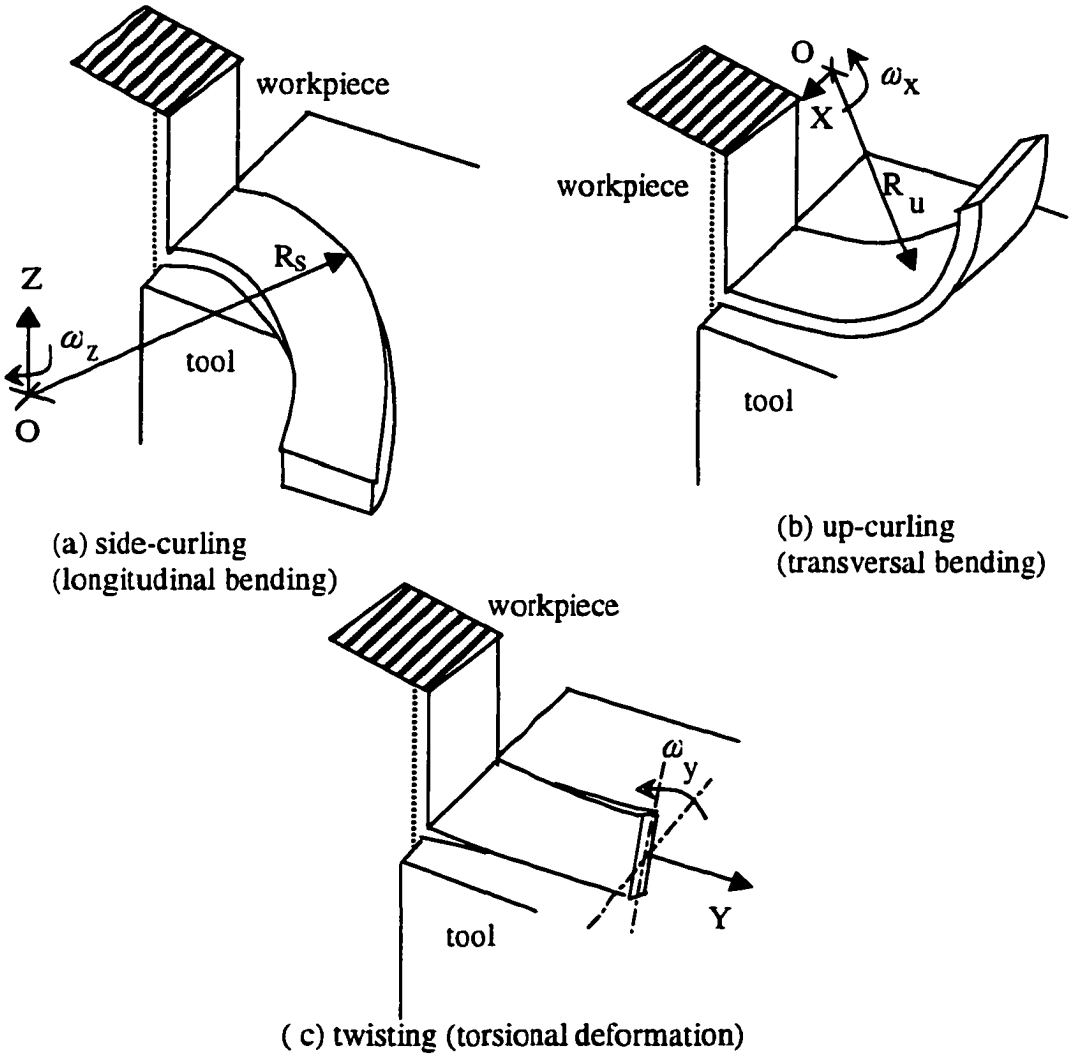

Fig. 3.3 3-D chip deformations

3.2.1.1 The chip motion and angular velocities of the helical chip

According to the 3-D chip deformation model, there are three orthogonal angular movements. The definition of these angular velocities is based on three orthogonal axes. Here, the X axis is defined by the tool-workpiece contact line or the cutting edge. The Y axis is the rake face of the tool. The X-Y plane forms the rake face. The Z-axis is perpendicular to

the rake face and the three axes form a right-hand coordinate system. The origin of the coordinate system is set at the middle point of the chip at the cutting edge.

The chip motion involves three angular velocities: ω_x, ω_y and ω_z. The initial chip speed at the edge of chip groove is V_0. The chip side-flow angle is η_s. Due to the restricted contact length, the chip flow at the groove edge has a streaming angle η_b. ω_x, ω_y and ω_z determine the chip movement characteristics in space. These angular velocities can be obtained by separating the side-curling, up-curling, and twisting effects from each other.

As shown in Fig. 3.4, the side-curling effects can be illustrated by removing up-curling and twisting effects. The angular velocity ω_z is defined as shown in Eq. 3-1:

$$\omega_z = \frac{V_0 \cos\eta_b}{\rho_{z0}} \tag{3-1}$$

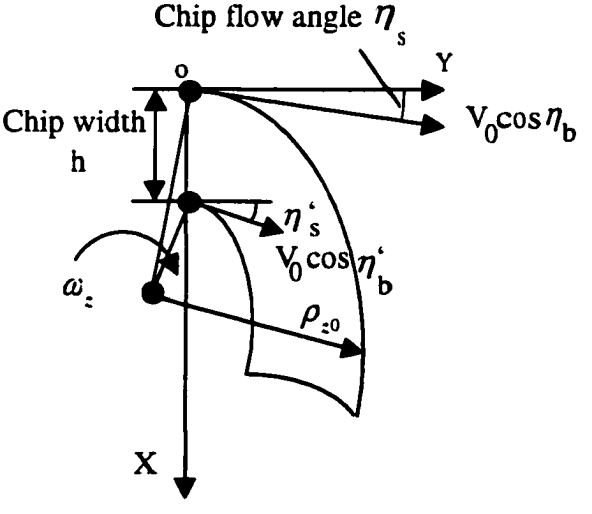

Fig. 3.4 Chip side-curling effect

where ρ_{z0} is the chip side-curling radius at the edge of groove and η_b is the streaming angle. This angular velocity can also be given in the form of angular velocity gradient (Eq. 3-2):

$$\omega_z = \frac{-\partial v}{\partial(x\cos\eta_s)} = \frac{V_0\cos\eta_b - V_0'\cos(\eta_s' - \eta_s)\cos\eta_b}{h * \cos\eta_s} \tag{3-2}$$

where h is the chip width, V_0' is the velocity at the edge of chip and η_s is the chip side-curling angle.

Similarly, by considering the chip up-curling effect alone, the up-curling radius can be analyzed as shown in Fig. 3.5. The radius is given by Eq. 3-3.

$$\omega_x = \frac{V_0\cos\eta_s}{\rho_{x_0}} \tag{3-3}$$

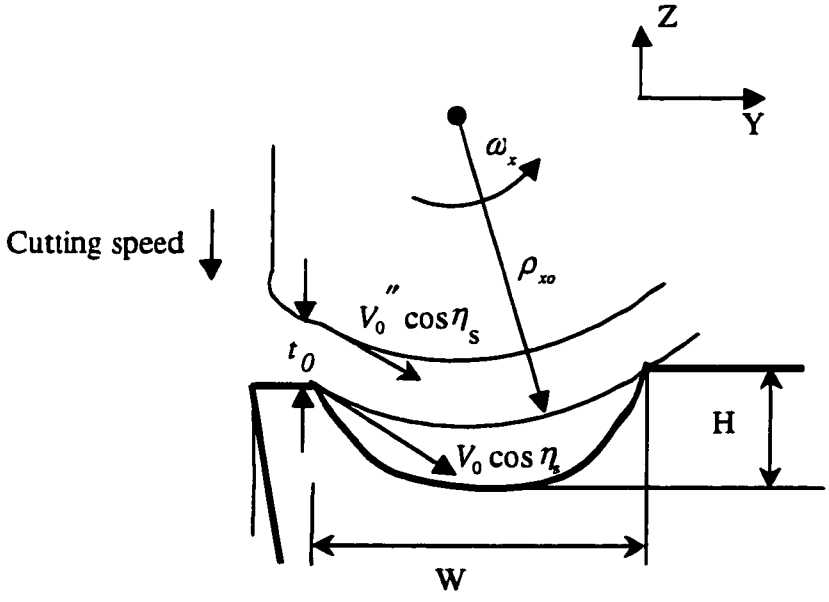

Fig. 3.5 Up-curl effect at the tool groove section

where ρ_{x0} is the radius of up-curling radius at the groove edge . The radius can also be given in the term of velocity gradient (Eq. 3-4):

$$\omega_x = \frac{-\partial(v\cos\eta_s)}{\partial z} = \frac{(V_0 - V_0^n)\cos\eta_s}{t_0} \tag{3-4}$$

where t_0 is the chip thickness at the groove edge.

The twisting effect, shown in Fig. 3.6, was recognized by Fang et al (1997b). The angular velocity ω_y can be obtained by dividing angle change with time (Eq. 3-5):

$$\omega_y = \frac{\phi V_0 \cos\eta_s \cos\eta_b}{W} \tag{3-5}$$

where ϕ is the chip twisting angle after traveling across the groove section, and W is the groove section width.

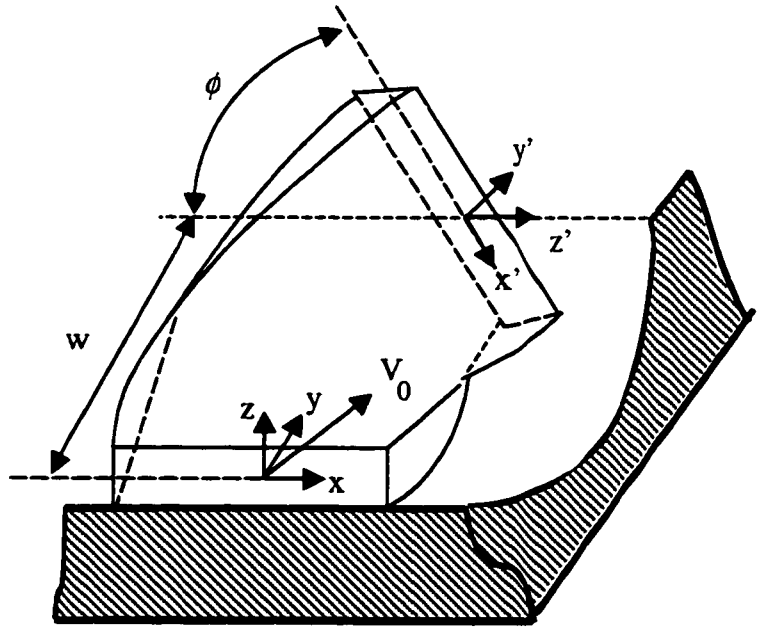

Fig. 3.6 Effect of chip twisting across a groove section

With the above three angular velocities about the three orthogonal axes, the resultant angular velocity is given in Eq. 3-6 by combining Eq. 3-1, 3-3, 3-5.

$$\omega = \sqrt{\omega_x^2 + \omega_y^2 + \omega_z^2} \tag{3-6}$$

3.2.1.2 Derivation of the kinematic analytic model

An analysis of the velocity-angular velocity relationships is shown in Fig. 3-7. The velocity V_0 can be decomposed into two perpendicular velocities, V_a and V_p, where V_a is along the resultant angular velocity ω and V_p is perpendicular to ω. The angle between V_0 and ω is α. As Eq. 3.7 and Eq. 3.8 show, it is easy to calculate the two velocities, V_a and V_p.

$$V_a = V_0 \cos\alpha \tag{3-7}$$

$$V_p = V_0 \sin\alpha \tag{3-8}$$

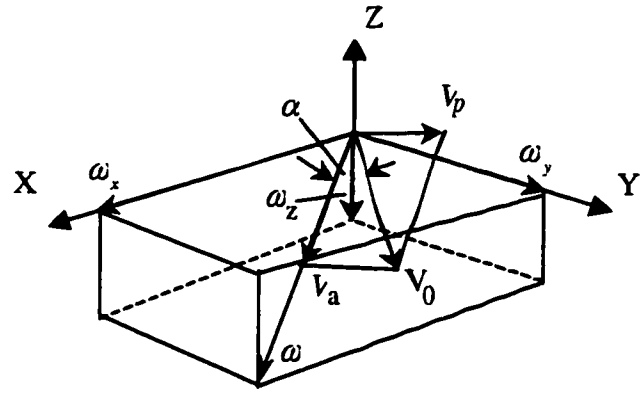

Fig. 3.7 Velocity analysis of the helical chip

To further derive the analytical model, V_0 is extended to point A as shown in Fig. 3.8. The angle of BOC is the chip streaming angle, η_b. The angle of COD is the chip side-flow angle, η_s. The angle AOE is α.

From Fig. 3.8, it is known that AD is perpendicular to OD, resulting in the relationship:

$$OA^2 = OD^2 + AD^2$$

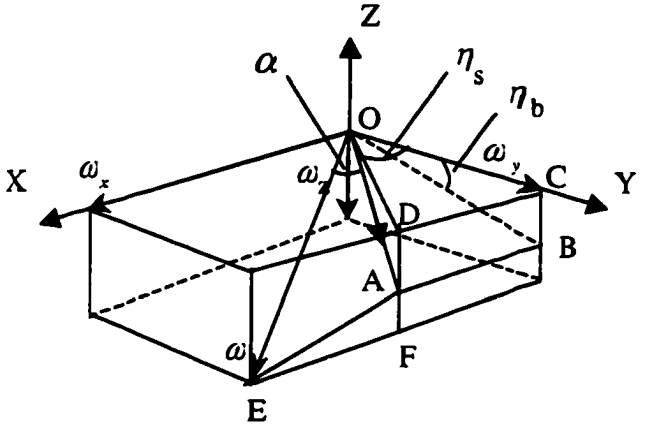

Fig. 3.8 Geometrical analysis of velocity

The geometrical analysis also indicates the following,

$$OD = \frac{\omega_y}{\cos\eta_s} \quad \text{and} \quad AD = BC = \omega_y \tan\eta_b$$

Thus OA can be obtained as shown in Eq. 3-9:

$$OA^2 = \omega_y^2 \left(\frac{1}{\cos^2\eta_s} + \tan^2\eta_b\right) = \omega_y^2 (1 + \tan^2\eta_s + \tan^2\eta_b) \tag{3-9}$$

Also, in the triangle of EAF, AF is perpendicular to EF:

$$EA^2 = EF^2 + AF^2$$

where EF and AF can also be obtained from the following geometrical analysis.

$$EF = \omega_x - \omega_y \tan\eta_s$$

$$AF = \omega_z - \omega_y \tan\eta_b$$

Then, EA is also determined as shown in Eq. 3-10:

$$EA^2 = (\omega_x - \omega_y \tan\eta_s)^2 + (\omega_z - \omega_y \tan\eta_b)^2 \tag{3-10}$$

Thus the angle of AOE or α can be calculated by Eq. 3-11.

$$\cos\alpha = \frac{OE^2 + OA^2 - EA^2}{2 * OE * OA} \tag{3-11}$$

By substituting Eq. 3-9 and Eq.3-10 into Eq.3-11, and letting OE equals ω, α is derived as shown in Eq. 3-12, and Eq. 3-13:

$$\cos\alpha = \frac{\omega^2 + \omega_y^2(1+\tan^2\eta_s+\tan^2\eta_b) - (\omega_x - \omega_y\tan\eta_s)^2 + (\omega_z - \omega_y\tan\eta_b)^2}{2*\omega*\sqrt{\omega_y^2(1+\tan^2\eta_s+\tan^2\eta_b)}}$$

$$= \frac{\omega^2 + \omega_y^2(1+\tan^2\eta_s+\tan^2\eta_b) - (\omega_x - \omega_y\tan\eta_s)^2 + (\omega_z - \omega_y\tan\eta_b)^2}{2*\omega*\sqrt{\omega_y^2(1+\tan^2\eta_s+\tan^2\eta_b)}}$$

$$= \frac{\omega_y + \omega_x\tan\eta_s + \omega_z\tan\eta_b}{\omega\sqrt{(1+\tan^2\eta_s+\tan^2\eta_b)}} \tag{3-12}$$

$$\sin\alpha = \sqrt{1-\cos^2\alpha}$$

$$= \sqrt{1-\left(\frac{\omega_y + \omega_x\tan\eta_s + \omega_z\tan\eta_b}{\omega\sqrt{(1+\tan^2\eta_s+\tan^2\eta_b)}}\right)^2}$$

$$= \sqrt{\frac{\omega^2(1+\tan^2\eta_s+\tan^2\eta_b) - (\omega_y + \omega_x\tan\eta_s + \omega_z\tan\eta_b)^2}{\omega^2(1+\tan^2\eta_s+\tan^2\eta_b)}}$$

$$= \sqrt{\frac{(\omega_x^2+\omega_y^2+\omega_z^2)(1+\tan^2\eta_s+\tan^2\eta_b)-(\omega_y+\omega_x\tan\eta_s+\omega_z\tan\eta_b)^2}{\omega^2(1+\tan^2\eta_s+\tan^2\eta_b)}}$$

$$= \frac{\sqrt{(\omega_x-\omega_y\tan\eta_s)^2+(\omega_z-\omega_y\tan\eta_b)^2+(\omega_z\tan\eta_s-\omega_x\tan\eta_b)^2}}{\omega\sqrt{1+\tan^2\eta_s+\tan^2\eta_b}} \qquad (3\text{-}13)$$

The helical chip radius ρ_0 then can be calculated as shown in Eq. 3-14:

$$\rho_0 = \frac{V_0\sin\alpha}{\omega}$$

$$= \frac{V_0\sqrt{(\omega_x-\omega_y\tan\eta_s)^2+(\omega_z-\omega_y\tan\eta_b)^2+(\omega_z\tan\eta_s-\omega_x\tan\eta_b)^2}}{\omega^2\sqrt{1+\tan^2\eta_s+\tan^2\eta_b}} \qquad (3\text{-}14)$$

The helical chip pitch, p, is also available (Eq. 3-15):

$$p = 2\pi\rho_0 c\tan\alpha$$

$$= 2\pi\frac{V_0\sin\alpha}{\omega}\frac{\cos\alpha}{\sin\alpha}$$

$$= 2\pi\frac{\omega_y+\omega_x\tan\eta_s+\omega_z\tan\eta_b}{\omega^2\sqrt{(1+\tan^2\eta_s+\tan^2\eta_b)}}V_0 \qquad (3\text{-}15)$$

3.2.2 Analysis of the kinematic model

The equations derived in section 3.2.1.2 provide internal relationship between the chip angular velocities and the chip shape. Eq. 3-12, 3-13, 3-14 and 3-15 use ω_x, ω_y, ω_z, η_s, η_b and V_0 to represent chip radius and pitch. From the equations in the section 3.2.1.1 (Eq. 3-1, 3-2, 3-3, 3-4, 3-5 and 3-6), all three angular velocities can be calculated in the form of V_0. In other words, chip shape can be determined by V_0, η_s, η_b and some other parameters. Except for the twisting angle ϕ, these parameters have been studied in various different approaches.

Since all the parameters are related to or result directly from the cutting conditions, the chip shape can be modeled from the cutting conditions and from the tool geometry.

3.2.2.1 Model assumptions

The above model was developed under some predefined assumptions, which must be fully presented in order to understand the model's use and its limitation: twisting angular velocity approximation, groove shape, material uniform and temperature distribution.

Twisting angular velocity approximation. Eq. 3-5 is derived from the basic definition of angular velocity, the angle ϕ traveled with a period of time T, as shown in Eq. 3-16:

$$\omega_y = \phi / T \tag{3-16}$$

where T is the time to travel across the groove section. T is obtained from the assumption that the chip travels at a constant speed of $V_0 \cos\eta_b \cos\eta_s$ horizontally. However, this speed is only correct at the start edge of the groove section. Due to side-curling and up-curling, the horizontal speed changes from time to time. The trajectory of the chip is in fact an eclipse. To avoid over-complicated calculations, the initial horizontal speed of $V_0 \cos\eta_b \cos\eta_s$ was used in Eq. 3-5. This assumption is a good approximation when both the up-curling radius and side-curling radius are considerably larger than the groove width W. In a practical use, this would mean that ,

$$R_u = \rho_{x0} > 5*W \qquad \text{and} \qquad R_s = \rho_{z0} > 5*W$$

Groove shape. Practically,the variation of a groove shape along the cutting edge and the cross-section of the groove are also complex. A typical example is the backwall height. In the model in Fig. 3.5, the backwall is at the same height as the rake face. In fact, there are

designs with lowered backwall and raised backwall. The model above did not consider these factors to simplify model deduction. The influence of these groove shapes is discussed in section 3.2.2.2.

Material uniform and temperature distribution. In the whole modeling process, the material is considered to have uniform properties and the influence of temperature distribution along the chip length is negligible. The chip itself is taken as an elastically bent body.

3.2.2.2 Complex groove shape factors

The groove section used in the initial kinematic model falls short of the complexity of current tool groove designs. To actually use the model in complex groove design, it must be revised to consider all the possibilities of the groove section: backwall height, complex groove cross-section contour, and varied groove cross-section along cutting edge.

Backwall height. As shown in Fig. 3.9, there are three basic groove sections, each with a different backwall height. The actual width that a chip travels in a groove section is W' instead of W. To account for the complex groove shape factors, W' (calculated as shown in Eq. 3-17) must be substituted for W in the equations of the kinematic model.

$$W' = \sqrt{W^2 + d^2} \tag{3-17}$$

Complex groove cross-section contour. The kinematic model does not use any variable that signals the effect of the groove cross-section contour. The shape of the cross-section actually plays an important role in forming the shape of the chip.

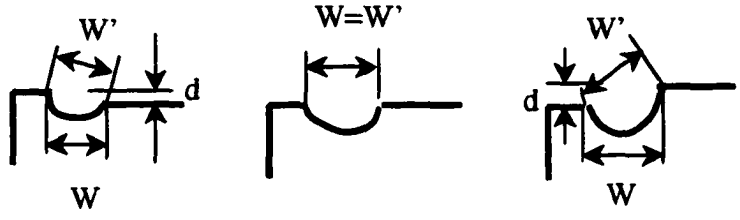

Reduced backwall Typical groove Raised backwall

Fig. 3.9 Consideration of different backwall height

This cross-section is not present in the kinematic model because an assumption is made that the chip will always be formed between the groove edges, and there is no other contact between the chip and the groove section. However, this assumption does not hold for the complex chip groove, because the contact point often shifts. This shifting is shown in Fig. 3.10. The reason for the shift is the change of the chip streaming angle and chip speed V_o.

The solution to this problem of complex groove contour is not to assume that the length that a chip has traveled is a constant (W). Rather, W is a function of the streaming angle and the groove shape.

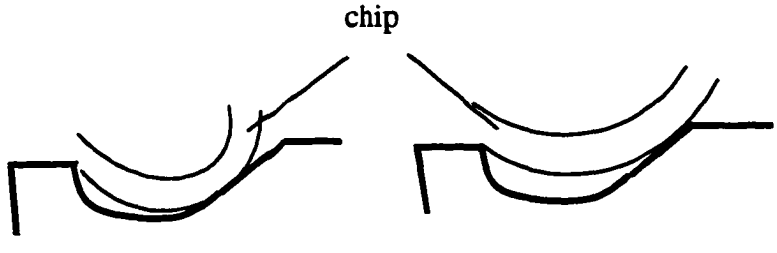

Fig. 3.10 Complex groove cross-section's influence on chip shape

Varied groove cross-section along cutting edge. Another feature of a complex tool design is varied groove cross-section as shown in Fig. 3.11. Since the kinematic model is based on calculations at the middle point of the chip width, the groove width variation would not show any impact in the model. To take its influence into account, one has to understand which variable the groove width variation affects.

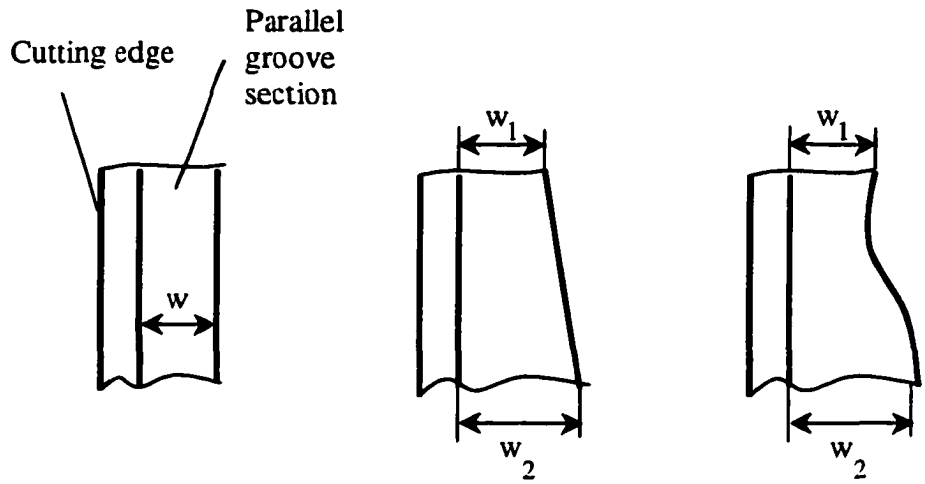

Fig. 3.11 Complex groove section: grooves with varied width

Fig. 3.6 shows that the chip has twisted at an angle of ϕ at the ending edge of the groove. In fact, the width variation would create extra forces on the chip and enforce the chip twisting effect. As shown in Eq.3-5, the angular velocity ω_y increases in proportion to the increase of ϕ. According to Eq. 3-14, the chip radius ρ_o will decrease if the angular velocity ω_y increases.

A coefficient can be added into Eq. 3-5 to represent the influence of the width variation factor. Then Eq. 3-5 becomes Eq. 3-18:

$$\omega_y = \frac{\lambda \phi V_0 \cos\eta_s \cos\eta_b}{W} \tag{3-18}$$

where λ is the coefficient for width variation. For a parallel groove, this coefficient is 1.

3.3 Mathematical modeling of the cutting tests

The theoretical analysis of 3-D chip kinematics help to cast light on better chip control for complex tool design. Combined with other analysis on chip velocities and angles, this knowledge will enable the tool designer to get a more complete view of chip control performance before a tool insert is even manufactured.

Currently, there are two variables whose theoretical predictions are still not satisfactorily in compliance with experimental results. These variables are the chip streaming angle and chip velocity. The kinematic model would require these variables as a starting point for theoretical 3-D chip behavior prediction. Nevertheless, the information obtained from the analysis has led to a better understanding of 3-D chip formation and the chip breaking mechanism.

For this dissertation, experimental cutting tests were carried out to observe and verify 3-D chip formation. The experimental results were used in comparison with the information derived in section 3.2. To facilitate the current need for predicting chip forms and chip breaking, models were constructed in accord with theoretical knowledge. These experiments lead to a proposed semi-empirical model for complex groove tools.

3.3.1 Hypothesis from current 2-D and 3-D cutting knowledge

As one can see, the 3-D chip formation model is much more complicated than the 2-D process. There are many jumps in knowledge from 2-D chip formation to 3-D chip formation. Even so, many assumptions in the 3-D process are based on 2-D experience. Therefore, it is necessary to test these assumptions. Prior to the 3-D kinematic analysis, all cutting experiments were carried out to verify 2-D chip formation and chip breaking theories. There were no tests designed for 3-D cutting practice, although some tests used 3-D complex cutting tool inserts.

These hypotheses given below come from either 2-D chip formation knowledge or from 3-D analysis. These hypotheses will be examined in section 3.3.2.

Hypothesis 1: Feed rate positively contributes to the chip radius.

This hypothesis can date to the experimental results from Henriksen in 1954. A rather contradictory conclusion was that the radius is expected to be in reverse proportion to the chip thickness and that the chip thickness is proportional to the feed rate (Trim and Boothroyd, 1968). 3-D analysis shows that the contribution of feed rate comes from its influence on the chip curl angles.

Hypothesis 2: The depth of cut is not a factor of the chip radius.

In most orthogonal analysis, chip width is assumed be the same as the depth of cut. The focus of studies was rather on the chip thickness and its influence on chip formation. This notion does not exist in the 3-D analysis of complex groove geometry. Chip radius is related to all cutting conditions and the tool geometry. But the exact relationship between the depth of cut and the radius is not clear, since it does not appear directly in the Eq. 3-14.

There are clearly more questions that need to be examined. The above are just two examples of what can be learned in the cutting experiments.

3.3.2 Cutting experiments

In order to study the chip formation and breaking characteristic of complex 3-D tool inserts, different combinations of cutting condition were used to verify each factor's contribution. In addition, eight types of inserts were used for mathematical modeling of 3-D chip formation. These different types of inserts, listed in Table 3.1, were selected based on their different configuration in groove cross-section shape, groove width and restricted contact length. The machine used in the cutting tests is a HITACHI SEIKI HITEC-TURN20SII CNC lathe, as shown in Fig. 3.12.

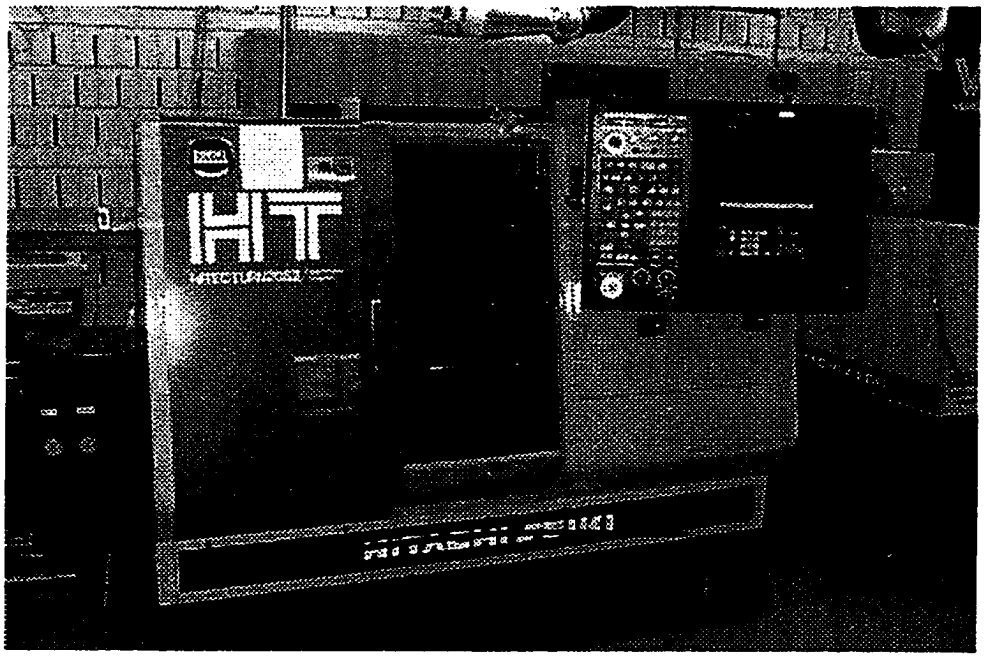

Fig. 3.12 CNC lathe used in the cutting experiments

Table 3.1 Inserts used in the cutting experiments

No.	Insert Photo	Insert Type	No.	Insert Photo	Insert Type
1	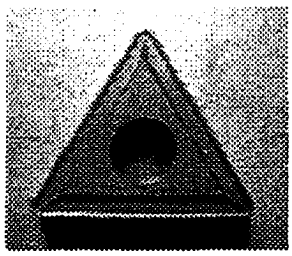	TNMG 322 56	5	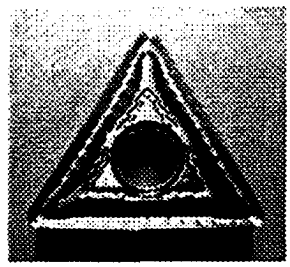	TNMG 332 NG
2	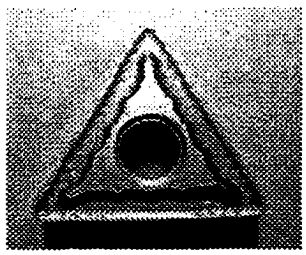	TNMG 332 M5	6	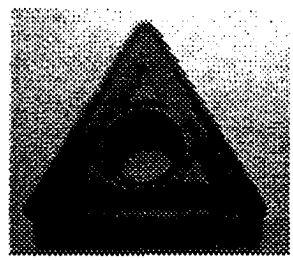	TNMG 322
3	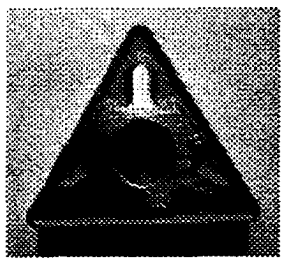	TNMG 332 MF3	7	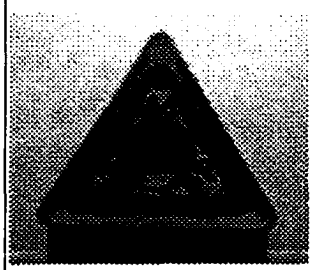	TNMG 332 PP
4	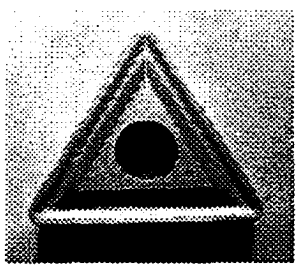	TNMG 332 MR5	8	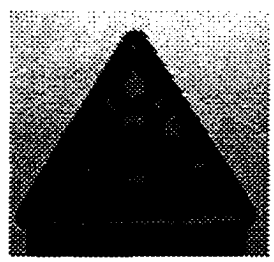	TNMG 332 FF

The work material was medium carbon steel, 1045 steel (with 0.45% C). The experiments used two cutting speeds: 50 m/min and 100 m/min. Five feed rates were used: 0.1 mm/rev, 0.2 mm/rev, 0.4 mm/rev, 0.6 mm/rev, and 0.8 mm/rev. The 0.8 mm/rev choice was used only when the machine could withstand the working load, especially when the depth of cut was also high. The depth of cut also varied from 0.5 mm to 4 mm. Metal chips from the cutting tests were filtered at a screening placed under the workpiece. These chips' dimensions were then measured and used for 3-D chip analysis.

3.3.3 Cutting experimental results

These experiments, designed specially for complex 3-D inserts, provide a good opportunity to examine the hypotheses proposed in section 3.3.1. The results of these experiments will not only help us increase understanding of 3-D chip behavior, but might also lead to the successful construction of a chip prediction model. All the experimental data are listed in Appendix 1.

Fig. 3.13 shows the relationship between the feed rate and the chip radius. The results are based on the depth of cut at 1 mm and 2 mm using TNMG 332-MF3 insert. There is a parabolic relationship between the chip radius and the depth of cut. Experimental results from other inserts types show a similar relationship. In Fig. 3.13, when the feed rate is lower than 0.2mm/rev, the chip radius drops with the increase of the feed. The drop is due to an increase in the chip streaming angle. When the feed rate increases, the chip radius starts to increase as well. The thickness of the chip is the overwhelming factor in determining the chip radius. It is very hard for a chip to bend when it gets thicker. Based on the data shown in the graphs in Fig. 3.13, the cutting speed does not seem to influence the radius very much.

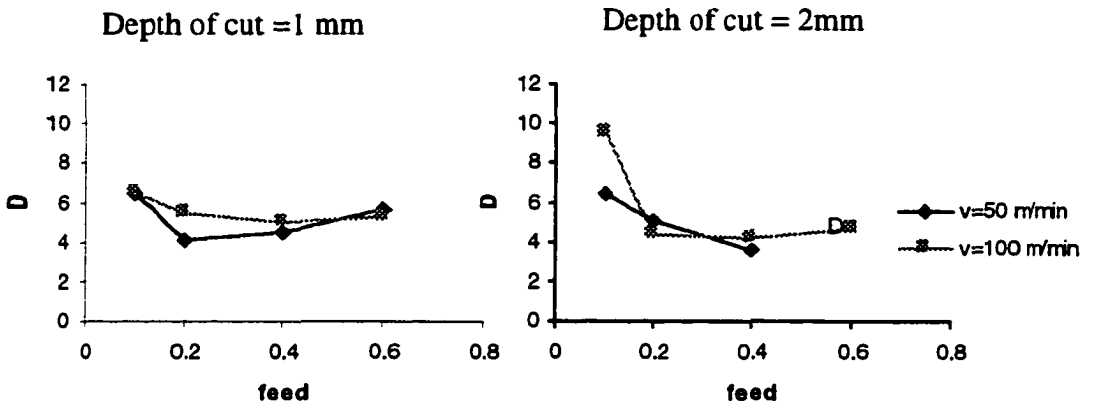

Fig. 3.13 Relationship between feed rate and chip radius (Insert: TNMG 332-MF3)

From Fig. 3.13, it is clear that Hypothesis 1 is incorrect. It overlooked the multiple influences of the feed rate. The feed rate can lead to a drop in the chip radius as well as an increase in the chip radius.

A special case occurs when the depth of cut is 0.5 mm or even less: there is no clear relationship between the feed rate and the chip radius. It is actually very easy to understand why this happens. With the depth of cut at 0.5 mm, the insert removes material using the cutting edge around its nose radius. With different feed rates, a chip travels across different groove sections. This variation contributes to the irregularity of the feed-chip radius relationship. The results from several different inserts using a depth of cut of 0.5 mm are shown in Fig. 3.14.

As for Hypothesis 2, Fig. 3.15 shows that there are some patterns to the relationship between the depth of cut and the chip radius. Therefore, Hypothesis 2 is also false. There are two things to be noted, first, the low feed rate curve does not match the pattern for the higher feed rate conditions; second, the pattern varies with different inserts.

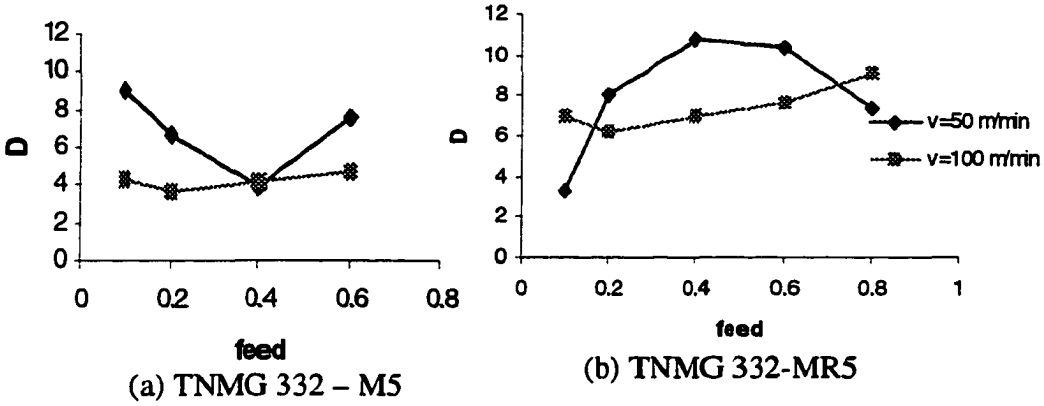

(a) TNMG 332 – M5

(b) TNMG 332-MR5

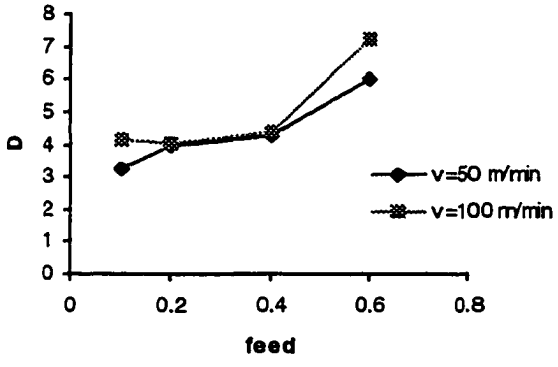

(c) TNMG 332-MF3

Fig. 3.14 Relationship between chip radius and feed when the depth of cut is 0.5 mm

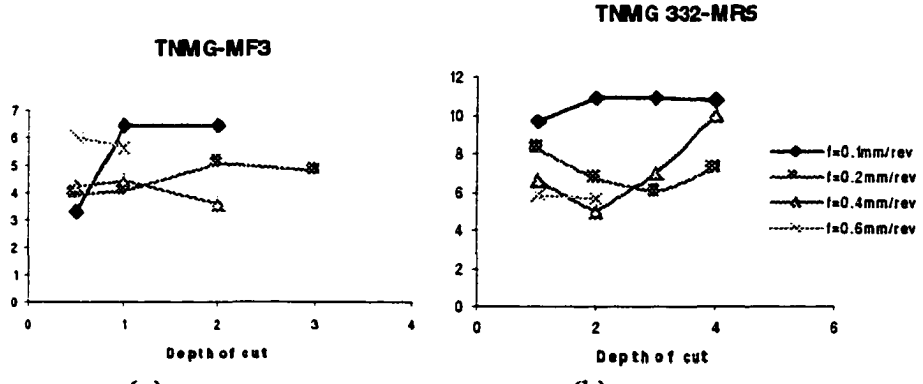

(a)

(b)

Fig. 3.15 Effect of depth of cut on chip radius (cutting speed v=50 m/min)

The first observation is due to the elastic property of the thin chips produced at very low feed rates. The second observation is the result of different chip-breaker configurations for each insert. For inserts with varied width complex grooves, an increase in the depth of cut means that there are changes in effective groove width. Since each insert is configured differently, the change is also different. Therefore, the patterns vary with each insert being used.

3.3.4 Mathematical modeling

A successful model requires knowledge of the possible contribution of different physical variables towards the variable being modeled. Without prior knowledge, the modeling will become a guessing game, which will make it more difficult and potentially lead to a biased model. The analysis described in the previous section and the knowledge described in the literature review prevent this bias from occurring in the chip shape modeling for complex groove tools.

The cutting conditions, feed, speed and depth of cut, are known to contribute to the chip formation process. Tool insert geometry, such as restricted contact length, effective groove width W' and groove depth, also contributes to the chip formation. With these variables in mind, the question that must be answered is how to organize them so that an accurate model can be obtained quickly.

Here, two interim variables are designed to help the model building process, R_1 (Eq. 3-19) and T (Eq. 3-20).

$$R_1 = \frac{(w'/4. - f)^2}{h} \tag{3-19}$$

$$T = d * v / f \tag{3-20}$$

where W' is the effective groove width, f is the feed rate, h is the groove depth, d is the depth of cut, v is the cutting speed and R_I and T are the two interim variables. These two variables come from the previous knowledge of chip formation. Eq.3-19 takes the key component of Eq. 2-13, and substitute the feed rate to for the chip thickness. Eq. 3-20 is derived from the possible chip radius with cutting conditions. The experimental results show that feed rate is in a parabolic relationship with the chip radius; thus, it is placed in as the denominator. Both the depth of cut and the cutting speed are possible positive components in T. These interim variables are added because the 3-D kinematic analysis suggested there is no simple relationship between these input conditions and the chip radius.

This mathematical modeling process used the least square method. The mathematical detail of the method is provided in Appendix 2. All the variables are standardized in order to achieve the best result. Exponential relationships are assumed for some variables. The proposed model for the chip radius is given in Eq. 3-21,

$$R = C_1 * T^{C_2} * d^{C_3} * L^{C_4} * e^{C_5 * T} * e^{C_6 * R_1} * e^{C_7 * L} * e^{C_8 * W'} \tag{3-21}$$

where C_1 through C_8 are constants, L is the restricted contact length and R is the chip radius. Eq. 3-21 is reformatted into Eq. 3-22 in order to make it easier for modeling calculation.

$$\ln(R) = \ln C_1 + C_2 \ln(T) + C_3 \ln(d) + C_4 \ln(L) + C_5 * T + C_6 * R_1 + C_7 * L + C_8 * W' \tag{3-22}$$

Through statistical regression analysis, the model constant is obtained as shown Eq. 3-23. The overall modeling result for the chip radius is shown in Fig. 3.16. Some of the experimental results using different inserts are shown in Fig. 3.17 through Fig.3.22.

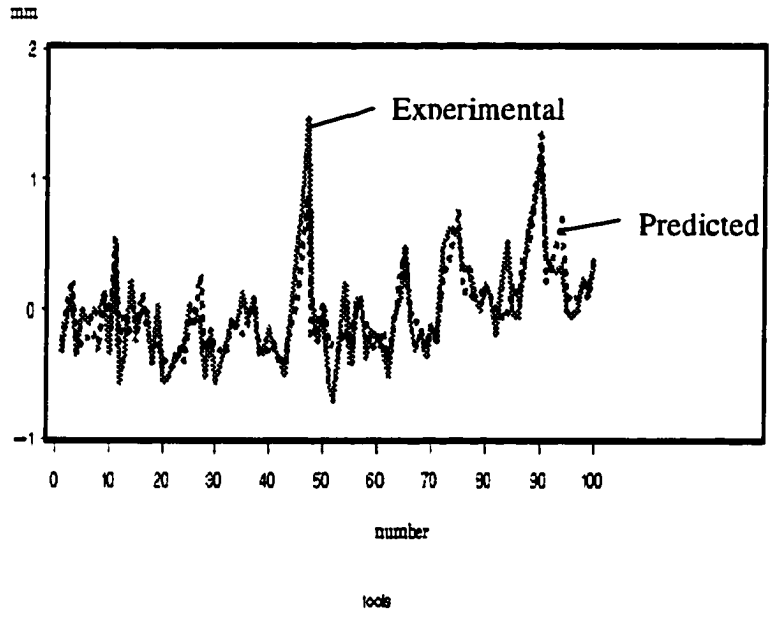

Fig. 3.16 Overall model result for chip radius

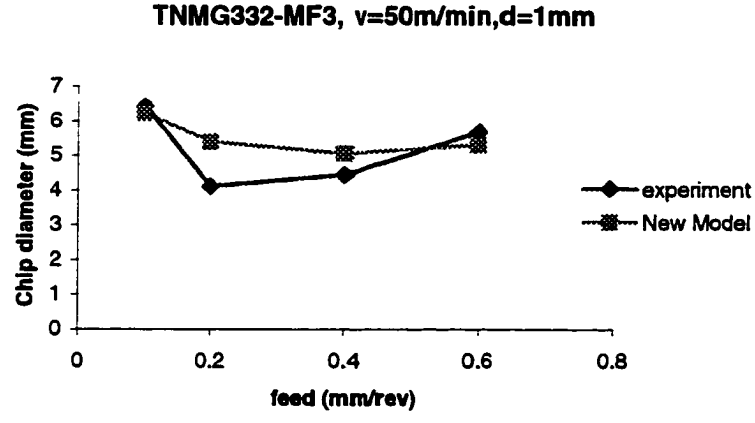

Fig. 3.17 Experimental data vs. modeling results (TNMG332, v=50m/min, d=1mm)

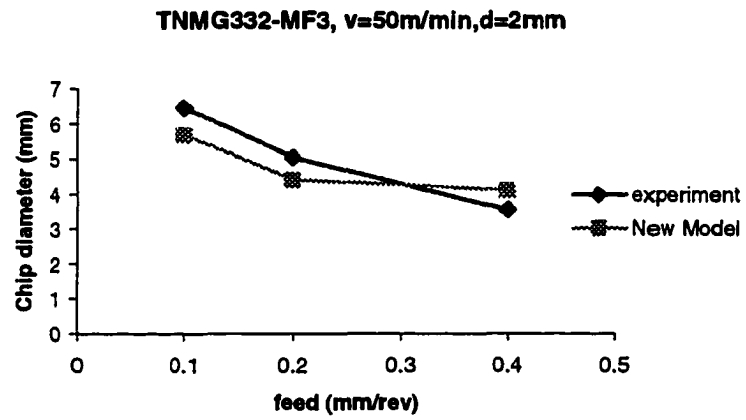

Fig. 3.18 Experimental vs. modeling results (TNMG 332-MF3, v=50m/min, d=2mm)

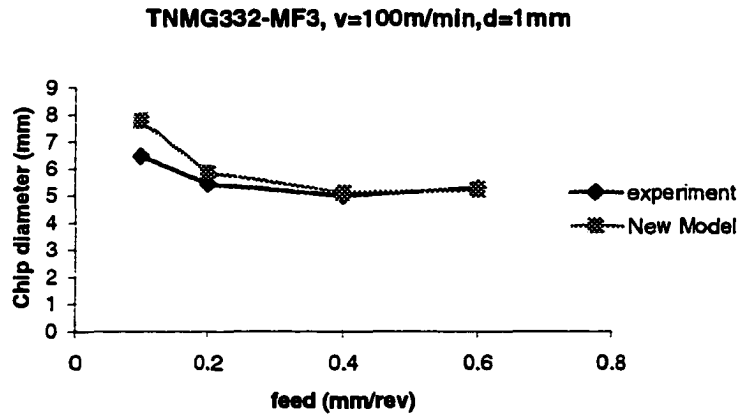

Fig. 3.19 Experimental vs. modeling results (TNMG 332-MF3, v=100m/min, d=1mm)

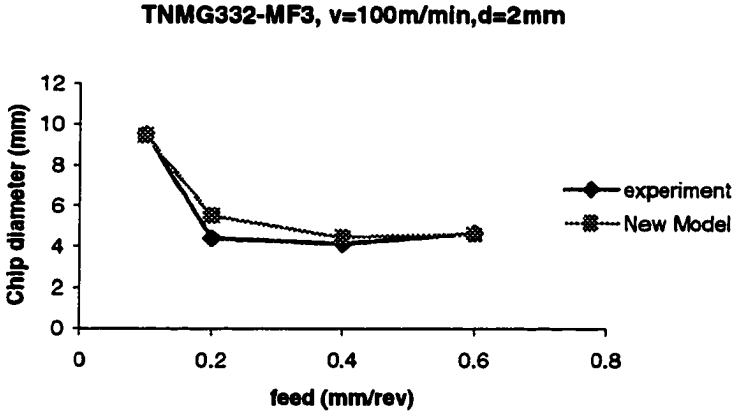

Fig.3.20 Experimental vs. modeling results (TNMG 332-MF3, v=100m/min, d=2mm)

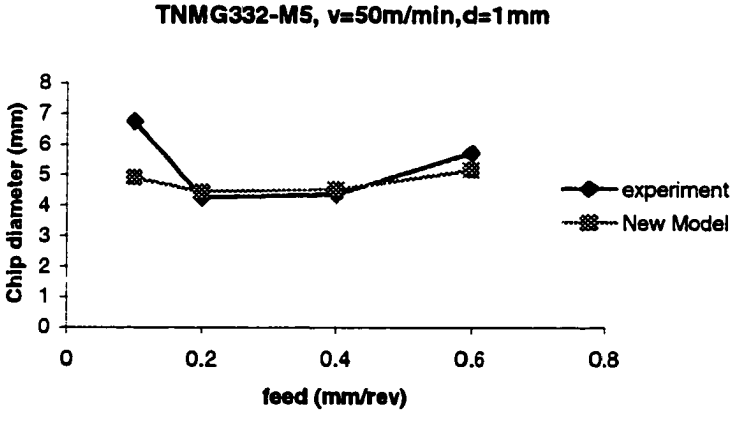

Fig. 3.21 Experimental vs. modeling results (TNMG 332-M5, v=50m/min, d=1mm)

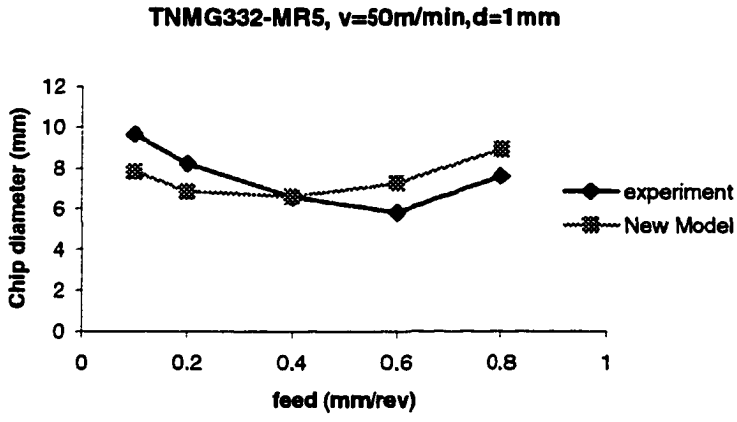

Fig. 3.22 Experimental vs. modeling results (TNMG 332-MR5, v=50m/min, d=1mm)

$$R = 2.88 \times 10^{-5} T^{-0.091} d^{-0.178} L^{-4.576} e^{-0.000572*T} e^{0.359*R_t} e^{23.075*L} e^{0.188*W} \tag{3-23}$$

Using a similar approach to model number of turns of the chip, an interim variable is defined in Eq. 3-24:

$$M = \frac{v}{f * d} \tag{3-24}$$

The number of turns can be modeled as shown in Eq. 3-25.

$$N = 0.0307 M^{0.2659} R^{1.209} e^{-0.133R} e^{0.0428W'} e^{1.35L} e^{-0.251h} \tag{3-25}$$

where R is the predicted chip radius and N is the number of turns. N is coded as

N=0, chip is straight chip;

N=0.2, chip is snarl chip;

N=0.4, half-turn chip;

N=0.6, full-turn chip;

N=0.8, 3-9 turns;

N=1.0, infinite turns.

The new model shows very satisfactory result in comparison to the experimental data. This model of chip geometry for complex groove inserts will enable designers to predict chip shapes even before manufacturing an insert. The application of this model will be discussed in the next chapter.

CHAPTER 4 CHIP-CONTROLLED FEATURE DESIGN FOR CUTTING TOOL INSERT

As discussed in Chapter 1, the design problems associated with complex cutting tools can be categorized into two major areas, systematic design process and design validity. This chapter started with design process model. Conclusions drawn from the design process modeling were used to deal with problems in complex cutting tool design. A customized tool insert design application was developed and chip control prediction was integrated into the application to improve the design process. A case study of the customized design is then presented as a showcase for the design methodology.

4.1 Modeling the design process

As described in Chapter 1, design process modeling has been addressed in previous research (Suh, 1978 and Takeda 1990). The motivation behind design process modeling is to make the engineering design process more of a science than an art, relying more on scientific and mathematical principles than on the intuition of individual designers. The ultimate goal of design process modeling research is to enable computer programs to automatically make many design decisions for human beings.

Evolutionary design (Takeda, 1990) is an important concept because it reveals the motions within a design process. In real life, design is truly a cyclical improvement process. This iterative pattern of the design cycle is similar to the feedback loop in the areas of system

and control. Instead of electrical signals, the design process operates on information. In a broader sense, the design process deals with an abstract type of signal, or information.

The design process can be represented through block diagrams. The simplest product design process is illustrated in Fig. 4.1, where the functional requirement for a design goal is the input signal R(s) of a system, and the output signal is Y(s), which is the prototype.

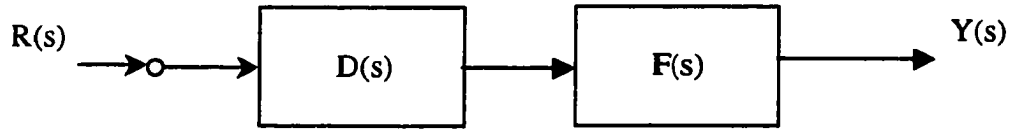

Fig. 4.1 The simplest design-manufacturing system

In Fig. 4.1, the D(s) block represents a designing process, while the F(s) block represents a manufacturing process to make prototypes. The ideal goal is to get a product at the output end that meets all the requirements, resulting in the system transfer function: T(s)= Y(s)/R(s)=1. For an open loop system (as in Fig. 4.1), this goal is very unlikely to be achieved. Thus an improved design process model is shown in Fig. 4.2.

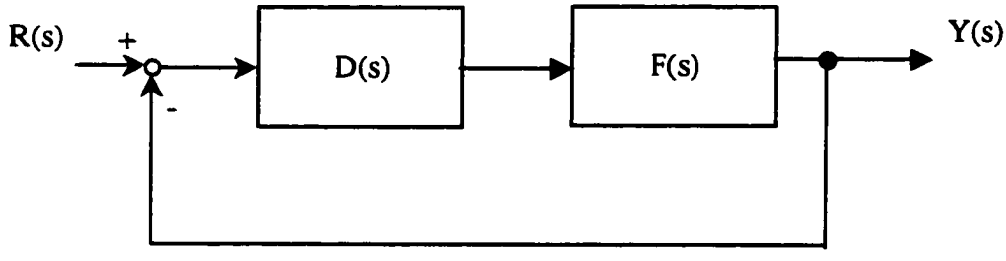

Fig. 4.2 An evolutionary design process

In the evolutionary design process model shown in Fig. 4.2, a feedback mechanism is going from the output to the input. The prototypes are compared to the original design requirements and are modified with possible improvements. The model in Fig. 4.2 is the basic design process that has been repeated over and over by all designers, although some designers may not even realize they are utilizing this process. This model is the same as the evolutionary model discussed in Chapter One.

The model in Fig. 4.2 is a much stable model than that in Fig. 4.1. The main difference comes from the feedback information from prototype. This would lead to a possibility that the design process can be improved through the addition of more feedback.

From the decision-based design theory, it is understood that a design process is composed of many discrete decision-making steps. At each step, some design parameters are defined or chosen. For example, one may choose the cutting tool insert nose radius at one step and define the insert angle at another step. The design process D(s) can be subdivided into m small steps, namely S_1, S_2, ..., S_m. These decision steps at the base level are so small that it is very hard to define a feedback at the base level.

In order to add an additional feedback, several decision steps are grouped together, forming a functional step. D(s) can be represented with functional steps, namely D_1, D_2, ..., D_n. One way to view the functional steps is to consider a typical functional step in insert design. Instead of defining a dimension in each single step, a typical functional step defines all the macro insert geometry. Suppose a feedback is added at a functional step, D_i. The modification model is shown in Fig. 4.3. The feedback function is H(s).

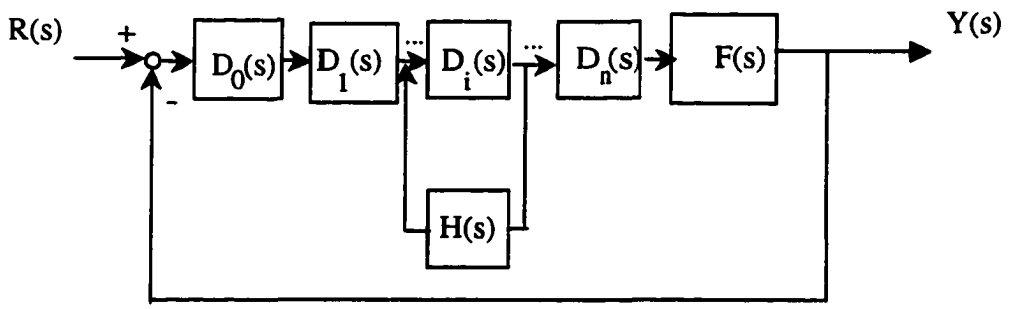

Fig. 4.3 Discrete design process with supplemental feedback

As a simple illustration of how this model works, suppose the following:

$$D_i(s) = \frac{1}{s+1},\ D_1(s) * D_2(s) * \ldots * D_{i-1}(s) * D_{i+1}(s) * \ldots * D_n(s) = \frac{1}{s+1}$$

$$F(s) = \frac{1}{s+1}, \text{ and } H(s) = \frac{1}{s+1}$$

The transfer function for Fig. 4.2 is then

$$T(s) = \frac{1}{s^3 + 3s^2 + 3s + 2}$$

and the transfer function according to the new model in Fig. 4.3 is

$$T(s) = \frac{1}{s^4 + 4s^3 + 7s^2 + 7s + 3}$$

To evaluate the system performance, the impulse response charts are shown in Fig. 4.4. Apparently, the new model with additional feedback showed better performance. This result leads to the conclusion that additional feedback within the discrete decision-making steps make the design goal easier to achieve.

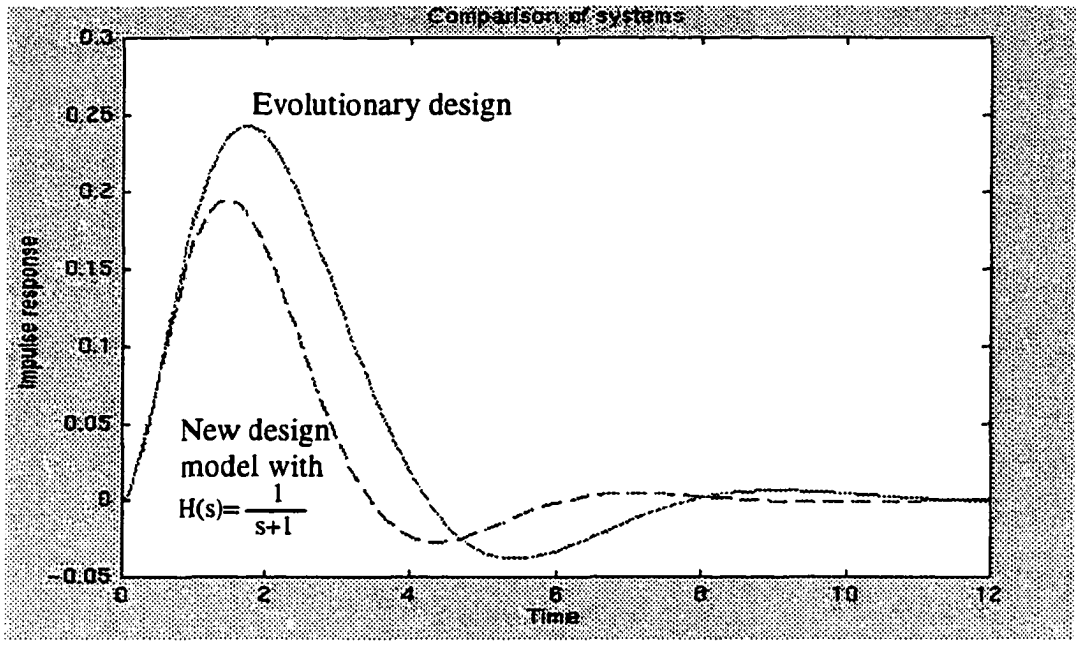

Fig. 4.4 The impulse response from the two design models

The significance of the new model is that it shows a path for systematically modifying the steps within the design process, which can lead to positive results. The key to the modification of the process is the additional feedback function. However, an arbitrary selection of such feedback does not guarantee that the improvement made upon the model will be successful; the feedback can also lead to system oscillation. As an example of how this oscillation might occur, assume H(s) is changed to a new value:

$$H(s) = \frac{1}{2s^2 + s + 1}$$

and the system transfer function then becomes

$$T(s) = \frac{2s^2 + s + 1}{2s^5 + 7s^4 + 10s^3 + 11s^2 + 7s + 3}$$

Fig. 4.5 shows that this new transfer function incurs more oscillation than the original design model. It clearly shows that a careful selection of the local feedback function is needed. This phenomenon implies that there exists an optimal feedback function for the particular design step.

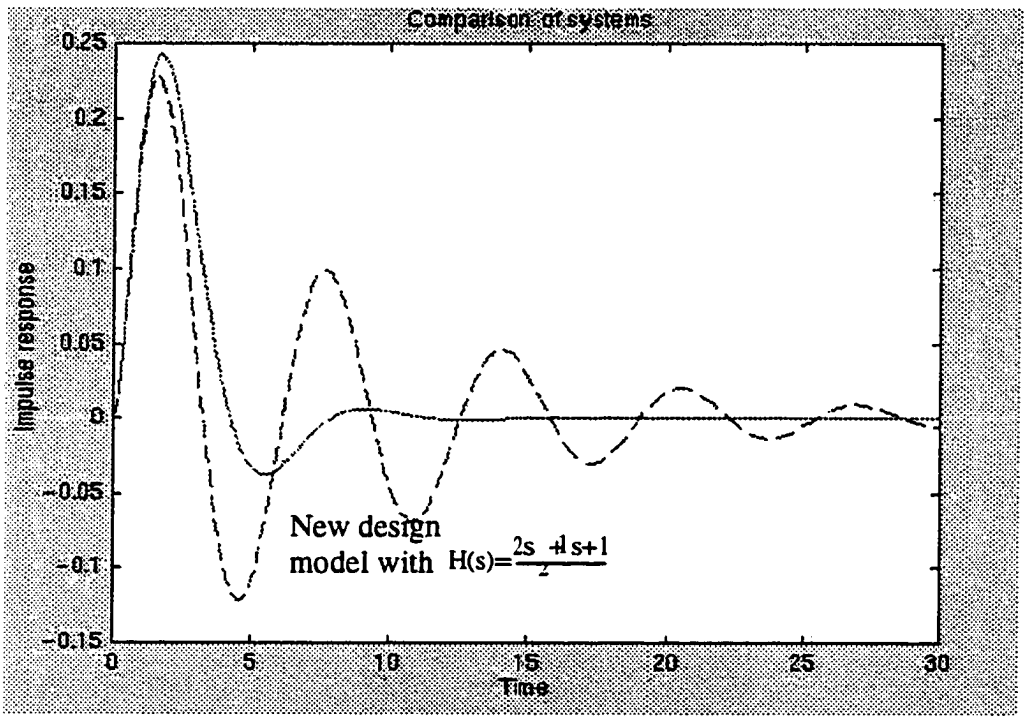

Fig. 4.5 Oscillating effect after improper feedback addition

To use this new model in a design process, one has to first, find ways of creating the discrete functional steps to allow local feedback being added; and second, find out how to select the feedback function. In a design process, a lot of specialized knowledge is deployed to find the relationship between design requirements and possible design solutions. The nature of local feedback is to judge/predict whether the solution will fulfill the requirements. From this understanding, if a design step is set too small, there will not be any improvement

because the results step are not sufficient to add local feedback. Conceivably, a proper step size is that which generates enough amount of information to allow certain functional predictions. Thus, the criterion for the feedback function is its accuracy in functional prediction.

4.2 Feature-based design for complex tool insert

Complex tool insert design is a tedious process because there is no easy way to manage the complex surface shapes. The design modeling analysis above provides means to analyze the complex cutting tool insert design process. For a complex insert, there are many dimensions to be determined before an insert is fully defined. Each dimension is a single design step. These steps need to form meaningful functional steps in order to add any functional feedback.

In the context of complex insert design, the primary function of concern is the chip control performance. Thus, the functional feedback would have to provide chip control performance prediction for a functional step. The design of tool surfaces becomes how to group small design steps into functional steps. The concept of tool surface features is introduced as a special partition of the whole geometry, with each surface feature contributing to chip control performance. Each surface feature designed then would become a functional step within the tool design process. This is feature-based design process is shown in Fig. 4.6.

In the process, Non-Uniform Rational B-Spline (NURBS) is used as a tool to model complex surface shapes.

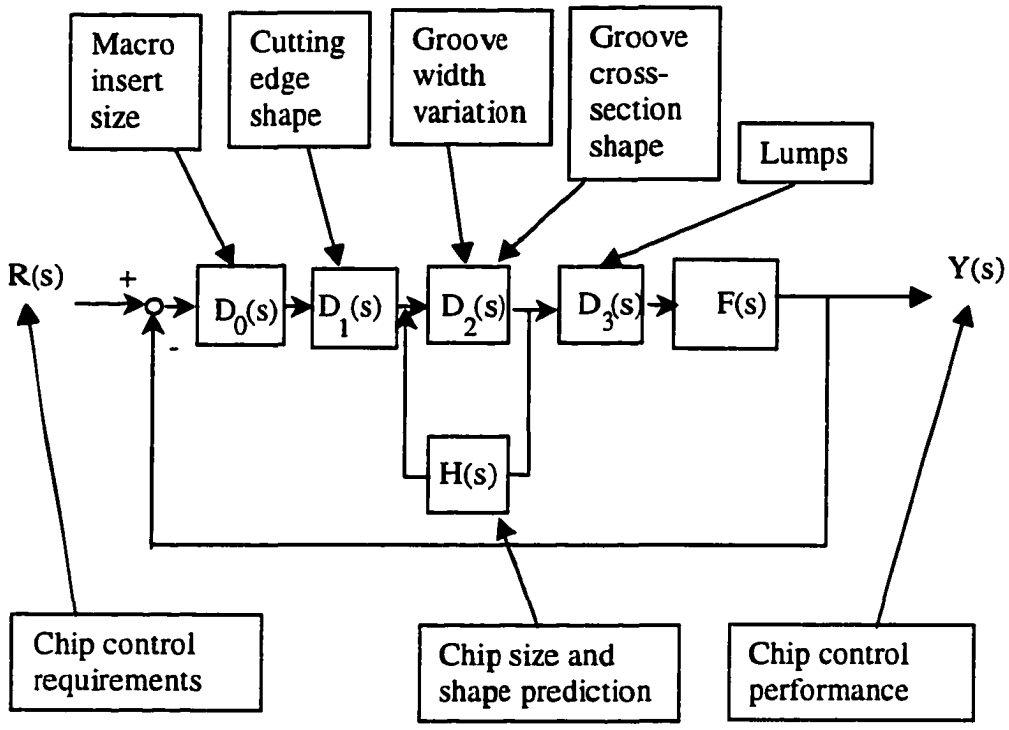

Fig. 4.6 Design process model of the feature-based tool insert design

4.2.1 NURBS as a powerful surface modeling tool

Traditional surface modeling used polynomial curve, which used simple polynomial functions of high degrees to represent geometric complexity. This approach is very inconvenient if there are only local modifications within a large curve/surface. One would have to redefine the whole curve/surface. The introduction of NURBS came as a response to the demand for flexible curves and surfaces that allow local modification.

4.2.1.1 NURBS definitions

B-spline was the basis of NURBS. A pth degree B-spline is defined in parametric form as

$$C(u) = \sum_{i=0}^{n} N_{i,p}(u) P_i \qquad a \le u \le b \tag{4-1}$$

where P_i are the control points, and the $N_{i,p}(u)$ are the pth-degree B-spline basis function defined on the non-periodic knot vector, U:

$$\mathrm{U} = \{\, \mathrm{a}, \ldots, \mathrm{a}, \mathrm{u}_{p+1}, \ldots, \mathrm{u}_{m-p-1}, \mathrm{b}, \ldots, \mathrm{b} \} \tag{4-2}$$

The B-spline basis function is defined as

$$N_{i,0}(u) = \begin{cases} 1 \; if & u_i \le u < u_{i+1} \\ 0 & otherwise \end{cases} \tag{4-3}$$

$$N_{i,p}(u) = \frac{u - u_i}{u_{i+p} - u_i} N_{i,p-1}(u) + \frac{u_{i+p+1} - u}{u_{i+p+1} - u_{i+1}} N_{i+1,p-1}(u) \tag{4-4}$$

A B-spline surface is defined by the bi-directional control points net and two independent knot vectors, U and V. The surface points are

$$S(u,v) = \sum_{i=0}^{n} \sum_{j=0}^{m} N_{i,p}(u) N_{j,q}(v) P_{i,j} \tag{4-5}$$

where $P_{i,j}$ are points on the control points net.

NURBS curves and surfaces are widely used in CAD/CAM software as the tool to design complex geometric entities. NURBS concepts were developed from B-Spline and offer greater flexibility as the weight factor is added.

A pth degree NURBS curve is defined as

$$C(u) = \frac{\sum_{i=0}^{n} N_{i,p}(u) w_i P_i}{\sum_{i=0}^{n} N_{i,p}(u) w_i} \qquad a \le u \le b \tag{4-6}$$

where w_i is the weight factor.

Similarly a pth degree by qth degree NURBS surface is defined as

$$S^w(u,v) = \sum_{i=0}^{n}\sum_{j=0}^{m} N_{i,p}(u)N_{j,q}(v)P^w{}_{i,j}$$

With the addition of the weight factor, all commonly used surfaces can be represented in the form of NURBS.

4.2.1.2 Freeform surface generation with NURBS surface

The most frequently used NURBS surface in tool design is the swept surface. A swept surface can be defined by Eq. 4-7,

$$S(u,v) = T(v) + M(v)C(u) \tag{4-7}$$

where M(v) is a 3x3 matrix incorporating rotation and non-uniform scaling of C(u) as a function of v, and T(v) is the trajectory to be swept along. Fig. 4.7 shows the typical freeform swept surface used in groove feature generation.

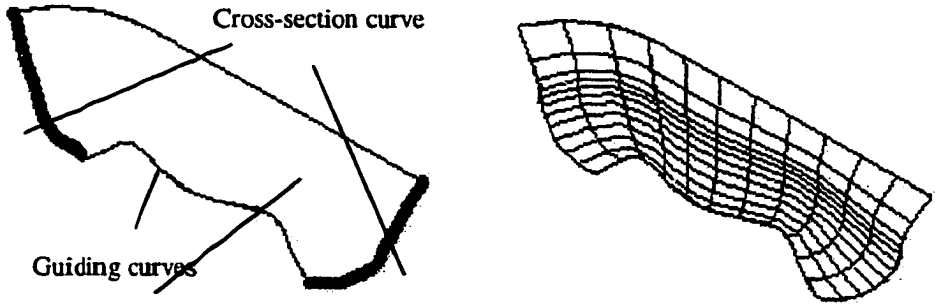

(a) Before sweeping (b) The swept freeform surface

Fig. 4.7 Swept surface used in a varied width groove generation

4.2.2 Application of tool surface features into the design process

After careful study of the insert surface structure, the following features are used in the feature-based tool insert design: groove surface feature, top feature, side feature and lump feature. The function of each surface feature is described in the following paragraphs.

Groove surface feature. The groove feature was first introduced to increase the curling of a metal chip. It has become a standard surface feature in modern tool inserts. The kinematic analysis of chip formation shows that the groove surface also influences the chip flow speed, chip angular velocities and chip breakability. A complex groove surface may also have a complex cross-section curve other than a simple arc, as well as varied groove width along the cutting edge.

The groove feature can be defined in various ways. Swept freeform surface is used here for the groove definition. The customized application provides a few options for users to define the surface. A particular developer may add or reduce the options, shown in Fig. 4.8, according to his or her need.

Top feature. Top feature is the surface expanded from the center hole and connecting to the groove surface. It is actually not an independent surface feature because its function is achieved in conjunction with the groove feature. The transitional surface to the groove feature, called as the backwall surface, defines the guiding boundary for the groove surface sweep. A guiding curve that is not parallel to the cutting edge creates a varied width groove feature. There are also some predefined shapes available as shown in Fig. 4.9.

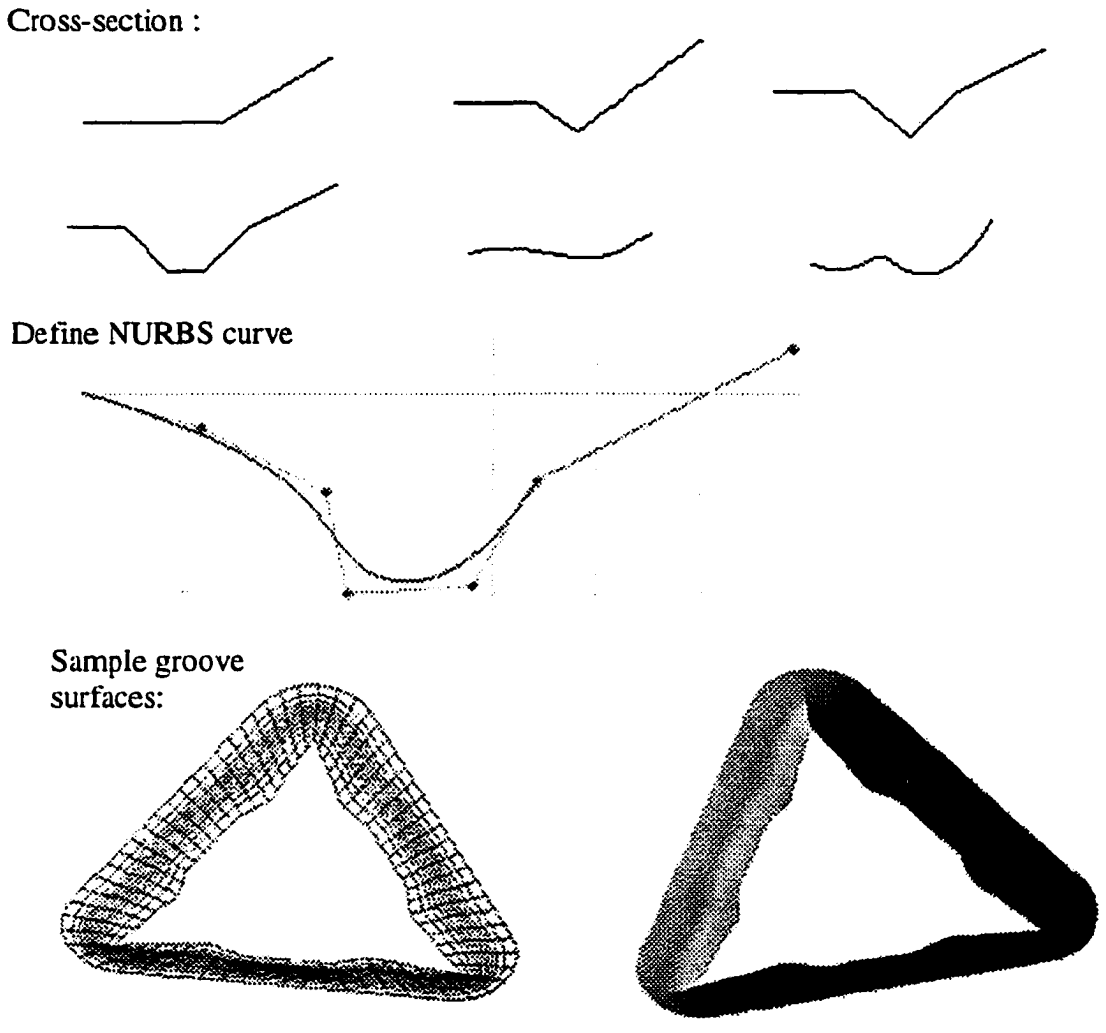

Fig. 4.8 Groove feature definition and sample groove surface

Side feature. Side feature refers to the cutting edge curve. The traditional side feature was a flat curve. Experiments showed good chip breaking performance for inserts with wavy cutting edges. The mechanism of how a wavy cutting edge works is not yet fully known. A possible reason for such performance improvement is that the chip produced by this kind of cutting edge has a non-rectangular cross-section. The uneven stress distribution across the chip cross-section may contribute to chip breaking.

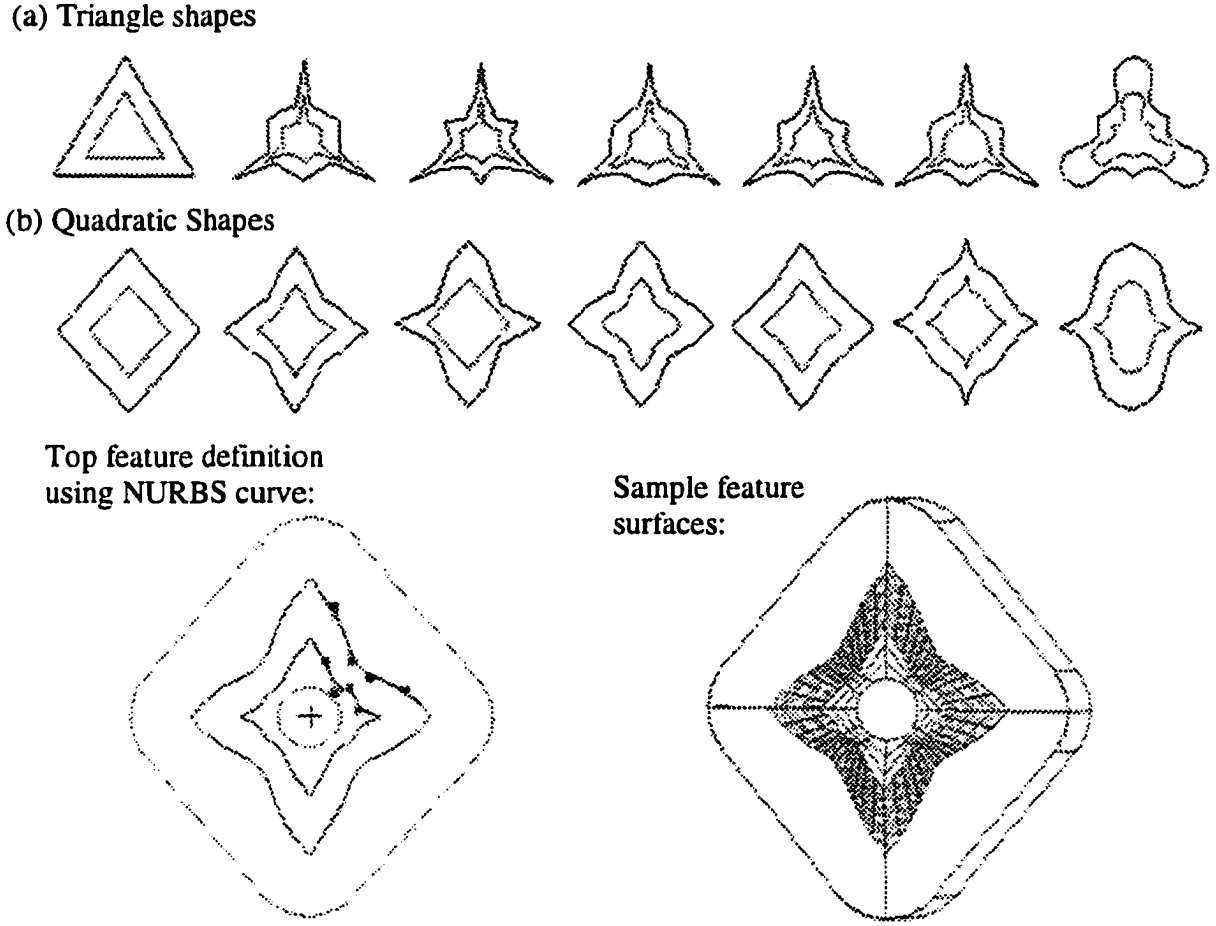

Fig. 4.9 Top feature definition

Lump feature. A lump is an obstruction type chip breaker. It is usually a simple extrusion placed on the cutting tool insert surface. This special geometry interacts with chips generated in a cutting process and delimits the directions in which chips can grow. In some insert designs, lumps are placed to work together with the groove surface to enhance the control of the chip.

4.2.3 Feature surfaces integration

Although feature surfaces are defined because they perform different functions, their functions will not work unless they are assembled together to become a complete product. The integration of different features requires careful handling. Because of its symmetry, only a small portions of a triangle or quadratic shape insert needs to be defined. All other portion of the insert can be obtained by mirroring and rotation. The boundaries between surface features should be aligned well and the boundaries at mirroring or rotation edges should maintain smooth transactions. Finished designs of triangle and quadratic shape tool inserts are shown in Fig. 4.10.

4.2.4 Customized design application

As discussed from previous sections, determining how to group small steps together into functional features is a key element in improving the design cycle. One of the obstacles to improving the design process in this manner is the lack of specialized design software that allows designers to group functional elements together into a feature categories so that feedback information can be provided about each feature.

It is very easy to get powerful CAD software that has many graphical functions. The drawback of these general CAD tools is that they do not help the designer make decisions on which design to choose and how to select parameters. Without the ability to add local feedback function into the design process, there is little room for the improvement of the design process. This problem particularly affects those design processes that rely highly on functionality performance prediction, such as complex cutting tool insert design.

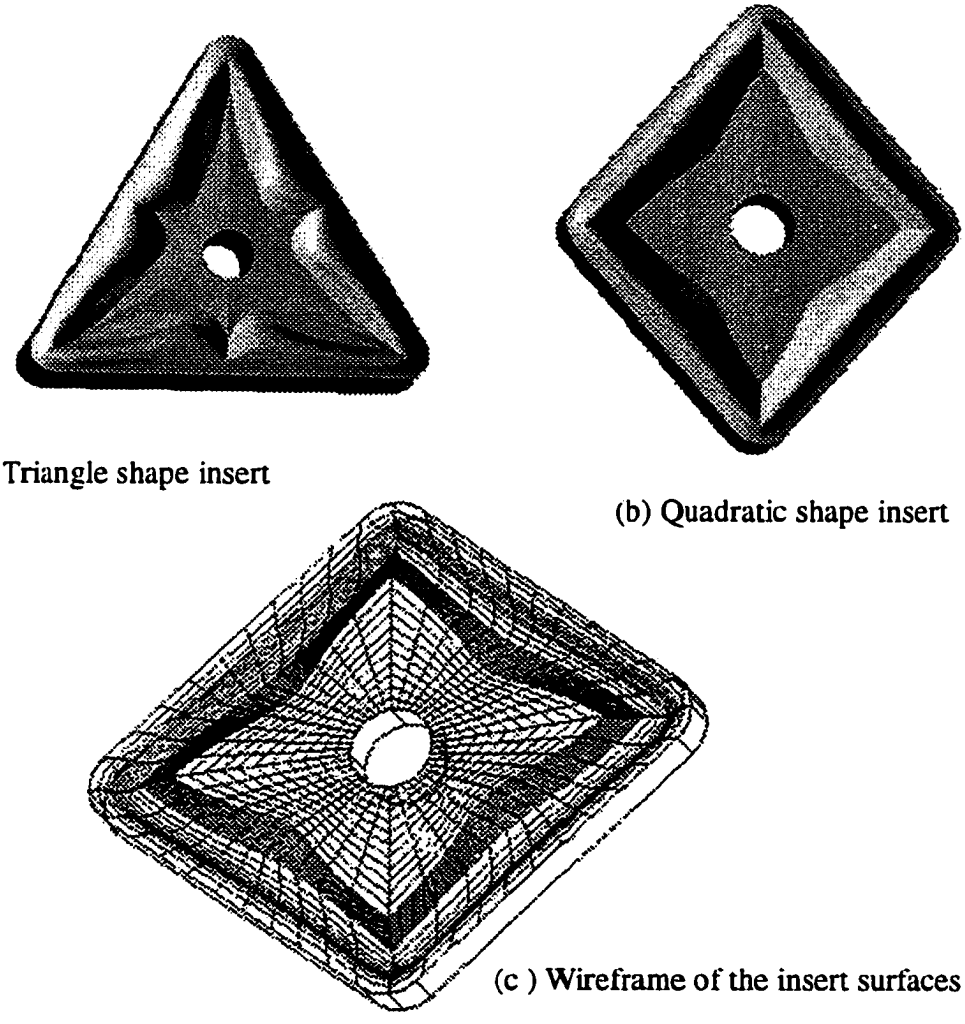

(a) Triangle shape insert

(b) Quadratic shape insert

(c) Wireframe of the insert surfaces

Fig. 4.10 Cutting tool inserts from feature-based design

Customized application is the solution to the problem of how to add "intelligence" into the applications. Customized application requires the designer to define the overall framework of the design process to allow functional prediction/feedback at major steps.

There are two major approaches to customized design: develop a design package from scratch and construct all application programs; or define the framework and use available graphic interface language to implement it. The first approach is time-consuming and difficult. The second approach is flexible and easy to expand upon, although it is subject to function availability in the graphic interface language.

In the application of complex groove tool insert design used for this disseration, both approaches have been tried and compared. The first approach took more than six months for a customized application. Using the second approach and the same design strategy, only two weeks were needed for the application program to function. The graphic interface language used was UG/OPEN GRIP from Unigraphics.

GRIP, which is an acronym for Graphics Interactive Programming, is a programming language. By using a vocabulary of English-like words, GRIP can perform most of the operations in commercial CAD package (Unigraphics). Commands are available to create geometric and drafting objects, execute external functions and modify existing geometry. GRIP provides the capabilities desired for an intelligent design tool.

4.3 Integrating chip control into the design process

Even when a tool insert feature has been selected, whether the design achieves the desired function requirements remains to be seen. The design's validity is of great importance because further work would be void if the current feature design is invalid in its function. In the cutting tool insert design, one obvious way of evaluation is to manufacture sample inserts and make cutting tests to examine the performance. This is a lengthy and costly process.

Section 4.1 suggested adding a local feedback loop to predict the functional performance of the current design step. In the particular case of complex tool insert design, this feedback function is the chip control model.

The chip control model required is a 3-D prediction model that is able to detect the influence s on complex 3-D chip groove surface: the groove feature which defines the cross-section, and the top feature which defines the groove sweeping pattern. Prior to the research work described in Chapter 3, there was no model that took account all the factors that influence the chip shape. The theoretical analysis described in Chapter 3 significantly unveiled these factors. The mathematical model derived from the cutting experiments provides the means need to fulfill the chip prediction task.

From Chapter 2, it is known that all current chip forms can be represented in helical shape equations. To observe a predicted chip form, one only needs to acquire the parameters for such chip shape. The key parameters are chip radius R, chip pitch p, number of turns n, chip width d, chip thickness t, chip side-curling radius r and chip tilting angle θ. With these seven parameters, the chip shape can be accurately determined.

For the purpose of chip control, not all seven parameters are required. The chip control is only affected by the chip size and when the chip is going to break. Thus, R and n are the two primary parameters, which can be determined through Eq. 3-23 and Eq. 3-25. Other secondary parameters can be ignored because they will not influence the breakability of the chip.

To actually implement the chip prediction model, there are other factors that have to be taken into consideration. The first one is the effective chip groove width. With a varied width design, the effective chip groove width has to be measured at the middle point of the chip width. Chip shape prediction will show the chip forms at different cutting conditions. These predictions are based on work material of 1045 steel, a medium carbon steel. There is no way to predict the chip formation of other work material without extensive cutting tests.

Even with the model in place, chip formation knowledge is necessary to avoid any wrong prediction caused by the model accuracy. For example, if the chip radius prediction is high (e.g. 10 mm), and the number of turns is predicted to be less than 1, when feed rate is low and the depth of cut is also low, then there is likely an error with the number of turns prediction.

By using the chip control prediction function, designers are able to foresee the performance of a tool insert while it is being designed. Modifications can then be made quickly to obtain better chip-controlled cutting tool inserts.

4.4 Case study of predicted chip chart and real cutting test

This section provides a case study that demonstrates the chip control prediction capability of the customized design application and how it will be able to provide fast feedback information to the designer to improve the design process.

Fig. 4.11 (a) shows the insert designed with the customized application. Fig. 4.11 (b) is a real insert manufactured commercially. Since their surface shapes are similar, the insert shown in Fig. 4.11 (b) is used in cutting experiments as the designed insert in Fig. 4.11 (a).

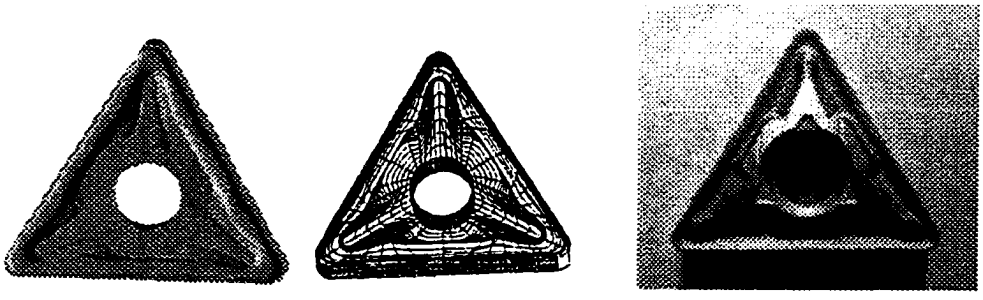

(a) Customized design (solid and mesh form) (b) TNMG 332- M3

Fig. 4.11 Tool insert used in chip shape prediction

When the insert is designed as shown in Fig. 4.11 (a), the software demonstrates that the 3-D mathematical model would predict chip forms as in Table. 4.1. The cutting chip produced in a real cutting environment is listed also for comparison. The number of turns is coded into six categories as discussed in section 3.3.4.

Table 4.1 Comparison of predicted chip data and experimental data (v=100m/min)

Feed (mm/rev) / Depth of Cut (mm)		0.1	0.2
1	Experiment	R=2.93 mm N=1 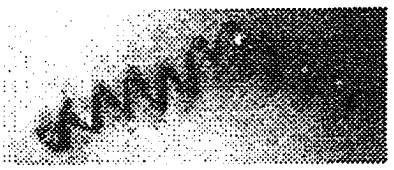	R=1.78 mm N=0.6 
	Predicted	R=2.70 mm N=1 	R=2.18 mm N=0.62 
2	Experiment	R=2.71 mm N=1 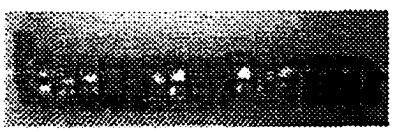	R=2.52 mm N=0.6 
	Predicted	R=3.85 mm N=0.8 	R=2.39 mm N=0.64 

Table 4.1 (continued)

Feed (mm/rev) / Depth of Cut (mm)		0.4	0.6
1	Experiment	R=1.69 mm N=0.4 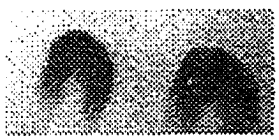	R=2.72 mm N=0.8 
	Predicted	R=2.25 mm N=0.49 	R=2.77 mm N=0.60 
2	Experiment	R=2.30 mm N=0.6 	R=2.60 mm N=0.4 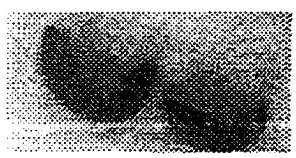
	Predicted	R=2.16 mm N=0.50 	R=2.57 mm N=0.48 

As this comparison shows, these two sets of chips are similar in size and shape. Thus demonstrating that chip control can really predict chip shape. Designers will be able to use this feedback information to modify groove shape in order to achieve maximal chip control performance.

CHAPTER 5 VIRTUAL REALITY AS AN EMERGING SIMULATION TOOL

During the last years, virtual reality (VR) has proved its potential for engineering simulation, especially for abstract model analysis. It is a great test platform for chip control simulation. This chapter looks at the basic concepts and theories of virtual reality. In particular, the stereoscopic theory is discussed in detail. Then, the literature review will focus on the use of VR in different fields of manufacturing.

5.1 Introduction to virtual reality

Generally, virtual reality refers to an interactive synthetic environment. The key elements of a virtual reality application are interaction, immersion and imagination.

A virtual reality system usually consists of three elements: human, VR hardware devices and VR software. The system diagram is show in Fig. 5.1. Human is the basis for all virtual reality applications, yet it is so often easily forgotten when defining the system. The human body interacts with hardware devices to provide crucial information for the software to process. At the same time, it receives feedback such as display or force-feedback through the devices.

Typical VR hardware devices include graphic display units, sound system, hand interaction tools and position trackers. Some VR systems even have force-feedback devices. Graphic display can be stereo graphical display using stereo glasses or head-mounted display, and it can also be streamed video. The viewing area can range from a limited-size

monitor screen to a wall screen that fully surrounds the user. The sound system provides audio feedback to a user.

The hand interaction tool refers to the data glove, the cyber glove, the pinch glove, the wand or the joystick. Although their functions differ, all of them supply hand information to the device driver.

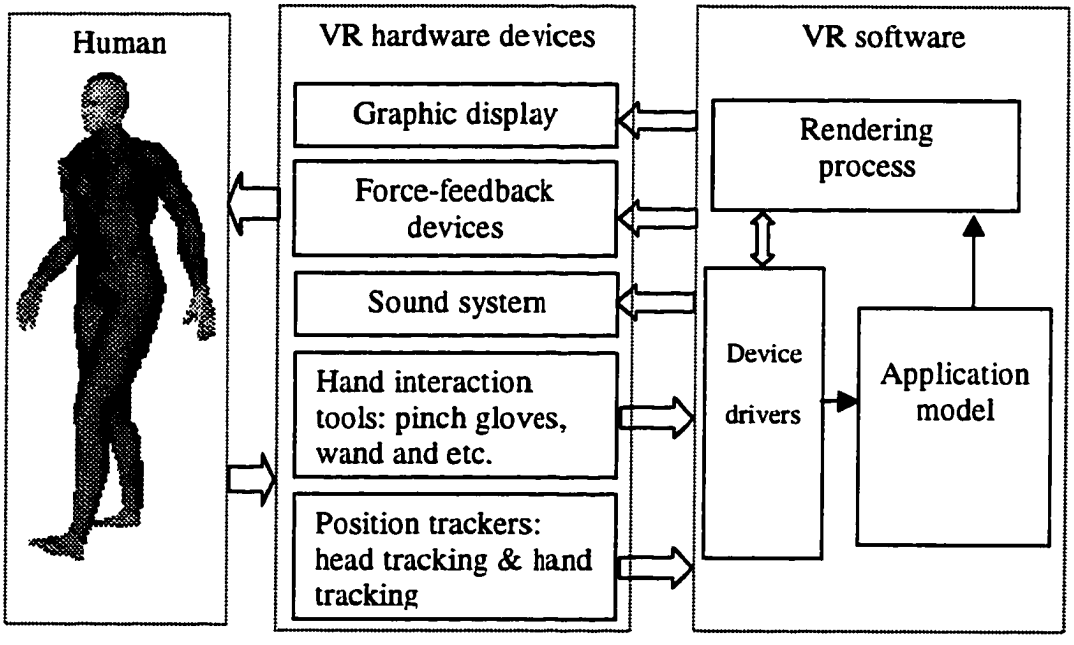

Fig. 5.1 System diagram of a VR system

Position trackers are a critical component of a virtual environment. Usually, there are both hand tracking and head/body tracking. Hand tracking provides the hand position and orientation while head/body tracking deals with head/body position and orientation. Tracking and hand interaction tools combined provide complete human interaction information to the application software.

VR software consists of two major parts: system software and application model. System software is composed of device drivers and rendering process. Device drivers process signals from various hardware devices and provide all the information to the user application process. The application model then updates the rendering process with regards to the human behavior. As the commercialization of VR grows, nowadays, a VR application developer only needs to design the application part of the VR software while system software such as CAVE and WorldToolkit is commercially available. This greatly reduces the cost and development cycle of a new VR application.

5.2 Stereoscopic model for graphical display

One of the important qualities of virtual reality is the display of computer generated images. The question comes as how to make these images look the same as in the real world.

5.2.1 Human eye stereo viewing theory

Human eyes see things three-dimensionally. The reason lies not only on the depth cues of eyes, but also on the stereoscopic nature of human eyes. In computer graphics, there are depth cues used to define spatial relationship among different objects, such as light and shade, relative size, interposition, texture gradient, perspective and so on. All these terms are also called monocular cues as they exist with a single (imaginary) eye. These cues are determined by objects' relationship in three-dimensional world. A single eye can perceive some three-dimensional information from these cues. This is why common graphic display can provide a seemingly three-dimensional view of the world.

Each of our eyes sees the same object differently. This is illustrated in Fig. 5.2. Each eye sees the world from a different point of view. There will certainly be disparity between the images that each eye views. The brain then processes these images into a single image of the real world. This stereo viewing nature of our eyes provides the stereo depth cue needed for a three-dimensional image. The disparity of images is created by the distance between eyes, interpupillary distance or interocluar distance. The resultant sense of depth is called stereopsis.

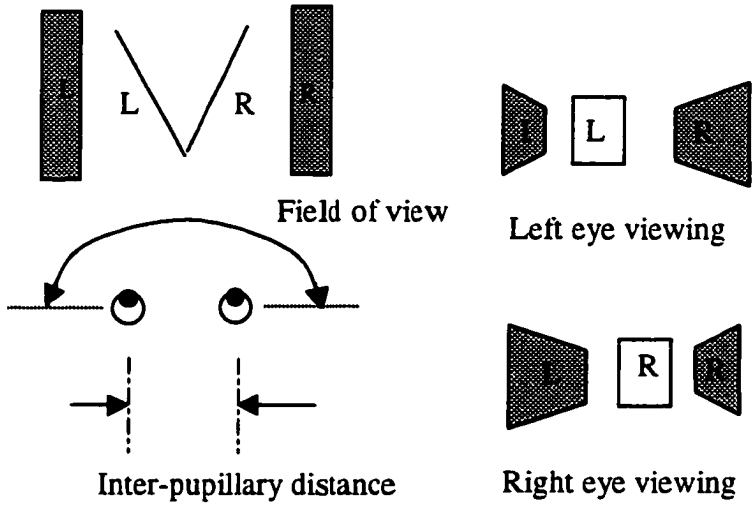

Fig. 5.2 Stereo viewing nature of human eyes

5.2.2 How the stereo glasses provide stereoscopic cue

Graphical display is similar to human eyes. A planar display does not create any disparity in eye retinae, thus no stereoscopic cue is generated from that. If different images are fed to different eyes, will the eyes perceive stereoscopic cue? This question can be answer from analysis of the display method.

A stereoscopic display would provide images with parallax values. Parallax is referred as the distance between left and right corresponding image points. It is similar to retinae disparity but it is measured on the display screen. Parallax can also be given in terms of angular measure. Parallax can be zero, positive and negative. The key to stereoscopic cue lies on the parallax values created by the different images fed to each eye.

Horizontal image translation is one of the techniques used to provide such stereoscopic cue. This method of display uses horizontal translation of two perspective views. Suppose the screen lies in the xy plan, and the center of projection lies on the positive z-axis at (0,0,d), an arbitrary point A (x,y,z) will be plotted at point A'(x',y') according to perspective viewing.

$x' = x\, d/(d-z)$

$y' = y\, d/(d-z)$

Assuming the interpupillary distance of a viewer is T. Left-eye and right-eye images are created for stereoscopic viewing by calculating projections from two different eye positions onto a single screen. The point A would be plotted at $A_{left}(x_l, y_l)$ for left eye and at $A_{right}(x_r, y_r)$.

$x_l = (x\, d + z\, T/2) / (d-z)$ $\qquad$ $x_r = (x\, d - z\, T/2) / (d-z)$

$y_l = y\, d/(d-z)$ $\qquad$ $y_r = y\, d/(d-z)$

Stereoscopic display calculates and renders both images to the screen. An emitter is used to synchronize the image with stereo shutter glass to make sure that the left eye only sees the left eye image and the right eye only sees the right eye image. Thus a viewer can use the stereoscopic cue to feel all objects are three-dimensional. This technique has been used in both desktop monitors and large projection screens.

5.3 Literature review on VR as an emerging simulation tool

Virtual reality is one of the most exciting and effective techniques to make a model of engineering systems and to simulate engineering processes for various purposes, such as design and manufacturing processes.

Due to the apparent benefits of visual effects, design is one of the first areas that saw VR as a leading technology of great potential. Back in 1995, Taylor et al developed a desktop virtual manufacturing workshop that visualized the design process and presented solid product component with NC codes.

Auto manufacturers in Germany had implemented virtual prototyping for design evaluations (Dai et al, 1996). Their presentations were based on a digital model instead of physical prototypes. The application simulation used BOOM as the VR tool.

VanDoren (1998) has found that building a control system in a computer-based virtual world allows all manners of extreme conditions and 'what-if' scenarios to be tested safely.

Xiao et al (1996) established a virtual machining environment - GMPS, which reads NC codes and simulates material removal and checks collision and interference. But it is more like a graphical visualization simulation.

Among all the developers, NIST is the leading researcher in simulating manufacturing process (Jones and Iuliano, 1997). They designed testbeds in the virtual world for continuous simulation of production equipment and processes, and discrete-event simulation models of various production systems.

CHAPTER 6 VR AS A TEST-BED FOR CHIP CONTROL SIMULATION

With an understanding of VR concepts and its usage in manufacturing, this chapter starts with the need and requirements of a virtual simulation tool for chip control simulation of complex cutting tool inserts. It then introduces the systematic design of such application. Following that, a brief discussion of the latest manufacturing knowledge used in the application will illustrate the remarkable achievement of such advanced simulation tools.

6.1 The need of VR as a model testing platform for chip-controlled insert design

In Chapter 3, a mathematical chip model about complex tool insert was developed. This predictive model shows satisfactory matching with experimental results in the case study in Chapter 4. It would not be adequate for a complete model examination since only discrete test points were selected. A complete validation would require examination of the model under all input conditions. Although graphical plots of the mathematical function can show some trends of the model, there are too many variables in the model to allow one to understand the validity of the prediction through plots. An interactive visualization of cutting chip is desired for such task.

Once the mathematical model becomes a valid tool in customized design application, designers can make use of it in the complex insert design. Usually a designer will only examine chip performance in a limited number of cutting conditions as design feedback. There may be cutting conditions being overlooked that enable the insert to generate undesirable chip forms. It will be of great waste of both time and money if the fault is found

only after prototype testing. A virtual simulation tool would also fulfil the testing task. The primary requirement for such tool is stereo graphical chip representation.

The requirements for the simulation and visualization are more just graphic animation. Interactive input and stereo viewing are also needed. VR simulation provides a great means to solve above problems. There are several benefits from the adoption of VR technology. The first and ultimate benefit of using VR is the considerable saving in costs. As discussed in the previous chapter, many industries had used VR in design and simulation. No real material objects need to be built anymore. Anything can be achieved in a virtual world.

The second benefit is its graphical and multimedia advantage over other simulation technology. Many process tests rely on people to imagine the possible results and so such tests are not very intuitive to researchers. When it comes to a complex mathematical model, visual representation would provide much more insight information about the model than equations.

Therefore, it is clearly understood that there is a great need to develop a VR test platform that simulates the chip formation in machining process.

6.2 The system components for a virtual model testbed

Fig. 5.1 shows the system components for a complete VR system. Not all of them are required for every VR application. The objective of an application determines the priority of the system components. There are also many choices of devices to be used for a given type of component.

From the above section, it is known that the vital element is the graphic display. To achieve best visual effect, 3-D viewing is preferred over 2-D viewing. The interaction

devices and position trackers are important as they enable interactive viewing effects. These devices are required for the application. Other devices, like audio system, are not needed for the model simulation.

The selection of graphic hardware is then based on the cost effect for 3-D viewing hardware. Available systems are desktop monitor, head-mounted display (HMD), BOOM and CAVE projection system. BOOM is not selected as it is very hard to maneuver in the scene. Table 6.1 compares various factors associated each system.

A CAVE type projection system provides multi-viewing and full immersive effect. It is, however, the most expensive type of graphic system. Head-mounted display (HMD) also provides immersive feeling and it is less expensive. HMD allows only one person to view at a time. Graphical monitor can also provide 3-D viewing, which is the least expensive way to view 3-D. The boundary of screen, however, would create a disruption of 3-D viewing effect. If the budget permits, the VR test-bed should use at least a HMD. In application described below, a CAVE type system is used for viewing.

6.3 Schematic design of manufacturing simulation

The initial objective to develop a virtual manufacturing simulation platform is to create an interactive machining lab to replace machining tests. The machining laboratory can be used as a test-bed for machining operation and chip model validation. The machine would also use CNC codes to create different cutting conditions. A fully developed platform would require many areas of knowledge as shown in Fig. 6.1.

Table 6.1 Comparison between different VR stereo display systems

System / Property	Projection system (CAVE)	Head-mounted display (HMD)	Desktop stereo monitor
Stereo device	Shutter glasses	CRT/ LCD screens	Shutter glasses
Immersiveness	Full	Full	N/A
Field of view (degree)	180 (4 walls) <180 (one wall)	180	Usually less than 90
Stereo effect	Good	Good	Poor
Realism	High	High	Low
Disorientation	Low chance	High chance (totally rely on HMD)	Low chance
View audience	multiple	Single	mulitple
Expense ($)	> 200k	10k-20k	2k
Tracking	Position trackers	Position trackers	Position trackers / keyboard
Interaction devices associated	Glove/ wand	Glove/ wand	Glove/ wand/ keyboard
Problems	the person in control has best stereo effect	Cable may entangle as the user cannot see himself/herself	Poor viewing effect due to image disruption at monitor border and low field of view

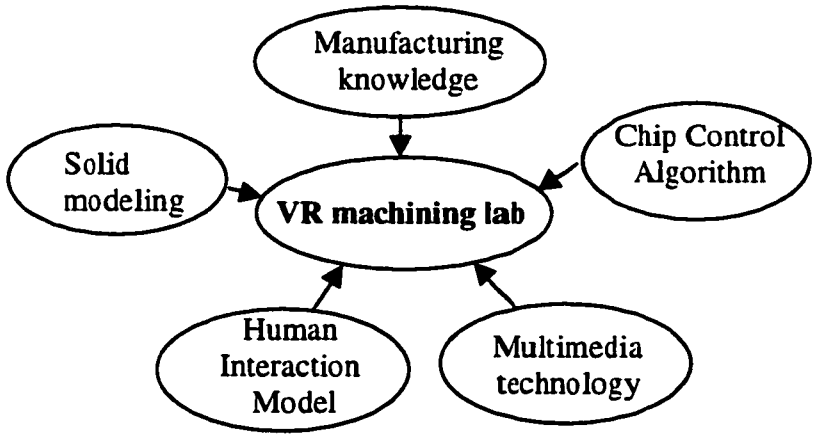

Fig. 6.1 System components of VR machining lab

A successful VR application requires all relevant process knowledge and machining theories to be implemented within the simulation process. Here, modeling of real-world machining includes physical models of various machine-tools and cutting tools, geometric models of workpieces coupled with manual operation or NC G-code programs, 3-D chip formation model, cutting forces model, tool life models, surface roughness models, and so on. Fig. 6.2 shows the machining theories and process models to be implemented.

The basic flow chart of the manual machine is shown in Fig. 6.3. The flowchart for virtual CNC machine is similar to that of the manual machine. The only difference is that operators can either manually control the machining operation or write their own NC G-code program to perform the CNC function to cut the part. There is a G-code engine used to analyze G-code program and to calculate the tool trajectory and finished workpiece shape.

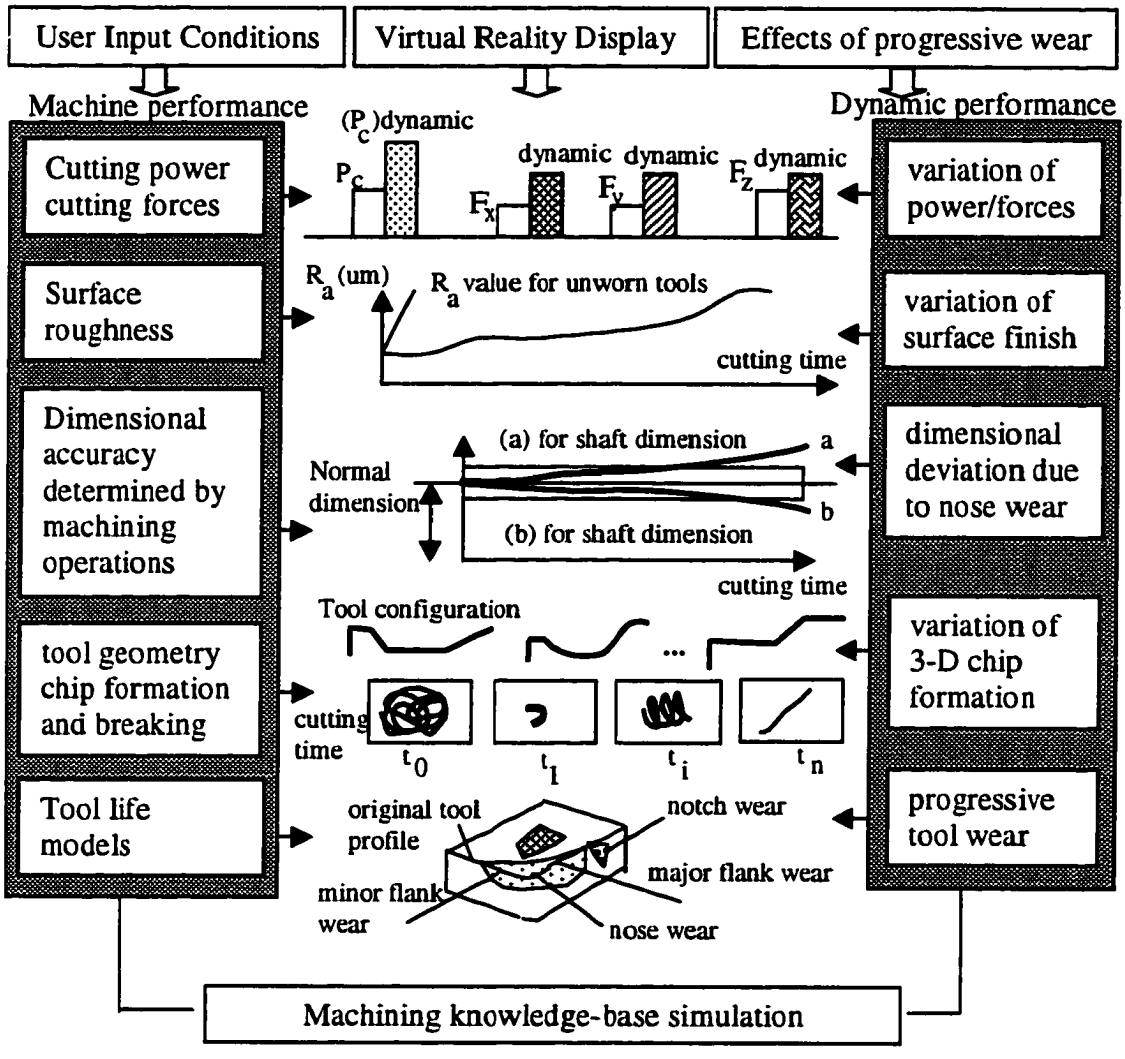

Fig. 6.2 Implementation of machining models in a virtual machining system

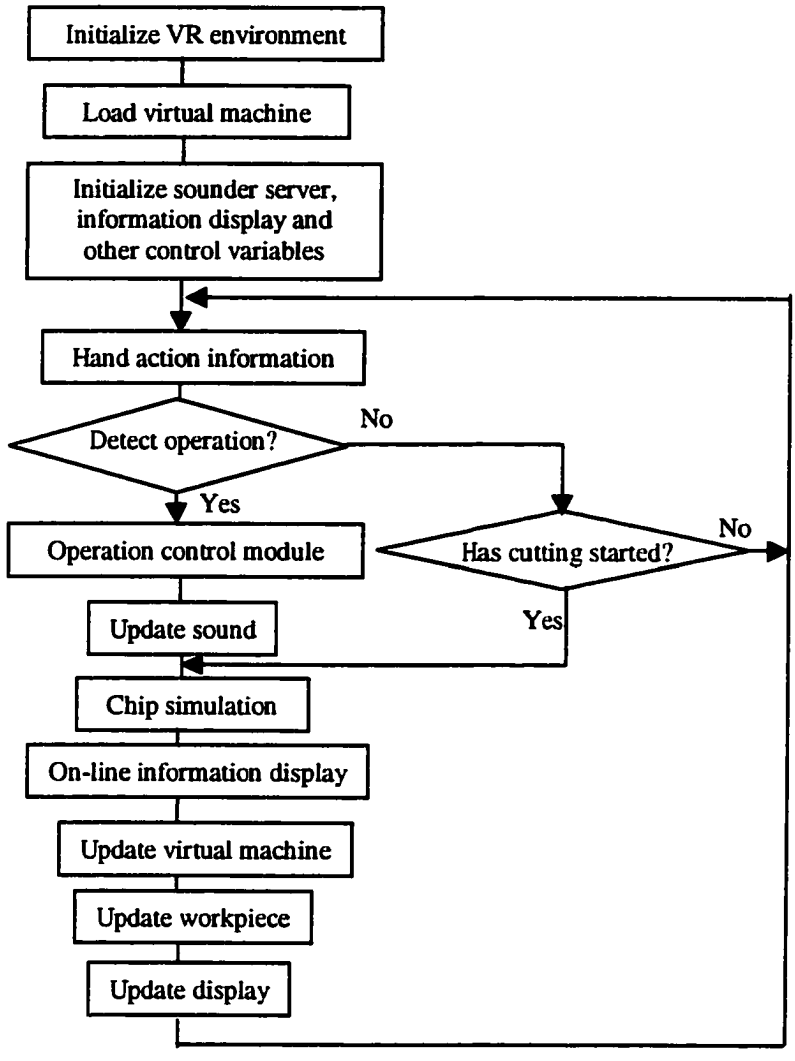

Fig. 6.3 Flowchart of a virtual manual machining simulation

All the virtual machines have to integrate machining process models, machine design, cutting tools, and dynamic animation modules together to make a fully simulated machining process. Once all the modules are in place, the virtual machines can be used as the testing and simulation platform for the 3-D chip model for complex cutting tool inserts.

6.4 Development of the virtual machining lab

A fully functional virtual machining lab has to be able to simulate the whole process and provide detailed process information at each consequential moment. Process information would include the machine conditions, workpiece geometry after cutting, finished surface roughness and so on. The simulation nature of the virtual machines allows the operator to modify input conditions and observe the results. The following sections will introduce the process models adopted in the simulation.

6.4.1 Surface roughness prediction

The surface finish quality is an essential consideration for selecting finish turning conditions. It would greatly benefit operators to allow this information to be available in the virtual machine simulation. There is a correlation between the finished surface roughness and cutting conditions (feed rate, depth of cut and cutting speed). Also, metal chips generated in the cutting process often come into contact with the workpiece surface and consequently influence surface quality. The chip factor is determined by the configuration of the cutting tool inserts, especially the chip breaker type. Another factor that may influence the final surface finish quality is the workpiece material. As each kind of material presents different mechanical property, each material type will certainly demonstrate different surface behavior after cutting.

There are hundreds of kinds of tool inserts with different chip-breaker configuration. There are also many arbitrary combinations of cutting conditions and many types of work material to choose from. Predicting surface finish quality under all the possibilities is a major

task for production engineers. Fang and Safi-jahanshahi (1997) proposed a reference-based model for predicting surface roughness in finish machining of steels.

This model used empirical equations to show the effects of cutting conditions on surface finish. There were linear, second order and exponential models being developed. Here, only the exponential equations based on general groove tool is adopted.

$$R_a = 6.25200 * v^{-0.173748} * f^{0.284038} * d^{0.029483} \tag{6-3}$$

where f is the feed rate, v is the cutting speed and d is the depth of cut.

The reference-based model then relies on coefficients deducted from experimental correlation to model the different configurations of chip-breaker and work material.

$$R_a(i,j) = w_{0.j} + w_{1.j}(C_{0.i} + C_{1.j}(R_{a(ref)})) \tag{6-4}$$

Where $R_a(i,j)$ is the final surface roughness prediction, w_{0j} and $w_{i,j}$ are the work material coefficients, $C_{0,i}$ and $C_{1,i}$ are the chip-breaker coefficients and $R_{a(ref)}$ is the surface roughness prediction from the previous empirical equation Eq.6-3.

For the virtual turning machine, work material factor can be omitted as only 1040 is selected for the simulation purpose. Thus $w_{0j}=0$ and $w_{i,j}=1.0$. $C_{0,i}$ and $C_{1,i}$ are stored in a database and can selected according to the chip-breaker configuration.The equation is simplified as,

$$R_a(i,j) = C_{0.i} + C_{1.j}(R_{a(ref)}) \tag{6-5}$$

6.4.2 NC G-code engine

The key component to virtual CNC machine is the G-code engine that can interpret any G-code program and assign cutting trajectory. There are several formats of CNC

programming language exist. Each programming language corresponds to a kind of CNC controller. G-code is a widely used CNC programming language. It can be used on controller produced by many companies, such as Fanuc. G-code is executed in the order of sequence numbers unless there is a subprogram block. The general syntax specifies machine control parameters, tool positions, tool change, coolant operation and so on.

In a real machine, CNC controller executes one command and waits untill the command is accomplished before it goes to the next one. With a G-code engine running, the virtual machine controller receives the machine's control commands and performs functions accordingly. Due to the particular rendering process of VR program, G-code engine can provide machine-state information at any time interval. The difference between CNC controller and virtual G-code controller can be illustrated in Fig. 6.4

In Fig. 6.4 (b), the virtual G-code engine controller counts each time interval within a given command execution cycle. The controller updates machine states at each interval and return these states for graphic rendering. In other words, the controller cuts each command cycle into small segments and provides a detailed result of the command execution.

The virtual G-code engine only provides tool positions and other machine state information, it does not provide any information on the geometric information of the workpiece after the metal cutting process. A virtual machine has to rely on separate geometric calculation to determine final workpiece shape.

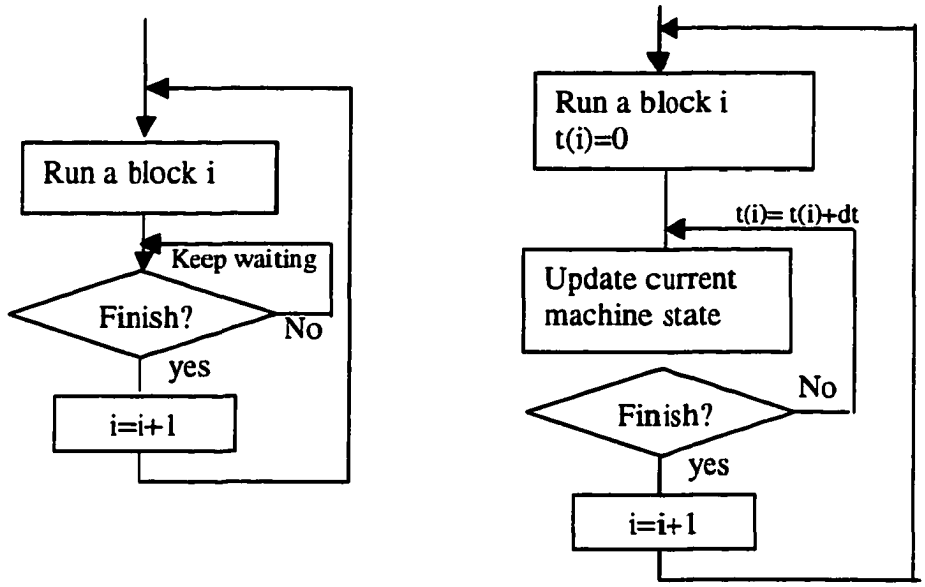

(a) CNC controller (b) Virtual G-code engine controller

Fig. 6.4 The difference between CNC controller and G-code engine controller

6.4.3 Geometric calculation in lathe

When cutting tool moves towards the workpiece, geometric calculation is used to figure out the intersection of the workpiece and the tool. Thus, the shape of workpiece after cutting can be determined.

For lathe, the problem is considered as a two-dimensional problem of intersections. Suppose the nose radius of cutting tool is R. The effect of a round cutting tool tip can be simulated by a small square with each edge length of R. This can be illustrated as Fig. 6.5 (a) and (b). When R << tool displacement, this approach is acceptable.

Fig. 6.5 (c) and (d) demonstrated a typical turning trajectory. In such a material removal process, final workpiece shape is determined by finding out the intersecting points between the tool tip trajectory and the original workpiece profile. Special care has to be taken of the intersecting points as sometimes the computer may return a response of no intersection as a result of float point rounding.

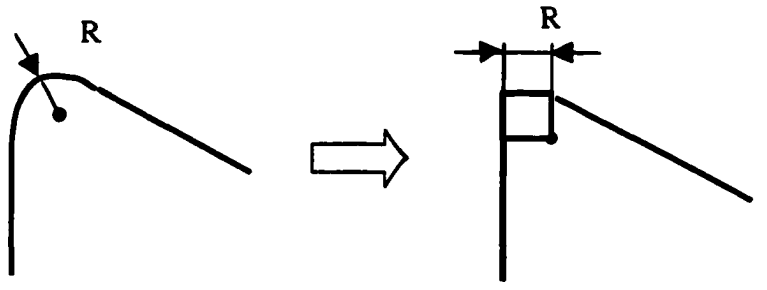

(a) real tool tip (b) simulated tool tip

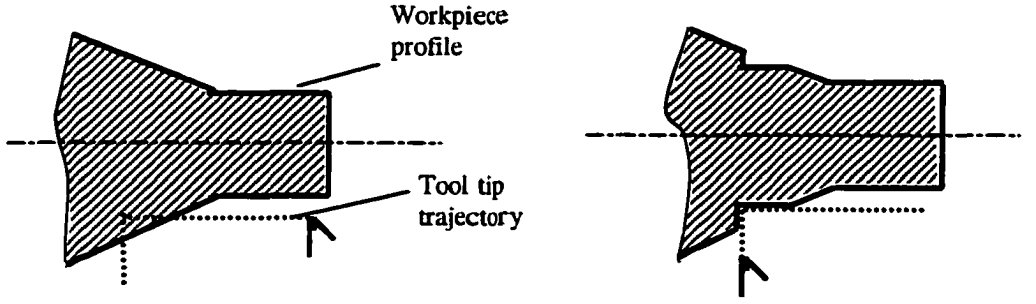

(c) before cutting (d) after cutting

Fig. 6.5 Simulated turning operation

6.5 Virtual machining lab development

The development library used in software development is C2 library, which is based on previous research done by Dr. Carolina Cruz-Neira at the University of Illinois at Chicago. The virtual machining lab program can run on both C2 facility and desktop simulation. As

shown in Fig. 6.6, C2 is an ideal place to experience the reality of such simulation. Desktop simulation has a limited feeling of stereo images due to the fixed edge effect of a computer monitor.

The virtual machining lab is composed of a manual lathe and a CNC lathe. Fig. 6.7 shows the CNC lathe.

In short, the virtual machining lab provides a safe, flexible, and cost-effective testing environment. The advantage of such system is that it gives all designers the opportunity to verify chip prediction model and validate insert design. Experiments under hitherto impossible situations become possible in the virtual environment. It is under this notion that the virtual machines are ideal test-beds for model simulation.

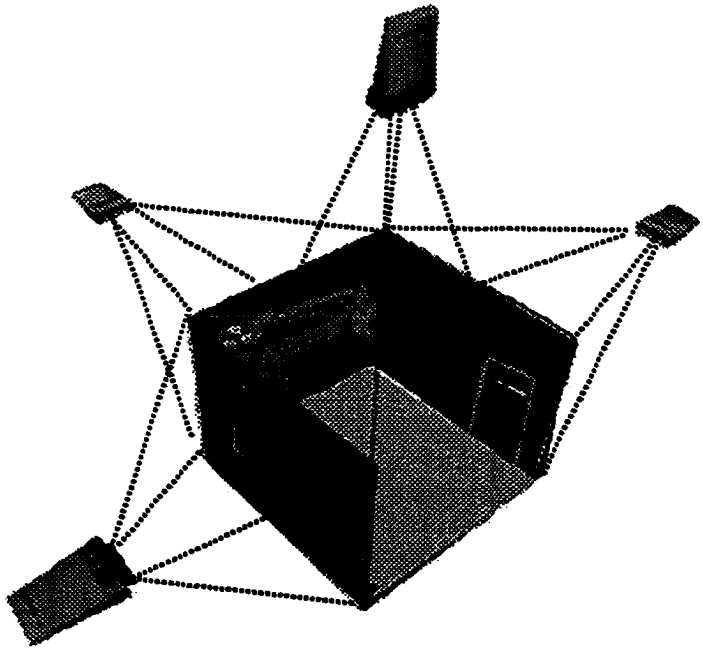

Fig.6.6 Virtual machining simulation in C2

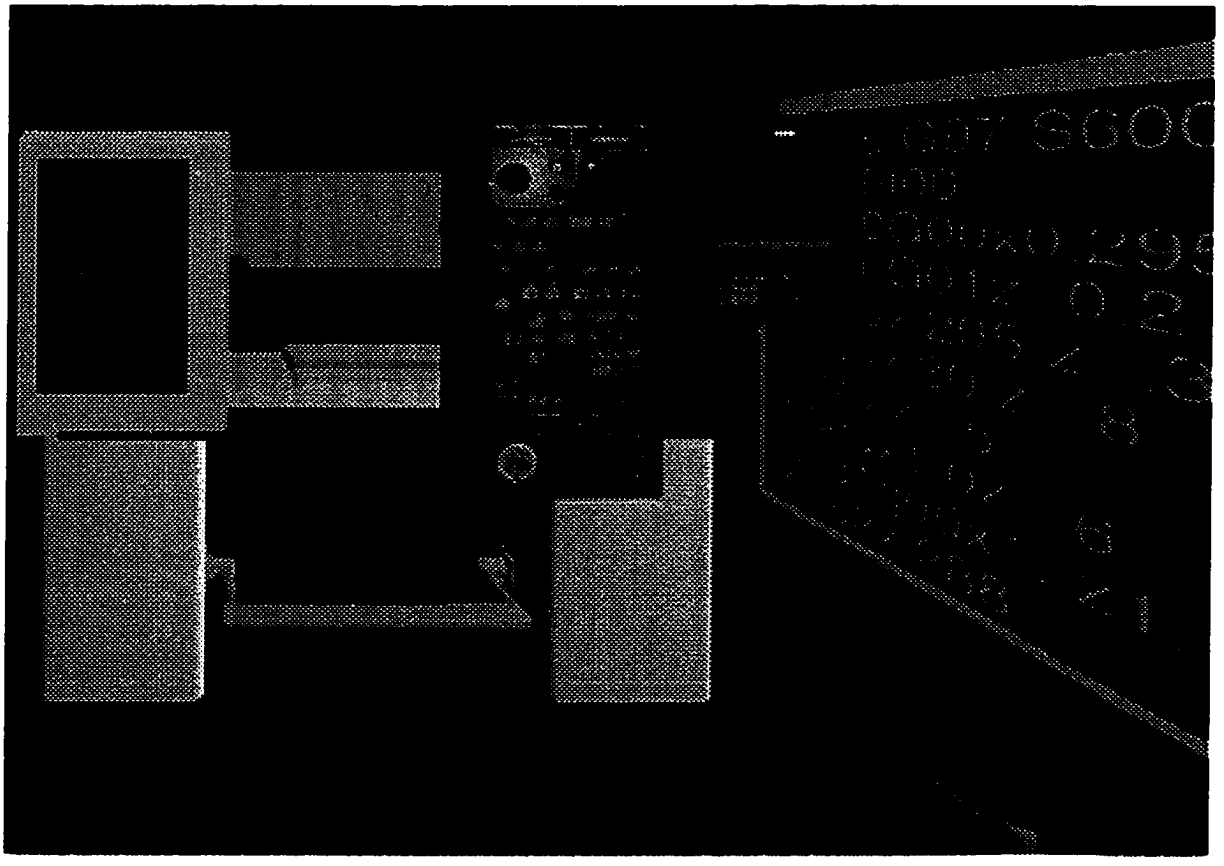

Fig. 6.7 Virtual CNC lathe simulation

CHAPTER 7 CONCLUSIONS AND DISCUSSIONS

This dissertation has identified the urgent need of research and development in chip control, tool design and manufacturing simulation. From the research work that had already been carried out in this dissertation, many achievements had been made. The following lists the conclusions drawn from the research work in this dissertation.

1. A new 3-D kinematic chip model was developed to depict chip behavior in a complex groove insert. This model is based on analysis of 3-D chip motions, which involve a linear velocity and three angular velocities. The model derived showed the analytical relationships between chip shape parameters and chip motion parameters. All angular parameters can be represented in the form of chip linear velocity and chip-curl angles, which are influenced by the cutting conditions. The model, therefore, proved that the chip shape/form is indisputably related to the cutting conditions.

A breakthrough also lies in the 3-D nature of this analytical model. In machining practice, complex 3-D tool inserts are extensively used. The chip control research on these cutting tools has to be enhanced to three-dimensional levels. This model thus provides a means for such research. This dissertation explained how the kinematic model could be modified to take accounts of all possible 3-D complex groove shapes. With this modified model, a chip shape can be readily predicted given quantified 3-D chip motion parameters.

2. A mathematical model has been constructed based on experimental data. The need for a mathematical model is imminent because it will help designers to foresee the chip forms as a result of their designs, and because there is still problem in accurately getting chip motion parameters which is required by the 3-D kinematic model. The mathematical model serves as

a tentative solution to the problem till advances can be achieved in predicting these motion parameters.

Previous research on chip formation, as well as the newly developed kinematic model, helped to create a successful prediction model for chip shape in a complex 3-D groove feature. This model takes the complex groove surface shape into account by adjusting the effective groove width. Hypotheses were tested in order to clarify some notions of chip shape and cutting conditions. The examination of hypotheses, again, proved the relationships between cutting conditions and chip geometry.

3. Improved design strategy: group discrete design steps according to functionality, and add local feedback control for each group. Block diagrams are used to model the design process. This dissertation demonstrated how the system transfer function could improve as a result of the addition of a local feedback. The keys to the improvement of a design process are: first, divide the vast amount of discrete steps into groups according to their performance functionality; second, find the appropriate local feedback functions which would predict the performance of these steps.

The result of such design strategy is customized design applications. A customized design application caters only for the special need of a designer. The structure of the design process can be modified to fulfill the new design strategy. The application will identify functions of different geometry and allow local feedback function being added.

4. Chip-controlled design for inserts with 3-D complex groove surfaces is a step further in achieving intelligent design. The current implementation of chip control into the tool design process has brought light to an often "blind" practice. The case study showed the close match of predicted chip control chart and real cutting test performance. This on-line

prediction means a designer can improve the design without waiting for the manufacturing test. Not only did this present a shortened design cycle, but this would also mean that tool inserts could be designed to satisfy special customer's requests on certain cutting conditions.

5. Virtual reality is an effective and interactive platform for chip model simulation. Information that is not available to real machine tools can be made possible in the virtual environment. The machining simulation has implemented manufacturing process knowledge. Without technical understanding of the manufacturing detail, the simulation would not be possible.

5. Future research and development is made possible through the work of the dissertation:

a. Chip modeling. With the kinematic model in place, one may develop accurate chip motion models and combine them with the kinematic model in order to create a complete chip control analytical model.

b. Design applications. Customized design would make use of models like chip control prediction model to improve a design process.

c. Virtual manufacturing: more simulation of manufacturing will be developed. Future machines would be able to be operated by people through virtual reality. Virtual reality will also provide a platform for product development, testing and manufacturing.

APPENDIX 1 EXPERIMENTAL DATA OF CUTTING TESTS

This appendix listed the raw data from the cutting tests described in Chapter 4. None of the data has been standardized, nor has they been encoded. There were eight inserts used in the tests. Table A1.1 to A1.8 shows the experimental results for each cutting tool insert. In these tables, the number of turn for chips is listed as *infinite* if the real number of turn exceeds 20, while it is listed as *snarl* if the chip is snarl chip.

Table A1.1 Experimental data for insert TNMG 322 56

Feed (mm/rev)	Speed (m/min)	Depth of Cut (mm)	Chip diameter (mm)	Chip turns
0.1	50	0.5	3.4	1.5
0.1	50	0.25	1.7	15
0.1	50	1	4.33	5
0.1	50	2	5.57	15
0.1	50	3	6.87	1.5
0.2	50	0.5	4.02	17
0.2	50	1	4.22	0.5
0.2	50	2	5.9	1.5
0.2	50	3	5.31	0.75
0.4	50	1	5.91	3
0.4	50	2	5.74	0.5
0.4	50	0.5	3.54	4
0.4	50	0.25	5.16	1.75
0.6	50	0.25	4.38	infinite
0.6	50	0.5	7.93	9
0.6	50	1	6.7	0.5
0.1	100	0.25	4.3	infinite
0.1	100	0.5	5.06	infinite
0.1	100	1	4.26	8
0.1	100	2	9.82	4
0.2	100	0.5	3.32	3
0.2	100	0.25	2.98	infinite
0.2	100	1	3.36	0.5
0.2	100	2	4.38	2
0.4	100	0.25	3.92	9
0.4	100	1	7.35	1.5
0.4	100	2	4.96	0.5
0.6	100	0.25	4.78	5
0.6	100	1	5.91	0.5
0.6	100	2	5.89	0.5
0.6	100	0.5	10.36	10

Table A1.2 Experimental data for insert TNMG 332 M5

Feed (mm/rev)	Speed (m/min)	Depth of Cut (mm)	Chip diameter (mm)	Chip turns
0.1	50	0.25	1.82	infinite
0.1	50	0.5	9.05	6
0.1	50	1	6.76	5
0.1	50	2	5.57	10
0.1	50	3	6.43	infinite
0.2	50	0.25	6.26	12
0.2	50	0.5	6.71	infinite
0.2	50	1	4.25	12
0.2	50	2	4.25	0.5
0.2	50	3	5.14	0.5
0.4	50	0.25	6.55	5
0.4	50	0.5	3.88	10
0.4	50	1	4.35	0.4
0.4	50	3	4.02	0.5
0.4	50	2	3.61	0.75
0.6	50	0.25	4.78	3
0.6	50	0.5	7.51	10
0.6	50	1	5.72	0.8
0.8	50	0.25	4.45	6
0.8	50	0.5	4.38	2
0.1	100	0.25	3.59	infinite
0.1	100	0.5	4.35	infinite
0.1	100	1	9.04	infinite
0.1	100	2	13.47	infinite
0.1	100	3	25.71	Snarl
0.2	100	0.25	4.88	4
0.2	100	0.5	3.69	infinite
0.2	100	1	6.51	9
0.2	100	2	4.71	0.5
0.2	100	3	5.7	1.5
0.4	100	0.25	7.42	6
0.4	100	0.5	4.22	infinite
0.4	100	1	3.39	3
0.4	100	3	2.95	0.75
0.4	100	2	4.43	0.35
0.6	100	1	7.3	1.5
0.6	100	2	3.96	0.5
0.6	100	0.25	6.1	3
0.6	100	0.5	4.76	2

Table A1.3 Experimental data for insert TNMG 332 MF3

Feed (mm/rev)	Speed (m/min)	Depth of Cut (mm)	Chip diameter (mm)	Chip turns
0.1	50	0.25	1.85	infinite
0.1	50	0.5	3.26	infinite
0.1	50	1	6.42	7
0.1	50	2	6.46	infinite
0.2	50	0.5	3.96	infinite
0.2	50	1	4.1	14
0.2	50	2	5.05	0.5
0.2	50	3	4.8	0.5
0.4	50	0.25	8.36	4
0.4	50	0.5	4.25	infinite
0.4	50	1	4.43	0.75
0.4	50	2	3.55	0.5
0.6	50	0.25	5.44	7
0.6	50	0.5	6	1
0.6	50	1	5.67	0.85
0.1	100	0.25	3.94	infinite
0.1	100	0.5	4.17	infinite
0.1	100	1	6.46	infinite
0.1	100	2	9.53	15
0.2	100	0.25	4.08	infinite
0.2	100	0.5	4.01	infinite
0.2	100	1	5.42	1.5
0.2	100	2	4.4	0.75
0.4	100	0.25	6.23	10
0.4	100	0.5	4.41	infinite
0.4	100	1	4.99	5
0.4	100	2	4.14	0.5
0.6	100	0.25	4.83	5
0.6	100	0.5	7.23	12
0.6	100	1	5.27	0.5
0.6	100	2	4.68	0.5

Table A1.4 Experimental data for insert TNMG 332 MR5

Feed (mm/rev)	Speed (m/min)	Depth of Cut (mm)	Chip diameter (mm)	Chip turns
0.1	50	0.5	3.3	11
0.1	50	1	9.65	infinite
0.1	50	2	10.9	infinite
0.1	50	3	10.9	infinite
0.1	50	4	10.8	infinite
0.2	50	0.5	8.08	infinite
0.2	50	1	8.2	infinite
0.2	50	2	6.69	1.25
0.2	50	3	5.95	infinite
0.2	50	4	7.2	infinite
0.4	50	0.5	10.7	14
0.4	50	1	6.57	1
0.4	50	2	4.91	0.5
0.4	50	3	7	0.75
0.4	50	4	10	0.5
0.6	50	0.5	10.4	7
0.6	50	1	5.8	0.5
0.6	50	2	5.66	0.5
0.8	50	0.25	10.97	10
0.8	50	0.5	7.4	1
0.8	50	1	7.6	0.75
0.1	100	0.5	7	infinite
0.1	100	1	11.04	infinite

Table A1.4 (continued)

0.1	100	2	13.9	10
0.1	100	3	19.5	infinite
0.2	100	0.5	6.23	infinite
0.2	100	1	8.94	infinite
0.2	100	2	8.38	1.25
0.2	100	3	7.86	infinite
0.2	100	4	8.34	infinite
0.4	100	0.25	8.58	snarl
0.4	100	0.5	6.94	infinite
0.4	100	1	5.9	1.5
0.4	100	2	5.58	0.75
0.4	100	3	5.9	0.5
0.6	100	0.25	7.69	10
0.6	100	0.5	7.63	infinite
0.6	100	1	7.58	1.5
0.6	100	2	6.81	1
0.8	100	0.125	2.79	infinite
0.8	100	0.25	11.79	Snarl
0.8	100	0.5	9.1	1
0.8	100	1	8.57	0.7

Table A1.5 Experimental data for insert TNMG 332 NG

Feed (mm/rev)	Speed (m/min)	Depth of Cut (mm)	Chip diameter (mm)	Chip turns
0.1	50	0.5	3.3	3
0.1	50	1	3.64	2
0.1	50	2	6.65	1
0.1	50	3	4.71	1
0.2	50	0.5	3.31	2
0.2	50	1	3.21	1.5
0.2	50	2	3.59	1
0.2	50	3	4.2	1
0.4	50	0.5	3.54	infinite
0.4	50	1	7.09	1
0.4	50	2	7.68	1
0.4	50	3	6.13	0.5
0.6	50	0.5	4.5	1
0.6	50	1	7.3	0.5
0.6	50	2	6.38	0.5
0.1	100	0.5	4.86	infinite
0.1	100	1	5.88	infinite
0.1	100	2	5.6	15
0.1	100	3	6.84	infinite
0.2	100	0.5	4.02	infinite
0.2	100	1	3.5	0.5
0.2	100	2	4.11	1
0.2	100	3	6.26	2
0.4	100	0.5	3.39	infinite
0.4	100	1	3.61	0.5
0.4	100	2	4.76	0.5
0.6	100	0.5	4.02	10
0.6	100	1	3.94	0.5
0.6	100	2	5.96	0.5

Table A1.6 Experimental data for insert TNMG 322

Feed (mm/rev)	Speed (m/min)	Depth of Cut (mm)	Chip diameter (mm)	Chip turns
0.1	50	0.5	2.56	10
0.1	50	1	4.52	3
0.1	50	2	6.83	2
0.1	50	3	12.29	1.5
0.2	50	0.5	2.66	3
0.2	50	1	6.6	1.5
0.2	50	2	6.32	1
0.2	50	3	6.04	0.5
0.4	50	0.5	7.46	7
0.4	50	1	7.25	0.75
0.4	50	2	8.3	0.5
0.6	50	0.5	5.62	9
0.6	50	1	8.12	1
0.6	50	2	8.72	0.5
0.1	100	0.5	5.3	infinite
0.1	100	1	5.85	10
0.1	100	2	6.38	3
0.2	100	0.5	4.41	12
0.2	100	1	5.18	1
0.2	100	2	6.68	1
0.4	100	0.5	5.23	7
0.4	100	1	4.67	0.5
0.4	100	2	6.76	0.4
0.6	100	0.5	10.36	2
0.6	100	1	6.52	0.75
0.6	100	2	6.6	0.5

Table A1.7 Experimental data for insert TNMG 332 PP

Feed (mm/rev)	Speed (m/min)	Depth of Cut (mm)	Chip diameter (mm)	Chip turns
0.1	50	0.5	2.32	15
0.1	50	1	3.97	8
0.1	50	2	6.3	1
0.1	50	3	8.76	1.5
0.2	50	0.5	4.76	17
0.2	50	1	7.17	4
0.2	50	2	4.61	0.5
0.4	50	0.5	7.17	15
0.4	50	1	5.29	0.75
0.4	50	2	6.07	0.5
0.6	50	0.5	5.09	infinite
0.6	50	1	6.27	0.5
0.6	50	2	5.53	0.5
0.1	100	0.5	5.7	infinite
0.1	100	1	6.31	20
0.1	100	2	5.56	2
0.2	100	0.5	6.33	infinite
0.2	100	1	6.81	10
0.2	100	2	6.43	0.5
0.4	100	0.5	6.94	infinite
0.4	100	1	5.93	0.75
0.4	100	2	5.16	0.5
0.6	100	0.5	6.46	infinite
0.6	100	1	5.49	1
0.6	100	2	4.71	0.3

Table A1.8 Experimental data for insert TNMG 332 FF

Feed (mm/rev)	Speed (m/min)	Depth of Cut (mm)	Chip diameter (mm)	Chip turns
0.1	50	0.5	2.38	10
0.1	50	1	4.12	2.5
0.1	50	2	8.47	3
0.2	50	0.5	3.13	infinite
0.2	50	1	3.63	1.5
0.2	50	2	4.74	0.4
0.4	50	0.5	5.49	20
0.4	50	1	4.76	0.5
0.4	50	2	6.6	0.25
0.6	50	0.5	5.99	6
0.6	50	1	5.7	0.5
0.6	50	2	6.33	0.5
0.1	100	0.5	4.66	infinite
0.1	100	1	6.28	infinite
0.1	100	2	9.56	4
0.2	100	0.5	4.54	infinite
0.2	100	1	4.27	0.75
0.2	100	2	4.3	0.5
0.4	100	0.5	4.54	infinite
0.4	100	1	4.3	0.75
0.4	100	2	4.07	0.5
0.6	100	0.5	5.32	7
0.6	100	1	4.68	0.4
0.6	100	2	4.5	0.5

APPENDIX 2 LEAST SQUARE METHODS AND STATISTIC ANALYSIS

Regression analysis is the statistical methodology for modeling and predicting values of one or more variables, known as *dependent* variables, from predictor (*independent*) variables. It can also assess the predictor variables effect on the response (*dependent*) variables.

A2.1 Classical Linear Regression Model

Assume v_1, v_2, ..., v_r to be r predictor variables that are considered to be related to a response variable Y. The classical linear regression model states Y is dependent on the continuous manner of the v_i and random error ε. As the values of predictor variables are fixed after obtained from an experiment, the error is viewed as a random variable with a certain distribution.

The model of regression is given below:

$$Y = \beta_0 + \beta_1 v_1 + ... + \beta_r v_r + \varepsilon \qquad \text{(A2-1)}$$

$$\text{Response Var} = \text{Mean (dependent on } v_1, v_2, ..., v_r) + \text{error} \qquad \text{(A2-2)}$$

This model is a linear function of all unknown parameters β_0, β_1,..., β_r. But predictor variables v_i may or may not be of the first order in the model.

After an experiment, with n independent observations on Y and the associated v_i obtained, the complete model yields n equations.

$$
\begin{aligned}
Y_1 &= \beta_0 + \beta_1 v_{11} + \beta_2 v_{12} + \ldots + \beta_r v_{1r} + \varepsilon_1 \\
Y_2 &= \beta_0 + \beta_1 v_{21} + \beta_2 v_{22} + \ldots + \beta_r v_{2r} + \varepsilon_2 \\
&\text{M} \quad \text{M} \\
Y_n &= \beta_0 + \beta_1 v_{n1} + \beta_2 v_{n2} + \ldots + \beta_r v_{nr} + \varepsilon_n
\end{aligned} \tag{A2-3}
$$

The errors are assumed to have the following properties:

1. $E(\varepsilon_j) = 0$;

2. $Var(\varepsilon_j) = \sigma^2$;

3. $Cov(\varepsilon_j, \varepsilon_k) = 0$, j≠k.

In matrix notation, the regression model is expressed as:

$$\mathbf{Y} = \mathbf{V} \beta + \varepsilon \tag{A2-4}$$

and $E(\varepsilon) = 0$, $Cov(\varepsilon) = \sigma^2 I$, where β and σ^2 are unknown parameters and the design matrix **V** has jth row $[v_{j0}, v_{j1}, \ldots, v_{jr}]$.

A2.2 Least-Square Estimation

Regression analysis is used to solve the equations of the classical model and attempts to find a suitable curve (model) to fit the original data. The least squares estimation is a method employed to select **b** (as an estimation of β), which minimizes the sum of squared differences

$$
\begin{aligned}
S(\mathbf{b}) &= \sum_{j=1}^{n} (y_j - b_0 - b_1 v_{j1} - \ldots - b_r v_{jr})^2 \\
&= (\mathbf{y}-\mathbf{Vb})'(\mathbf{y}-\mathbf{Vb})
\end{aligned} \tag{A2-5}
$$

The estimated parameter **b** is chosen by the criterion of Least Square Estimation. It is considered as unbiased estimation of β, denoted as $\hat{\beta}$.

Let **V** have full rank r+1≤n. The least square estimate of β in the classical regression model is given by

$$\hat{\beta} = (\mathbf{Z}'\mathbf{Z})^{-1}\mathbf{Z}'\mathbf{y} \tag{A2-6}$$

The residuals is calculated as

$$\hat{\varepsilon} = \mathbf{y} - \hat{\mathbf{y}} = [\mathbf{I} - \mathbf{V}(\mathbf{V}'\mathbf{V})^{-1}\mathbf{V}']\mathbf{y} \tag{A2-7}$$

Also, the

Residual Sum of Squares $$= \sum_{j=1}^{n}(y_j - \hat{\beta}_0 - \hat{\beta}_1 v_{j1} - \mathrm{L} \ - \hat{\beta}_r v_{jr})^2 = \hat{\varepsilon}'\hat{\varepsilon}$$

$$= \mathbf{y}'[\mathbf{I} - \mathbf{V}(\mathbf{V}'\mathbf{V})^{-1}\mathbf{V}']\mathbf{y} = \mathbf{y}'\mathbf{y} - \mathbf{y}'\mathbf{V}\hat{\beta}^{2} \tag{A2-8}$$

After decomposition, we obtain

$$\sum_{j=1}^{n}(y_j - \bar{y})^2 = \sum_{j=1}^{n}(\hat{y}_j - \bar{y})^2 + \sum_{j=1}^{n}\hat{\varepsilon}_j^2 \tag{A2-9}$$

$$\begin{pmatrix} total\ \ sum \\ of\ \ squares \\ about\ \ mean \end{pmatrix} = \begin{pmatrix} regression \\ sum\ \ of \\ squares \end{pmatrix} + \begin{pmatrix} residual\ \ (error) \\ sum\ \ of\ \ squares \end{pmatrix} \tag{A2-10}$$

By decomposition, the quality of the model fit can be measured by the coefficient of determination

$$\mathrm{R}^2 = 1 - \frac{\sum_{j=1}^{n}\hat{\varepsilon}_j^2}{\sum_{j=1}^{n}(y_j - \bar{y})^2} = \frac{\sum_{j=1}^{n}(\hat{y}_j - \bar{y})^2}{\sum_{j=1}^{n}(y_j - \bar{y})^2} \tag{A2-11}$$

The quantity of R^2 gives the proportion of the total variation in the y_j's attributable to the predictor variables.

Let $\mathbf{Y}=\mathbf{V}\beta+\varepsilon$, where $\mathbf{V}$ has full rank r+1 and ε is distributed as $N_m(0,\sigma^2\mathbf{I})$. The maximum likelihood estimator of β is the same as the least square estimator, $\hat{\beta}$.

A $100(1-\alpha)\%$ confidence region for β is given by

$$(\beta-\hat{\beta})'\mathbf{V}'\mathbf{V}(\beta-\hat{\beta})\leq (r+1)s^2F_{r+1,n-r-1}(\alpha) \qquad \text{(A2-12)}$$

where $F_{r+1,n-r-1}(\alpha)$ is the upper (100α) percentile of an F-distribution with r+1 and n-r-1 degree of freedom.

A2.3 Statistical model improvement for prediction model

Once the regression model is found fitting satisfactorily with the data, it is then cast into two major domain of application. First, the model can be used to estimate the regression function at certain point. Second, the model may predict or forecast a new observation at a point, which may be an existing point or a new one.

Let $\mathbf{v}_0=[1,v_{01},...,v_{0r}]'$ be a set of selected values for predictor variables, $\hat{\beta}$ be the least square estimation and Y_0 denote the response when predictor variables have the value of $\mathbf{v}_0$. The expected value of Y_0 is

$$E(Y_0 \mid \mathbf{v}_0)=\beta_0+\beta_1v_{01}+...+\beta_rv_{0r}=\mathbf{v}_0'\beta \qquad \text{(A2-13)}$$

Its least square estimation is $\mathbf{v}_0'\hat{\beta}$. When Y_0 is a new observation at $\mathbf{v}_0$, the prediction of Y_0 is more than a simple expected value. According to the regression model,

$$Y_0=\mathbf{v}_0'\beta+\varepsilon_0 \qquad \text{(A2-14)}$$

where ε_0 is normally distributed as N(0, σ^2) and is independent of ε, $\hat{\beta}$ and s^2.

$$\mathrm{Var}(Y_0 - \mathbf{v}_0' \hat{\beta}) = \sigma^2(1 + \mathbf{v}_0' (\mathbf{V}'\mathbf{V})^{-1} \mathbf{v}_0) \qquad \text{(A2-15)}$$

The above equation shows the variance of the forecast error, the scale of which reflects the model fitness and accuracy.

The difficulty of practical regression analysis lies in how to find out variables that are crucial for changes in dependent variable, delete insignificant ones and increase some variables of high order or special function, such as exponential or log function.

In fact, it is still a trial and error based technique, but there are some guidelines that can be used. One of the possible ways is to assume the present model "correct" and plot the residual plots against predictor variables and response variables. From the shape of various plots, it could then be decided if any items (e.g. high order terms) need to be added in.

Another way of doing the selection is called *step-wise* selection. This method applies well for selecting predictor variables from a large set. It is often difficult to formulate an appropriate regression function when a large number of variables are presented to the model all at once. A selection method is to try all the subsets of variables for regression, and check some criterion quantity such as R^2. Stepwise regression attempts to select important predictors without considering all the possibility. The method is to compare each variable's contribution to the response. If they are below the criterion value, it is then selected into the model.

A high R^2 does not necessarily mean a good regression model. There may be some potential problems for the model or even a misled biased model. One factor of great concern is the colinearity among variables. When $\mathbf{V}$ is not of full rank, some linear combination, such as $\mathbf{Va}$, must equal $\mathbf{0}$. In such a situation, it is said to be *colinear*. This in turn implies that

$\mathbf{V'V}$ does not have an inverse. Although for our regression situation, it is unlikely that $\mathbf{Va=0}$. Yet it may be very close to $\mathbf{0}$ for linear combination of $\mathbf{V}$, the inverse matrix $(\mathbf{V'V})^{-1}$ is still numerically unstable. The direct yield from this is large estimated variance for the $\hat{\beta}_i$'s and it is then difficult to detect the significant β_i.

REFERENCES

Albrecht, P., 1961, "New Development in the Theory of the Metal-Cutting Process, Part II: The Theory of Chip Formation," Trans. ASME, Journal of Engineering for Industry, pp. 557-571.

Armarego, E. J. A. and Wiriyacosol, S., 1978, "Oblique Machining eith Triangular Form Tools-I. . theoretical Investigation," Int. J. Mach. Tool Des. Res. v18, pp. 67-80"

Armarego, E. J. A. and Wiriyacosol, S., 1978, "Oblique Machining with Triangular Form Tools-II. Experimental Investigastion," Int. J. Mach. Tool Des. Res., v18, pp. 153-165.

Armarego, E. J. A., 1967, "Machining with Double Cutting Edge Tools—I. Symmetrical Triangular Cuts," Int. J. Mach. Tool Des. Res. v7, pp. 23-37.

Burdea, G., 1993, "Virtual Reality Systems and Applications," Electro'93 International Conference, Short Course, Edison, NJ, Apr. 28, pp. 164.

Colwell, L. V., 1954, "Predicting the Angle of Chip Flow for Single-Point Cutting Tools," Trans ASME, v76, n2, pp. 199-204.

Dai, F, Felger, W., Fruhauf, T. Gobel, M., Reiners, D. and Zachmann, G., 1996, "Virtual Prototyping Examples for Automotive Industries," Virtual Reality world '96, pp. 1-11.

Fang, Y. J., Basu, A. and Fang, X. D., 1997b, "A 3-D kinematic model of complex chip curling with chip breaker tools in metal cutting. Part I: Analytical Modelling," ASME International Mechanical Engineering Congress and Exposition, Manufacturing Science and Technology, v6, n2, pp. 177-182.

Fang, Y. J., Fang, X. D. and Basu, A., 1997c, "A 3-D kinematic model of complex chip curling with chip breaker tools in metal cutting. Part II: Analysis and Discussion," ASME International Mechanical Engineering Congress, Manufacturing Science and Technology, v6, n2, pp. 183-191.

Fang, X. D.; Fang, Y.J.; Hamidnia, S., 1997a, "Computer animation of 3-D chip formation in oblique machining," Journal of Manufacturing Science and Engineering, v 119, n3, pp. 433-438.

Fang, X. D., Fei, J. and Jawahir, I. S., 1996, "A hybrid algorithm for predicting chip form/chip breakability in machining," Int. J. Mach. Tools Manufact., v36, n10, pp.1093-1107.

Fang, X. D. and Jawahir, I. S., 1991, "On Predicting Chip Breakability in Machining of Steels with Carbide Tool Inserts Having Complex Chip Groove Geometries," Journal of Materials Processing Technology, v28, pp. 37-47.

Fang, X. D. and Jawahir, I.S., 1996, "An analytical Model for Cyclic Chip Formation in 2-D Machining with Chip Breaking," Annals of the CIRP, v45 n1, pp.53-58.

Fang, X. D. And Safi-jahanshahi, H., 1997, "A new algorithm for developing a reference-based model for predicting surface roughness in finish machining of steels," Int J Prod Res, v35, n1, pp. 179-199.

Feinberg, B. 1975, "No-Groove Inserts: A Design for Chip Control," Manufacturing Engineering, v75, n2, pp. 34-36.

Jawahir, I. S., 1988, "The Tool Restricted Contact Effect as a Major Influencing Factor in Chip Breaking: An Experimental Analysis," Annals of the CIRP v37, n1, pp. 121-126.

Jawahir, I. S., 1988, "A Survey and Future Predictions for the Use of Chip Breaking in Unmanned Systems," The International Journal of Advanced Manufacturing Technology, v3, n4, pp. 87-104.

Jawahir, I. S. and Oxley, P. L. B., 1988, "New Developments in Chip Control Research Moving Towards chip BreakaBility Predictions for Unmanned Manufacture," Proc. Int. Conf. ASME, Atlanta, pp. 311-320

Jawahir, I. S. and Oxley, P. L. B., 1988, "Efficient Chip Control at Reduced Power Consumption: An Experimental Analysis," Proc. 4th Int. Conf. On Manufacturing Engg., Brisbane, Australia, pp. 97-102.

Johnson, W, 1962. "Some Slip-line Fields for Swaging or Expanding, Indenting, Extruding and Machining for Tools with Curved Dies," Int J of Mechanical Sciences, v4, pp. 323-347.

Jones, A. and Iuliano, M., 1997,"Virtual manufacturing testbed," Proc of IEEE Int Conf on Systems, Man and Cybernetics, Orlando, pp. 737-742.

Katbi, K., 1990, "Chip Grooves," Cutting Tool Engineering, April, pp. 59-62.

Kauffman, D. C., 1954, "Carbide Tool Troubles," The Tool engineer, v33, n1, pp. 35-42.

Kirschman, C. F. and Fadel, G.M., 1998, "Classifying Functions for Mechanical Design, J of Mech Design," v120, pp.475-482.

Kluft, w., Konig,W., van Luttervelt, C. A., Nakayama, K. and Pekelharing, A. J., 1979, "Present Knowledge of Chip Control," Annals of the CIRP, v28, n2, pp. 441-453.

Liu, X. D., Lee, L. C., and Lam, K. Y. 1995,"A Slip-Line Field Model for the Determination of Chip curl Radius," Transactions of the ASME, v117, pp. 266-271.

Mesquita, R. M. D. and BarataMaruqes, M. J. M., 1992, "Effect of Chip-Breaker Geometies on Cutting Forces," Journal of Materials Processing Technology, v31, pp. 317-325.

Mittal, R. N., Juneja, B. L. and Sekhon, G. S., 1980, "A solution of the oblique controlled contact continuous cutting problem," Int. J. Mach. Tool Des. Res., v20, pp. 211-221.

Nakamura, S., Wuebbling, G. J., and Christopher, J. D., 1982, "Chip Control in Turning," SME Technical Paper.

Nakayma, K., 1960, "A Study on Chip-Breaker," Bulletin of JSME, v5, n17, pp. 142-150.

Nakayma, K., 1972, "Chip Form Geometry - Study on the Form of Chip in Metal Cutting (part I)," J of JSPE, v38, n7, pp. 34-40.

Nakayma, K., Ogawa, M., and Takeyama, H., 1978, "Basic Rules on the Form of Chip in Metal Cutting," Annals of the CIRP, v27, n1, pp. 17-21.

Nakayma, K. and Aria, M., and Suzuki, H. 1981, "Cutting Tool with Curved Rake Face—A Means for Breaking Thin Chips,"Annals of the CIRP, v30, n1, pp. 5-8.

Nakayma, K. and Aria, M., 1992, "Comprehensive Chip from Classification Based on the Cutting Mechanism," Annals of the CIRP, v41, n1, pp. 71-74.

North, B, 1989, "Indexable metal cutting inserts – industry trends," Powder Metallurgy, v32, n2, pp. 88-91.

Okushima, K., Minato, K., 1959, "On the Behavior of Chip in Steel Cutting," Bulletin JSME, v2, n5, pp. 58-64.

Oxley, P. L. B., 1962, An Analysis for orthogonal Cutting with Restricted Tool—Chip Contact," Int. J. Mech. Sciences, v4, pp. 129-135.

Rotberg, J., Ber, A., and Wertheim, R.,1991, "Chip Control in Cut-off Tools," Annals of the CIRP, v40, n1, pp. 77.

Rubenstein, C., Venuvinod, P. K., and Lau, W.S., 1986, "Analysis of Oblique Cutting with Controlled Controlled Contact Tools," Annals of the CIRP v35, n1, pp. 51-54.

Sadik, M. I. and Lindstrom B., 1993, "The Role of Tool-Chip Contact Length in Metal Cutting," Journal of Materials Processing Technology, v37, pp. 613-627.

Shi, T. and Ramalingam, S., 1991, "Slip-Line Solution for Orthogonal Cutting with a Chip Breaker and Flank Wear," Int. J. Mech. Sci. v33, n9, pp.689-704.

Shi, T. and Ramalingam, S., 1992, "Modeling Chip Formation with Grooved Tools," Int. j. Mech. Sci. v35, n9, pp. 741-756.

Shi, T. and Betts, C. A., 1993,"Technical Briefs," Transactions of the ASME, v115, pp. 160-163.

Shimomura,Y., Yoshioka, M., Takeda, H., Umeda, Y. and Tomiyama, T., 1998, "Representation of Design Object Based on the Functional Evolution Process Model," Journal of Mech. Design, v120, pp. 221-229.

Sikder, C., Babu, S. S., Chattopadhyay, A. B., and Venkatesh, V. C., 1991, "Effect of Becelling of carbide Turning Inserts on Chip Formation and Cutting Forces," Journal of Materials Processing technology, v28, pp. 15-24.

Stabler, G. V., 1951, "The Fundamental Geometry of Cutting Tools," The Institution of Mech. Engineers, v165, n63, pp. 14-26.

Stier, H., 1990,"Breaking the chip or living with it if you can't break it," Modern Machine Shop, v, p. 124.

Strenkowski, J. S. and Moon, K. J., 1990, "Finite Element Prediction of Chip Geometry and Tool/Workpiece Temperature Distributions in Orthogonal Metal Cutting," Transactions of the ASME, Journal of engineering for industry, v112, pp. 313-318.

Suh, N. P., Bell, A. C. and Gossard, D. C., 1978, "On an Axiomatic Approach to Manufacturing and Manufacturing Systems," Journal of Engineering for Industry, Trans of ASME, v100, n2.

Suh, N. P. and Rinderle, J. R., 1982, " Qualitative and Quantitative Use of Design and Manufacturing Axioms," v31, n1, pp. 333-338.

Sutherland, I., 1965, "The ultimate display," Proc. IFIP Congress, pp. 506-508.

Sutherland, I., 1968, "A head-mounted three dimensional display," Proc. Fall Joint Computer Conference, pp. 757-764.

Takeda, H., Veerkamp, P., Tomiyama, T. and Yoshikawa, H., 1990, "Modeling Design Process," AI Magzine, v11, n4, pp.37-48.

Taylor, R., Bayliss, G., Bowyer, A. and Willis, P., 1995, "A virtual workshop for design by manufacture," Proceedings of the Computers in Engineering Conference and the Engineering Database Symposium, pp. 921-926.

Ten Horn, B. L. and Schuermann, R. A., 1954, "Chip Control, How To Determine Tool Feed to Obtain Desirable Chip Form," The Tool Engineer, v33, n4, pp. 37-44.

Tipnis, V., 1981, "Turning with Advanced Inserts," Modern Machine Shop, June , pp. 89-100.

Tonshoff, H. K., Wulfsberg, J. P., Kals, H. J. J., Konig, W.,and VanLuttervelt, C. A., 1988, "Developments and Trends in Monitoring and Control of Machining Processes," Annals of the CIRP, v37, n2, pp. 611-621.

Trigger, K. J. and VonTurkovich, B. F., 1963, "Chip Formation in High-Speed Cutting of Copper and Aluminum," Trans. ASME, Journal of Engineering for Industry, v85, pp. 365-373.

Trim, A. R. and Boothroyd, G., 1968, "Action of the Obstruction Type Chip Former," The International Journal of Production Research, v6, n3, pp. 227-241.

Ueda, K. and Manabe, K., 1992, "Chip Formation Mechanism in Microcutting of an Amorphous Metal," Annals of the CIRP, v41, n1, pp. 129-132.

Usui, E. and Hirota, A., 1978, "Analytical prediction of Three Dimensional Cutting Process," Journal of Engineering for Industry, v100, pp. 229-235.

Usui, E. and Shaw, M.C., 1962, "Free Machining Steel—IV Tool with Reduced Contact Length," Transactions of the ASME, Journal of Engineering for Industry, February, pp. 89-102.

Usui, E. and Hoshi, K, 1963, "Slip-line Fields in Metal Machining which Involve Centered Fans," International Journal of Production Engineering Research Conference, ASME, pp. 61-17.

Usui, E., Kikuchi, K. and Hoshi, K., 1964, "The theory of Plasticity Applied to Machining With Cut-away Tools," Trans. ASME, pp. 95-104.

VanDoren., V. J., 1998, "Simulation simplifies `what-if' analysis," Control Engineering, v45, n9, pp.6.

VanLuttervelt, C.A., 1976, "Chip Formation in Machining Operation at Small Diameter," Annals of the CIRP v25, n1, pp. 71-76.

VanLuttervelt, C. A., 1989, "Characteristic Parameters of Chip Control in Turning Operation with Indexable Inserts and Three-Dimensionally Shaped Chip Formers," Annals of the CIRP, v38, n1, pp. 75-79.

Venu Vinod, P.K., Lau, W., and Barrow, G., 1978, "On a New Model of Oblique Cutting," Journal of Engineering for Industry, v100, pp. 287-292.

Venkatesh, V. C., Zhou, D. Q., Xue, W. and Quinto, D. T., 1993, "A study of Chip Surface Characteristics during the machining of steel," Annals of the CIRP, v42, n1, pp. 631-636.

Worthington, B., 1975, "The effect of Rake Face Configuration on the Curvature of the Chip in metal Cutting," Int. J. Mach. Tooi Des. Res., v15, pp. 223-229.

Worthington, B., 1976, "The Operation and Performance of a groove-Type Chip Forming Device," Int. J. Prod. Res. V14, n5, pp. 529-558.

Worthington, B. and Rahman, M. H., 1979, "Predicting Breaking with Groove Type Breakers," Int. J. Mach. Tool Des. Res., v19, pp. 121-132

Wright, P. K., McCormick, S. P., and Miller, T. R., 1980, "Effect of Rake Face Design on Cutting Tool Temperature Distributions," Journal of Engineering for Industry, v102, pp. 123-128.

Xiao, T., Han, X. and Yang, G., 1996, "Virtual machining environment – GMPS," ETFA'96, v1, pp. 167-171.

Yao, Y., Jawahir, I. S., Jamieson, D., and Fang, X. D., 1990, "Computer Animation of Chip Flow and Chip Curl in an Expert Process Planning System for Metal Machining," Transactions of the North American Manufacturing Research Institution of SME, pp. 161-166.

Yellowley, 1983, "The Utilization of Restricted Rake Face Contact Turning Tools," Annals of the CIRP, v32, n1, pp. 75-78.

Zdeblick, W. J. and Mason, F., 1992, "Blast Chips to Automate Turning ," American Machinist, July, v136, pp. 47-51.

Zhang, H. T., Liu, P. D., and Hu, R. S., 1988, "The Theretical Calculation of Naturally Curling Radius of Chip," Int. J. Mach. Tools Manufact. v29, n3, pp. 323-332.

Zhang, Y. Z., 1980, "Chip Curl, Chip Breaking and Chip Control of the Difficult-to-Cut Materials," Annals of the CIRP, v29, n1, pp. 79-82.